Final Report

DEVELOPMENT OF A BINDER FRACTURE TEST TO DETERMINE FRACTURE ENERGY

UF Project No.:   00084221

Contract No.:   BDK75 977-27

Submitted to:

UF | UNIVERSITY *of* FLORIDA

Dr. Reynaldo Roque, P.E.
Tianying Niu
George Lopp
Dr. Jian Zou

Department of Civil and Coastal Engineering
College of Engineering
365 Weil Hall, P.O. Box 116580
Gainesville, FL, 32611-6580
Tel: (352) 392-9537 extension 1458
Fax: (352) 392-3394

April 2012

DISCLAIMER

The opinions, findings and conclusions expressed in this publication are those of the authors and not necessarily those of the Florida Department of Transportation.

Prepared in cooperation with the State of Florida Department of Transportation.

SI* (MODERN METRIC) CONVERSION FACTORS

APPROXIMATE CONVERSIONS TO SI UNITS

Symbol	When You Know	Multiply By	To Find	Symbol
LENGTH				
in	inches	25.4	millimeters	mm
ft	feet	0.305	meters	m
yd	yards	0.914	meters	m
mi	miles	1.61	kilometers	km
AREA				
in²	square inches	645.2	square millimeters	mm²
ft²	square feet	0.093	square meters	m²
yd²	square yards	0.836	square meters	m²
ac	acres	0.405	hectares	ha
mi²	square miles	2.59	square kilometers	km²
VOLUME				
fl oz	fluid ounces	29.57	milliliters	ml
gal	gallons	3.785	liters	l
ft³	cubic feet	0.028	cubic meters	m³
yd³	cubic yards	0.765	cubic meters	m³

NOTE: Volumes greater than 1000 l shall be shown in m³.

Symbol	When You Know	Multiply By	To Find	Symbol
MASS				
oz	ounces	28.35	grams	g
lb	pounds	0.454	kilograms	kg
T	short tons (2000 lb)	0.907	megagrams	Mg
TEMPERATURE (exact)				
°F	Fahrenheit temperature	5(F-32)/9 or (F-32)/1.8	Celcius temperature	°C
ILLUMINATION				
fc	foot-candles	10.76	lux	lx
fl	foot-Lamberts	3.426	candela/m²	cd/m²
FORCE and PRESSURE or STRESS				
lbf	poundforce	4.45	newtons	N
psi	poundforce per square inch	6.89	kilopascals	kPa

APPROXIMATE CONVERSIONS FROM SI UNITS

Symbol	When You Know	Multiply By	To Find	Symbol
LENGTH				
mm	millimeters	0.039	inches	in
m	meters	3.28	feet	ft
m	meters	1.09	yards	yd
km	kilometers	0.621	miles	mi
AREA				
mm²	square millimeters	0.0016	square inches	in²
m²	square meters	10.764	square feet	ft²
m²	square meters	1.195	square yards	yd²
ha	hectares	2.47	acres	ac
km²	square kilometers	0.386	square miles	mi²
VOLUME				
ml	milliliters	0.034	fluid ounces	fl oz
l	liters	0.264	gallons	gal
m³	cubic meters	35.71	cubic feet	ft³
m³	cubic meters	1.307	cubic yards	yd³
MASS				
g	grams	0.035	ounces	oz
kg	kilograms	2.202	pounds	lb
Mg	megagrams	1.103	short tons (2000 lb)	T
TEMPERATURE (exact)				
°C	Celcius temperature	1.8C + 32	Fahrenheit temperature	°F
ILLUMINATION				
lx	lux	0.0929	foot-candles	fc
cd/m²	candela/m²	0.2919	foot-Lamberts	fl
FORCE and PRESSURE or STRESS				
N	newtons	0.225	poundforce	lbf
kPa	kilopascals	0.145	poundforce per square inch	psi

(Revised August 1992)

* SI is the symbol for the International System of Units. Appropriate rounding should be made to comply with Section 4 of ASTM E380.

1. Report No.	2. Government Accession No.	3. Recipient's Catalog No.
4. Title and Subtitle Development of A Binder Fracture Test To Determine Fracture Energy		5. Report Date April 2012
		6. Performing Organization Code 0054539
7. Author(s) Reynaldo Roque, Tianying Niu, George Lopp, and Jian Zou		8. Performing Organization Report No.
9. Performing Organization Name and Address University of Florida Department of Civil and Coastal Engineering 365 Weil Hall P.O. Box 116580 Gainesville, FL 32611-6580		10. Work Unit No. (TRAIS)
		11. Contract or Grant No. BDK75 977-27
12. Sponsoring Agency Name and Address Florida Department of Transportation Research Management Center 605 Suwannee Street, MS 30 Tallahassee, FL 32399		13. Type of Report and Period Covered Final 10/26/09-04/30/12
		14. Sponsoring Agency Code
15. Supplementary Notes		

16. Abstract

It has been found that binder testing methods in current specifications do not accurately predict cracking performance at intermediate temperatures. Fracture energy has been determined to be strongly correlated to fracture resistance of asphalt mixture, so a new fracture test and interpretation system was developed based on finite element analysis (FEA) and prototype testing on a servo-hydraulic testing machine to consistently measure fracture energy of binder at intermediate temperature. For evaluation, the new test was applied to a range of binders, including unmodified binder, SBS-modified binder, rubber-modified binder, and hybrid binder from pressure aging vessel (PAV) residue or recovered from field test sections. Statistical analysis was conducted on test results, which showed that the new fracture test and interpretation system clearly differentiated binders by fracture energy values. Expected trends in fracture energy between binders were observed. It was also shown that, for the same binder, fracture energy is independent of loading rate evaluated in this study and test temperature from 0 to 15°C. Thus, fracture energy appeared to be a fundamental property of binder, which does not depend on test condition, and can be determined by tests performed at a single temperature and loading rate. The results also showed that different types of binder have different characteristic true stress-true strain curves, which can be used to identify binder type, modifier type, and relative content. Basic principles were proposed to identify the presence of modifier from true stress-true strain curves. A detailed testing protocol was recommended. The protocol helps assure the appropriate loading rate range so that the complete true stress-true strain curve can be identified for accurate determination of fracture energy.

17. Key Word Fracture Energy, Asphalt Binder, Fracture Test, Direct Tension Test, Modified Binder, Hybrid Binder, and True Stress-True Strain Curve	18. Distribution Statement No restrictions. This document is available to the public through the National Technical Information Service, Springfield, VA, 22161.		
19. Security Classif. (of this report) Unclassified	20. Security Classif. (of this page) Unclassified	21. No. of Pages 138	22. Price

Form DOT F 1700.7 (8-72)   Reproduction of completed page authorized

ACKNOWLEDGMENTS

EXECUTIVE SUMMARY

Fatigue performance of asphalt mixture and pavement is known to be strongly influenced by fatigue resistance of asphalt binder. However, a recently completed study for FDOT (Roque et al., 2009) showed that binder testing methods in current specifications, including Dynamic Shear Rheometer (DSR) (G*sinδ), Elastic Recovery (ER), and Force-Ductility (FD) do not accurately predict cracking performance at intermediate temperatures. Fracture energy has been determined to be strongly correlated to fracture resistance of asphalt mixture (Roque et al., 2004). So, in the same FDOT study, an approach to determine cumulative energy to failure from FD results was developed and evaluated. The new approach resulted in improved ability to predict cracking performance at intermediate temperatures, even though the FD was not optimized to determine fracture energy accurately. Thus, it was inferred that a test to measure fracture energy of binder would be an excellent tool to evaluate fracture resistance of binder.

A new binder fracture energy test was developed based on nonlinear 3-D finite element analysis (FEA) to identify and optimize an appropriate specimen geometry that assured accurate determination of stress and strain on the fracture plane, which in turn assures accurate determination of fracture energy. The feasibility and validity of different specimen geometries identified were evaluated by conducting prototype direct tension tests using a servo-hydraulic loading frame in a temperature-controlled environment. A data interpretation system was established based on both nonlinear FEA and large strain formulation. A set of diagrams were proposed, based on nonlinear FEA results for convenience of performing the calculation procedure. In preliminary evaluations, the new fracture energy test and data interpretation system were shown to provide consistent and repeatable fracture energy of binder at intermediate temperatures.

For a more comprehensive evaluation, the new fracture energy test and data interpretation system were applied to a range of binders including unmodified binders, styrene butadiene styrene (SBS) polymer-modified binder, rubber-modified binders, hybrid binders, highly SBS-modified binder from pressure aging vessel (PAV) residue, as well as binder recovered from field test sections. For each binder, tests were performed at multiple loading rates and temperatures. Statistical analysis showed the new fracture energy test and data interpretation system significantly distinguished between different binders by fracture energy values. Expected trends in fracture energy between binders were observed. Statistical analysis also showed that for a given binder, fracture energy was independent of loading rates evaluated in this study and test temperatures from 0 to 15°C. Thus, fracture energy appears to be a fundamental property of binder, which does not depend on test condition, and can be determined by tests performed at a single temperature and loading rate.

However, it was also determined that erroneous results may occur if excessively high or low loading rates are used. A detailed testing protocol was recommended that helps assure tests are performed at appropriate loading rate ranges, within which accurate fracture energy is obtained. In addition, it was determined that erroneous tests resulting from inappropriate loading rates can be identified by way of the characteristics of the resulting true stress-true strain curve.

It was also found that the characteristic shape of the true stress-true strain curve from the fracture energy test was closely related to binder type, including presence of modifier or rubber and relative content. Therefore, the true stress-true strain curve can be used to identify the binder type, modifier type, and relative content. Basic principles for interpretation of the true stress-true strain curves were proposed for this purpose.

As for the binders tested, the highly polymer-modified binder PG 82-22 had significantly greater fracture energy than unmodified, SBS-modified, rubber-modified and hybrid binders. All hybrid binders had fracture energy higher than that of unmodified binders and comparable to SBS-modified binder. Two hybrid binders, Wright and Hudson, exhibited higher fracture energy than that of SBS-modified binder. The rubber-modified binders had fracture energy slightly greater than unmodified binders, but lower than other modified binders. Therefore, it appeared that polymer modifier is necessary to substantially increase binder fracture energy. Some hybrid binders (e.g., Hudson) exhibited higher fracture energy with a lower polymer content compared to polymer-modified binders (PG 76-22).

In conclusion, the new binder fracture energy test and data interpretation system developed appears to suitably measure fracture energy of unmodified and modified binder. In addition, it appears that the presence and relative content of modifier or rubber may be detectable from the test results. Several recommendations were made regarding implementation of this work, including the retrofit of existing binder direct tension test devices to perform the test developed and further use and evaluation of the test to determine binder damage rates and fracture properties of mastic.

TABLE OF CONTENTS

LIST OF TABLES

LIST OF FIGURES

CHAPTER 1
INTRODUCTION

1.1 Background

Fatigue performance of asphalt mixture and pavement is known to be strongly influenced by fatigue resistance of asphalt binder. However, a recently completed study for the Florida Department of Transportation (FDOT) (Roque et al., 2009) showed that the existing testing methods for asphalt binder in current specifications, including Dynamic Shear Rheometer (DSR) (G*sinδ), Elastic Recovery (ER), and Force-Ductility (FD) do not provide parameters that are consistently correlated with the relative cracking performance of mixtures at intermediate temperatures (i.e., 0 - 30 °C). Fracture energy is an important property related to fatigue resistance of asphalt mixtures. In the same FDOT study, an approach to determine cumulative energy to failure from FD results was developed and evaluated. The new approach resulted in improved ability to predict cracking performance at intermediate temperatures, even though the FD was not optimized to determine fracture energy accurately. The results indicated that a test designed specifically to obtain fracture energy would provide a better parameter related to fatigue resistance of binder. Also, there is a need for a system to determine mixture fracture energy from constituent properties (i.e., properties of aggregate and binder) for purposes of pavement structural design. Based on binder fracture energy, one should be able to predict mixture fracture resistance.

In concept, the direct tension (DT) test is a suitable approach to measure fracture energy of binder. However, because of its specimen shape (Figure 1-1), the traditional DT test exhibits excessively high variability (even for tensile strength) and does not properly represent the actual failure condition of binder between aggregates in mixture, which precludes accurate determination of fracture energy. Because the tensile stress is fairly uniform throughout the

1

relatively long middle section (see Figure 1-1), the specimen may crack anywhere within this section, which makes it impossible to accurately measure failure strain on the failure plane, which is required for accurate determination of fracture energy. Also, stress concentrations can develop where the cross-sectional area decreases, which often results in premature fracture. Finally, the specimen's geometry makes it difficult to apply a high enough strain rate to reduce the specimen's ductility, which makes the calculated fracture energy sensitive to any inaccuracy in simulation. For some highly ductile, high fracture energy binders, the fracture test may exceed the loading rate capacity of testing equipment without failure. These issues made it necessary to develop a new DT test that allows for accurate determination of stress-strain relationships of binder, from which fracture energy can be obtained.

Figure 1-1 A Superpave Direct Tension specimen

1.2 Objectives

The primary objective of this study is to develop a binder direct tension test and associated data interpretation methods that allow for determination of binder fracture energy at intermediate temperatures. It should be noted that "fracture energy" is a short form of the full term "fracture energy density". Both were used interchangeably throughout the report.

Detailed objectives can be summarized as follows:

1. Use 3-D finite element analysis (FEA) and prototype testing to develop and identify an optimized specimen configuration to determine fracture energy accurately.

2.   Develop and identify test procedures and appropriate measurement systems from which fracture energy can be determined accurately.

3.   Identify appropriate data interpretation procedures to calculate true stress and true strain, and to determine the instant of fracture initiation, such that fracture energy can be determined accurately.

4.   Evaluate the system developed by measuring fracture energy for a range of binders for which expected trends in fracture energy are known.

1.3 Research Approach

The research process consists of six tasks as follows:

1.   Literature Review

2.   Identify and Optimize Specimen Geometry

3.   Build Prototype System and Modify as Needed

4.   Identify Test Procedures, Measurement Systems and Data Interpretation Methods

5.   Perform Tests on a Range of Binders

6.   Evaluate System

In task 2 and task 3, a new specimen configuration was developed by FEA and prototype test. In task 4 and task 5, it was proved that the fracture energy of binder is independent of test temperature and loading rate. The optimal test condition (loading rate and temperature) was also identified. Task 5 tested and verified the new system can accurately predict cracking performance at intermediate temperatures.

CHAPTER 2
LITERATURE REVIEW

In order to improve fracture resistance of binder, many types of modifier including polymer and rubber have been applied to binder. Recently, various combinations of polymer, rubber and binder called hybrid binder have also been produced. However, it has been very difficult to quantitatively evaluate the fracture resistance of binders, and differentiate between them, particularly for modified binder.

At present, most relevant research is focused on traditional testing methods such as Dynamic Shear Rheometer (DSR), Bending Beam Rheometer (BBR), Elastic Recovery, Ductility, etc., with traditional parameters such as complex shear modulus G*, phase angle δ, etc., or some parameters derived from these tests such as yield energy and strain at maximum stress (Bahia et al., 2010).

Some researchers realized that traditional testing methods are not suitable for modified binders, and tried to develop new tests to improve accuracy. Rosales (2011) used the single-edge-notched beam (SENB) as an alternative to Bending Beam Rheometer (BBR) to determine both stiffness and fracture energy of modified binders, and found that the stiffness obtained through SENB is higher than that of BBR. The SENB is a typical fracture mechanics testing method. However, it is not suitable for highly ductile materials. Actually, the SENB was designed for binder at low temperature with brittle fracture, but not applicable to binder at intermediate temperature with ductile fracture.

Other researchers noticed the limitations of current binder tests. At the University of Florida, in a recently finished research project with hybrid binder, Roque et al. (2009) evaluated almost all existing binder testing methods including Dynamic Shear Rheometer (DSR), Bending Beam Rheometer (BBR), Multiple Stress Creep Recovery (MSCR), Elastic Recovery (ER) and

Forced Ductility (FD) test, and found that none of these tests able to accurately predict cracking performance at intermediate temperatures. Multiple Stress Creep Recovery (MSCR), Elastic Recovery (ER) and Forced Ductility (FD) tests were able to identify the presence of polymer-modified binder to some extent. In the same FDOT research project, Roque et al. (2009) developed an approach to determine cumulative energy to failure from FD results that showed improved ability to accurately predict cracking performance at intermediate temperatures. Even though the FD was not optimized to determine fracture energy accurately, the results indicated that a test designed specifically to obtain fracture energy could provide a much better parameter related to fatigue resistance of binder. Therefore, the research recommended developing a new binder fracture test to determine fracture energy.

Until now, most binder fracture energy tests are intended for use at low temperature. Ponniah et al. (1996) proposed fracture energy specifications for modified asphalts. They used three-point notched bending beam method to determine fracture toughness K_{IC}, then calculated fracture energy G_{IC} based on K_{IC}. Anderson et al. (2001) performed the three-point notched BBR test on a range of binders, and found that K_{IC} provides a much more discriminating ranking of resistance to thermal cracking than the Superpave criteria. Hoare et al. (2000) analyzed the results of three-point notched bending beam test, and found that fracture toughness and fracture energy are sensitive to the binder's morphology, polymer content, and stiffness. However, this method is only suitable for brittle binder specimen at low temperature when Linear Elastic Fracture Mechanics (LEFM) holds, but is not applicable for ductile binder at intermediate temperature. For rubber-modified binders in which the rubber is not completely digested, which are actually composite materials, a local notched crack tip may lead to a high variation in results. For this reason, the global fracture energy is a better indicator for rubber-modified binder.

For ductile binder at intermediate temperature, Andriescu et al. (2004) used double-edge-notched tension specimen to determine the essential work of fracture (i.e., the energy necessary for progression of fracture) and the plastic work of fracture (i.e., the energy necessary for the plastic deformation before fracture). It was found that this method provides an accurate way to measure failure properties of ductile binders. However, as mentioned above, the notched specimen shape may not be suitable for composite modified binders. On the other hand, the calculation of essential and plastic work of fracture was based on force, rather than on true stress on the fracture section, so it will result in inaccurate fracture energy values, particularly for ductile binders.

To test binder's ductile fracture energy at intermediate temperature is difficult, because it is not easy to accurately perform constitutive modeling of true stress-true true-strain for a complicated nonlinear viscoelastic or plastic modified binder which is often highly ductile and undergoes large deformation and fracture process. Constitutive modeling of true stress-true strain can be based on both Finite Element Analysis (FEA) simulation and prototype testing. However, there is usually a maximum strain level that FEA can accurately simulate based on large strain formulation. The mesh-free method, as an alternative to FEA, is good at dealing with large strain problems. However, at present, it is not mature enough and has its own limitations. It is also very time-consuming, which prevents it from practical use. The Extended Finite Element Method (XFEM), by use of additional discontinuous basis functions for crack opening displacement, is good at solving fracture problem because the mesh does not need to be updated along with cracking. The Extended Finite Element Method (XFEM) is being incorporated into some FEA software packages. In the future, we can expect a rapid development in nonlinear numerical simulation field. However, considering the different combinations of various materials and the

complicated material properties, accurate simulation of the large deformation and fracture

process will remain a challenge.

CHAPTER 3
DEVELOPMENT OF A NEW BINDER FRACTURE TEST

3.1 Development of Specimen Geometry by FEA

3.1.1 Reasons to Develop a New Specimen Geometry

According to previous research, fracture energy analysis based on direct tension testing can predict cracking performance at intermediate temperatures better compared to other binder tests. However, as mentioned earlier, the traditional direct tension test has some crucial deficiencies in terms of obtaining fracture energy accurately (see Chapter 1).

Accurate simulation of the deformed shape during extension is required to determine accurate stress and strain (true stress-true strain), which in turn is required for accurate determination of fracture energy. One key to achieving this is to limit the ductility or strain to failure of the asphalt specimen. Unfortunately, the relatively long middle section of the traditional direct tension test makes it difficult to apply a high enough strain rate to reduce specimen's ductility. In addition, fracture may occur anywhere along the relatively long middle section of the traditional direct tension test, making it nearly impossible to determine failure strain on the failure plane.

In conclusion, it is not possible to obtain true stress-true strain relationships, which are required to obtain fracture energy accurately, during fracture process using the traditional direct tension test. Therefore, new specimen geometry that overcomes the deficiencies of the existing direct tension test is needed to obtain fracture energy accurately.

3.1.2 Development and Optimization Process

3.1.2.1 Geometry No. 1

The geometry illustrated in Figure 3-1 was selected to more closely simulate the actual stress and strain states of asphalt binder within asphalt mixture, which leads to higher stresses and rates of loading. Results of 2-D FEA of this geometry are also illustrated in Figure 3-1.
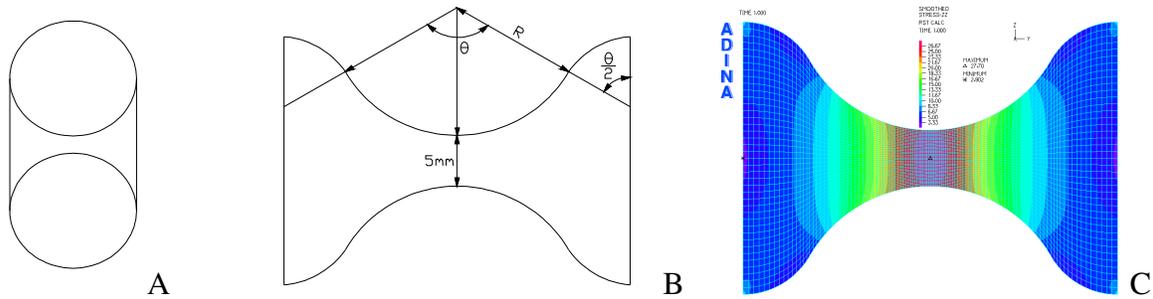
Figure 3-1 2-D FEA model. A) Simplified spheres, B) 2-D complex curves, C) Stress distribution by FEA

The highest stress concentration factor determined from the 2-D analysis was 2.05, which was not considered high enough to assure failure consistently in the central part of the specimen. Therefore, the geometry and analysis were extended to the 3-D shape shown in Figure 3-2.
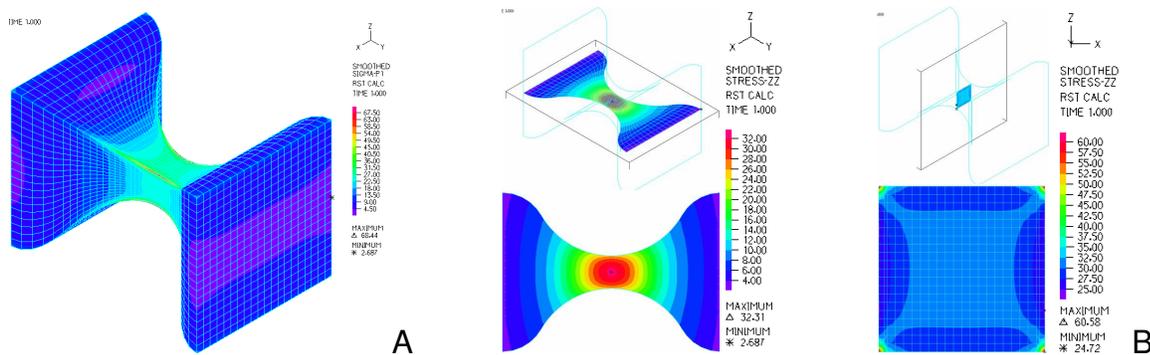
Figure 3-2 3-D FEA model. A) 3-D specimen shape, B) Stress distribution on horizontal and vertical cross-section by FEA

3-D FEA results indicated that a highly uniform, nearly isotropic stress state exists in the central narrow portion (3mm×3mm) of the specimen. Also, the tensile stresses are eleven times higher than tensile stresses near the edge (i.e., the stress concentration factor was 11; compared with 2.05 for the 2-D specimen), which helps ensure the specimen will fail first within its central

narrow region. For practical reasons (e.g., easier production of specimen and possible testing of mastics in the future), a specimen cross-section of 5mm×5mm was selected for prototype tests.

At first, an attempt was made to perform tests on the existing direct tension test machine. However, at relatively high loading rates, the tensile stress of the specimen exceeded the capacity of the DT machine, which would cause the testing system to stop. At relatively low loading rates, excessively large deformation to fracture was encountered, as shown in Figure 3-3. Development of data interpretation methods to determine true stress-true strain will be presented later in the report.
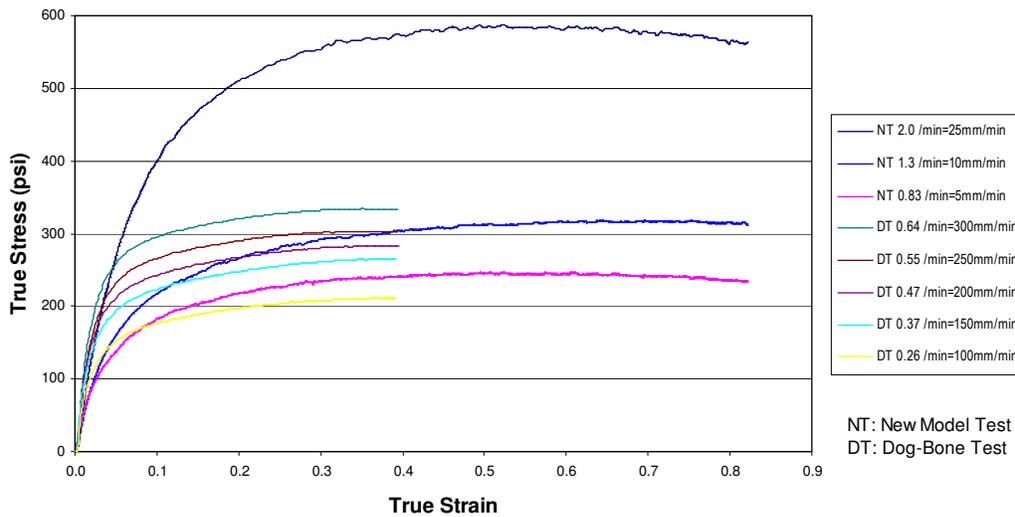
Figure 3-3 Geometry No. 1, true stress vs. true strain

As mentioned earlier, fracture at smaller deformation is preferred in order to avoid errors resulting from geometry changes that occur at very large deformations, which cannot be determined accurately. Therefore, the test was moved to a servo-hydraulic testing machine, i.e., a material test system (MTS) which can achieve high loading rates without exceeding its loading capacity.

In order to avoid any bending moment or torque caused by eccentricity, a special loading device with two guide bars and a movable load head connection was designed (Figure 3-4 A).

10
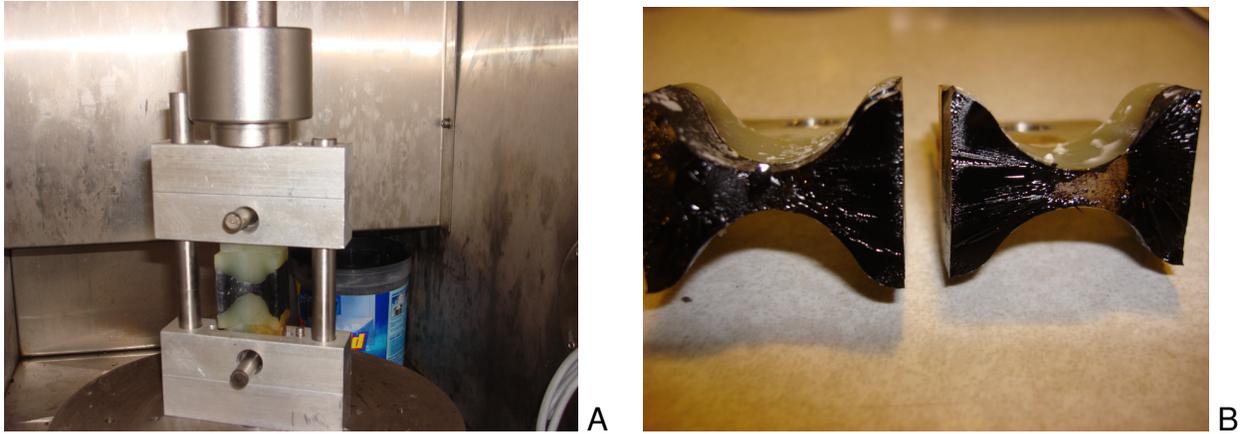
Figure 3-4 Geometry No. 1, testing on MTS. A) Asphalt pulled by the load head. B) Asphalt peeled off from the load head.

However, at 5°C, the asphalt consistently peeled off the load head (Figure 3-4 B), which showed that for this geometry, the adhesion between asphalt and load head was less than the cohesion within asphalt. Therefore, the specimen geometry had to be modified to eliminate the stress concentration on the contact surface of load head.

3.1.2.2 Geometry No. 2

In an attempt to solve the problem, concave grooves with curved chamfers were cast on both sides of the central portion of the specimen (Figure 3-5). Although this system solved the problem by making the stress concentration greater within the asphalt, this shape was considered to be too complicated for use in practice. Therefore, it was decided that a simpler geometry was needed.
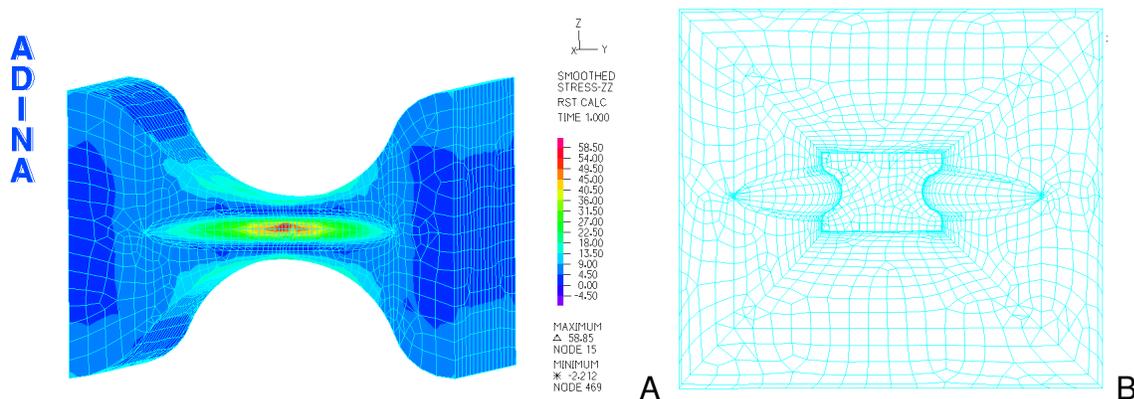
Figure 3-5 Geometry No. 2, FEA model. A) Concave on both sides. B) Vertical cross-section.

11

3.1.2.3 Geometry No. 3

The dog-bone direct tension geometry shown in Figure 3-6 was selected as a possible solution. Analyses were conducted to identify a geometry that resulted in a fairly uniform stress concentration throughout the cross-section at the center of the specimen. This geometry resulted in a stress concentration greater than 5 (relative to the stress near the loading heads), which was considered sufficient to consistently result in fracture in the central cross-section.
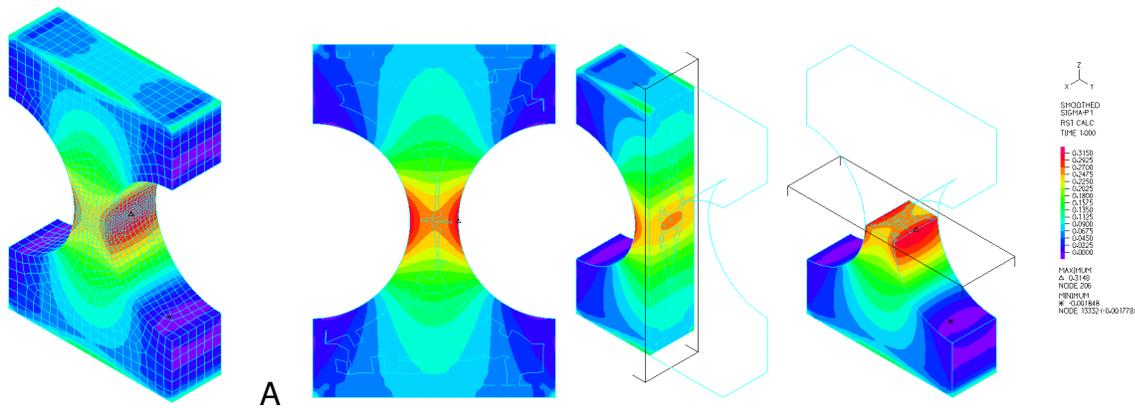
Figure 3-6 Geometry No. 3, FEA model. A) Dog-bone shape B) Stress distribution on vertical and horizontal cross section.

Preliminary tests were performed using the direct tension test machine at four loading rates (70, 100, 150, and 300 mm/min) and two temperatures (5 and 10°C) for two types of binder (unmodified PG 67-22 and styrene butadiene styrene (SBS) polymer-modified PG 76-22).

Figure 3-7 Geometry No. 3, asphalt peeled off from load head.

Unfortunately, all specimens cracked from the contact surface of load head (Figure 3-7), indicating that adhesion between asphalt and load head was still not enough to make the specimen crack in the middle.

It was also found that the extension rate of direct tension test machine (above 150 mm/min) was not accurate for SBS-modified binder PG 76-22. For programmed rates of 150 and 300 mm/min, rates of 120 and 258 mm/min were actually achieved. Therefore, the decision was made to perform the remainder of tests for this research using a servo-hydraulic loading frame. Figure 3-8 shows successful test results at two loading rates, which provided the first indication that fracture energy may be independent of loading rate.
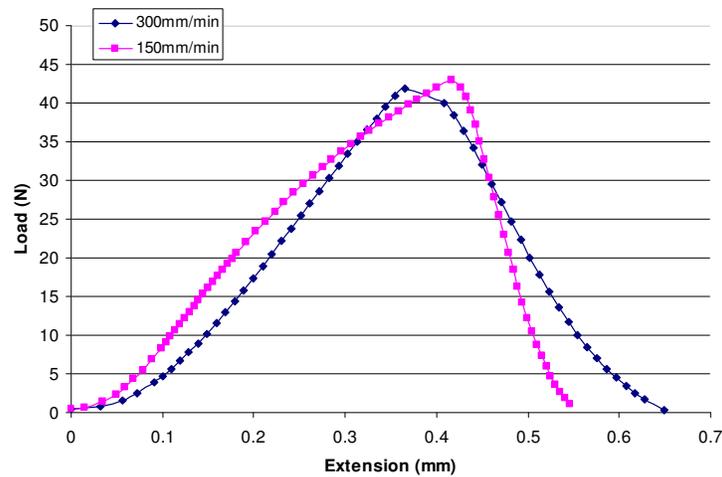
Figure 3-8 Geometry No. 3, PG 76-22, 5°C, 300 mm/min & 150 mm/min

However, most tests failed by loss of adhesion at the loading head, so there was a clear need to modify the geometry to strengthen the connection between asphalt and load head by increasing adhesion and by reducing any high stresses on the corners of load head. This led to Geometry No. 4 (Figure 3-9).

3.1.2.4 Geometry No. 4

The connection was strengthened by extending the asphalt specimen on both sides of load head, which increased adhesion (Figure 3-9). In addition, the corners of loading head were

rounded to eliminate stress concentrations caused by sharp corners, resulting in adhesive failure. Preliminary tests showed that the use of the new geometry (No. 4) effectively eliminated the adhesive failure and resulted in proper fracture occurred in the center. Figure 3-10 shows the final dimensions of Geometry No. 4.
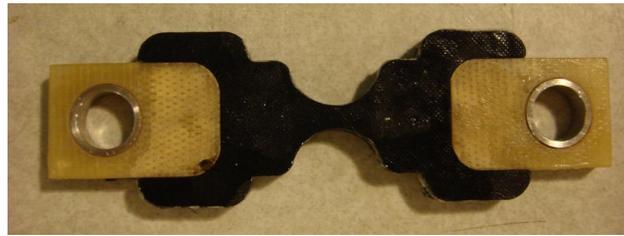
Figure 3-9 Geometry No. 4
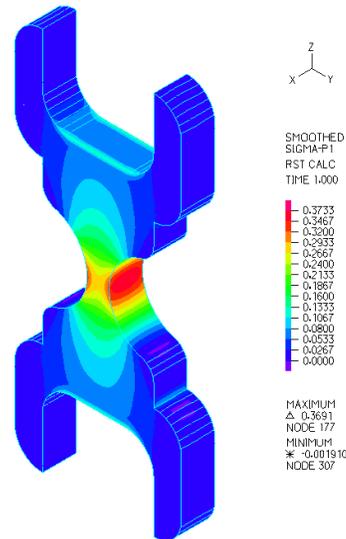
Figure 3-10 Dimensions of Geometry No. 4

FEA results presented in Figure 3-11 show that a relatively uniform stress distribution develops in the central cross section. Also, the stress concentration on the contact surface of load head has been eliminated.

The specimens were prepared by molds shown in Figure 3-12.
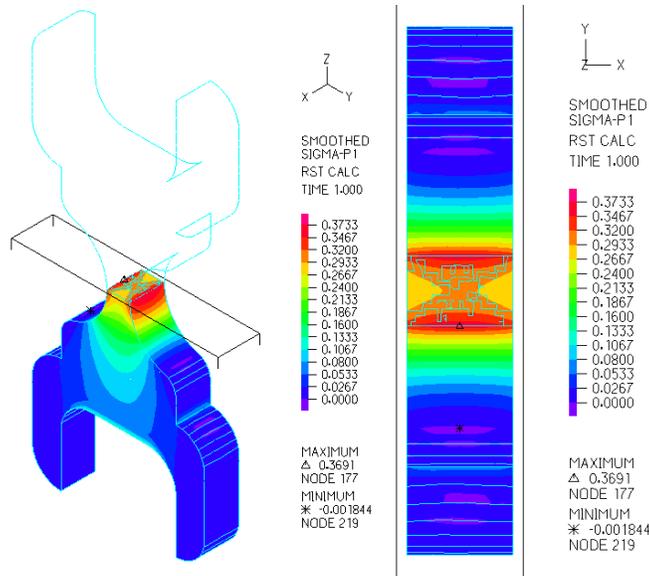
Figure 3-11 Stress distribution on horizontal cross-section by FEA
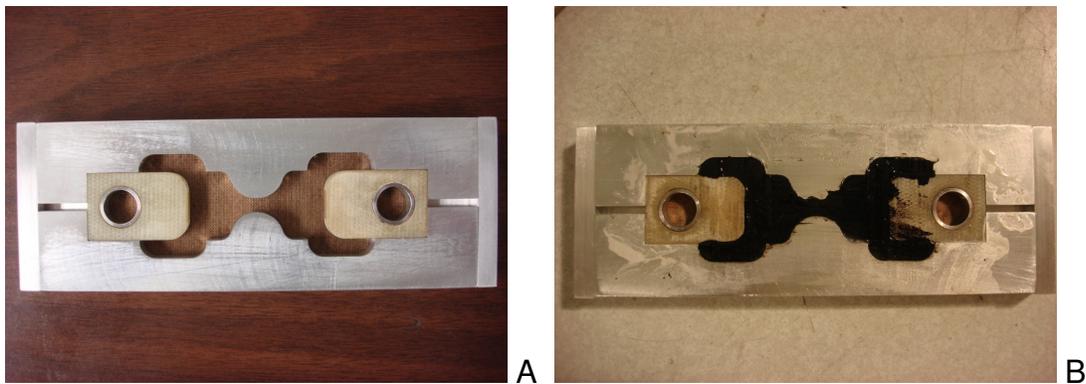
Figure 3-12 Preparation of specimen. A) mold. B) specimen in the mold.

As mentioned earlier, a special device consisting of two guide bars and a movable load

head connection was designed and installed to mitigate potential errors resulting from eccentric

loading (Figure 3-13).
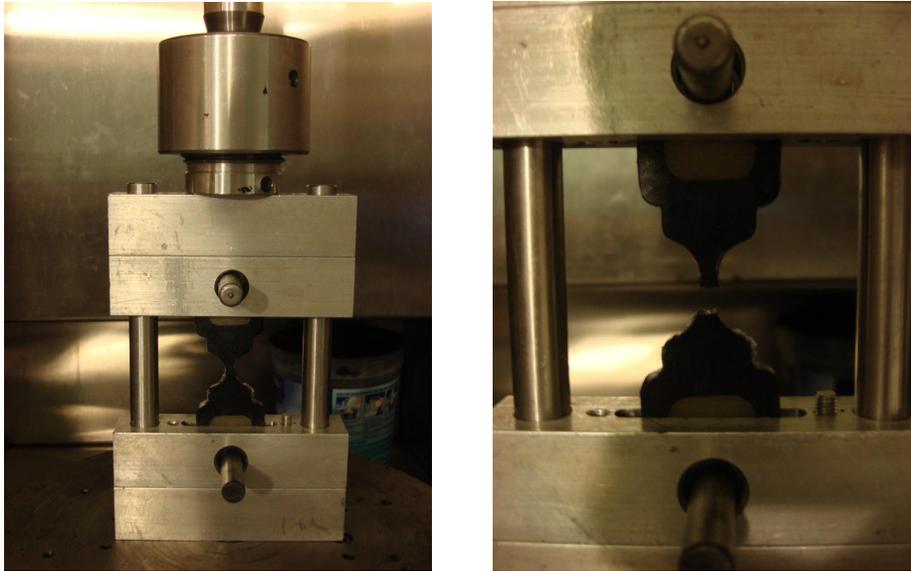
Figure 3-13 New DT testing equipment on MTS

Figure 3-14 shows typical fractured specimens for unmodified PG-67-22 binder and SBS-modified PG 76-22 binder. It is clear, particularly at lower loading rates, that the SBS-modified binder exhibited greater ductility.

Geometry No. 4 was finally selected as the optimal specimen configuration.
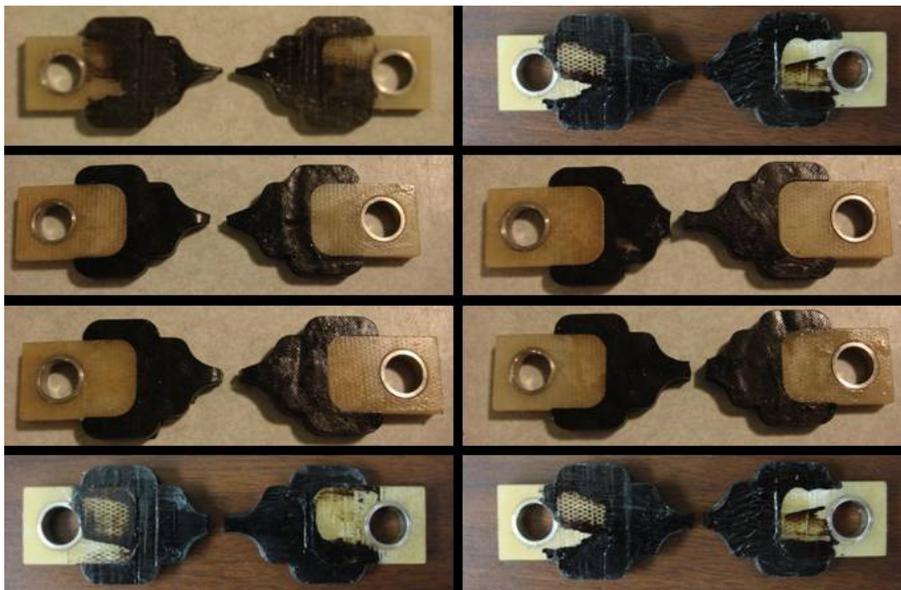
SBS-Modified Binder PG 76-22   Unmodified Binder PG 67-22

Figure 3-14 Fracture of specimens

3.2 Data Interpretation

3.2.1 Premature Failure Identification

At low temperatures and/or faster loading rates, any imperfection (flaw) of specimen may result in premature failure. These specimens do not crack at the exact center, which leads to erroneous test results that must be identified and discarded. In most cases it was relatively easy to identify premature fracture based on the geometric characteristics of the fractured specimen, the true stress-true strain curve and resulting fracture energy (Figure 3-15). The fracture energy of specimens that fail prematurely is dramatically lower (close to zero), compared to specimens that did not fail prematurely. However, in addition to this intuitive evidence, premature fracture can be consistently identified by the occurrence of an incomplete true stress-true strain curve. Details of how to do this are provided later in the report.

These results also implied that there is an optimal combination of temperature and loading rate range to consistently obtain fracture energy of binder; in other words, loading rates at which small imperfections do not result in premature fracture.

Proper Fracture   Premature Fracture
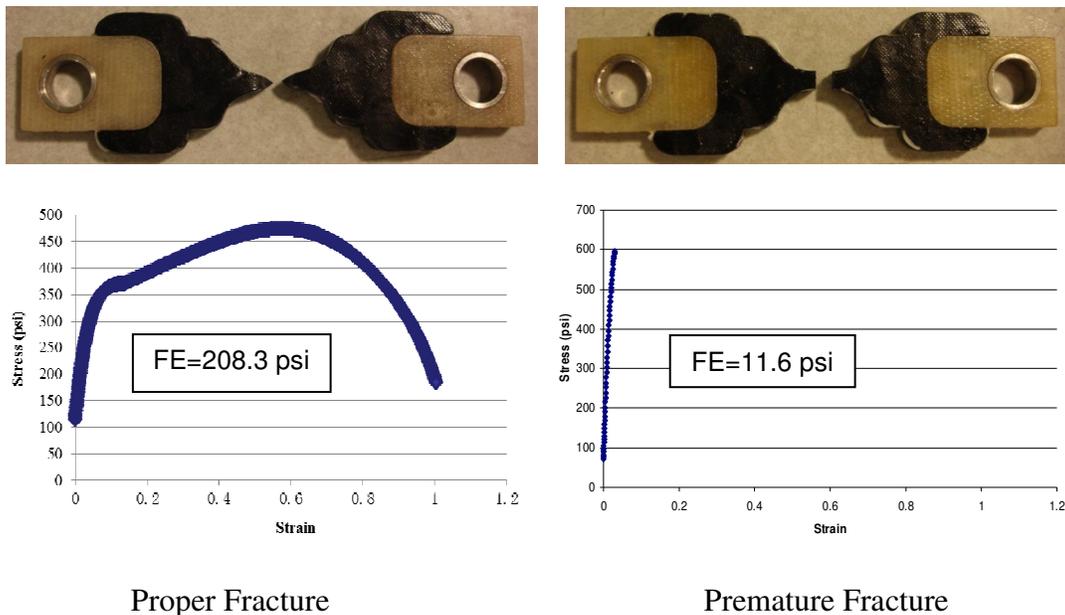
Figure 3-15 Identification of premature fracture

3.2.2 Calculation Procedure for Fracture Energy

The measured test results are in the form of force versus displacement. In order to accurately calculate fracture energy of binder, measured force must be transformed to average true stress and measured displacement must be transformed to average true strain in the central cross-sectional area of the specimen where fracture initiates and propagates. Therefore, actually this fracture energy is surface energy. Nonlinear FEA can be used to accomplish this up to a certain level of deformation, however, ductile cracks clearly exhibit necking because of larger deformation to failure, and FEA is not adequate to simulate this type of failure accurately even with large strain formulation. Accurate calculation would require knowledge of properties for each binder that is not available from common binder tests.

Therefore, a new data analysis procedure was developed to adjust the smaller strain FEA solutions by accounting for necking that occurs at larger deformations. The following steps are involved in the data analysis:

1. Transform measured force vs. displacement to average true stress vs. average true strain in the central cross-sectional area of the specimen using nonlinear FEA with large strain formulation (see Figures 3-16 and 3-17).

2. Plot the true stress-true strain curve transformed by FEA in Step 1.

3. Up to the first stress peak, the FEA true stress-true strain results may be taken as accurate and used as the true stress and true strain response.

True Strain(average on middle cross-section) vs. Extension

$$y = -4.86178401x^6 + 5.38784242x^5 - 1.83753292x^4 + 0.44188713x^3 + 0.24726061x^2 + 1.38315414x - 0.00000142$$
$$R^2 = 1.00000000$$
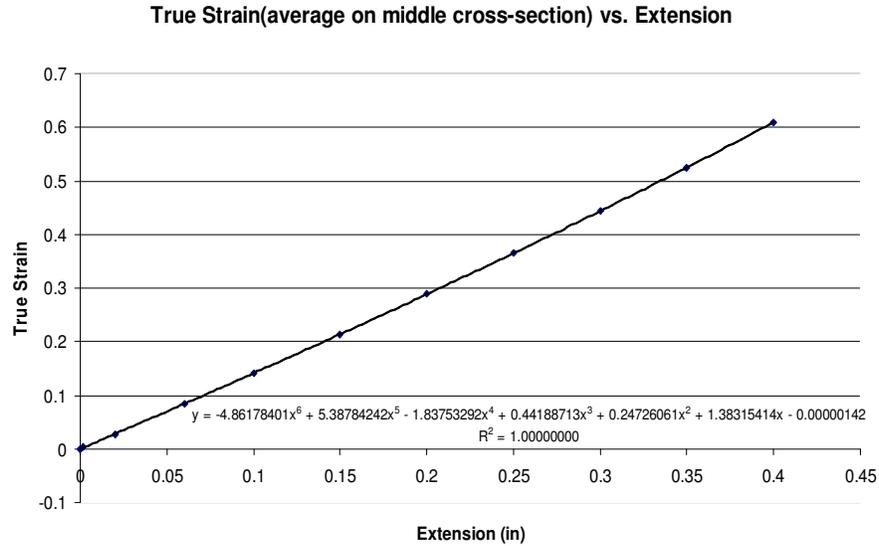
Figure 3-16 FEA results for transforming displacement to true strain

Average Stress on Middle Cross-Section / Load vs. Extension

$$y = 355.31994057x^6 - 336.69341655x^5 + 132.88607987x^4 - 10.33097936x^3 + 23.15689960x^2 + 27.93221846x + 26.67485395$$
$$R^2 = 1.00000006$$
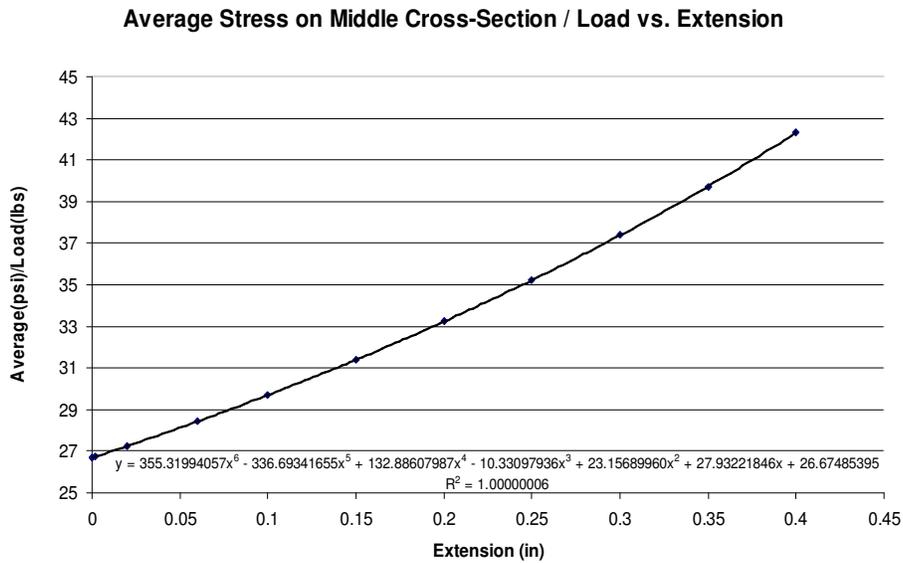
Figure 3-17 FEA results for transforming force to true stress

4. After the first stress peak, we can approximately think that only necking develops in the middle section of specimen, therefore the extension of middle necking part is equal to measured displacement. So after the first stress peak, we only need to take out the middle necking part to calculate its true strain. Based on specimen dimensions and observations

19

during testing, the initial length of the section undergoing necking is about 3mm (Figure 3-18 A), and it is elongated to L_1 at the first stress peak (Figure 3-18 B), and then it undergoes necking (Figure 3-18 C).
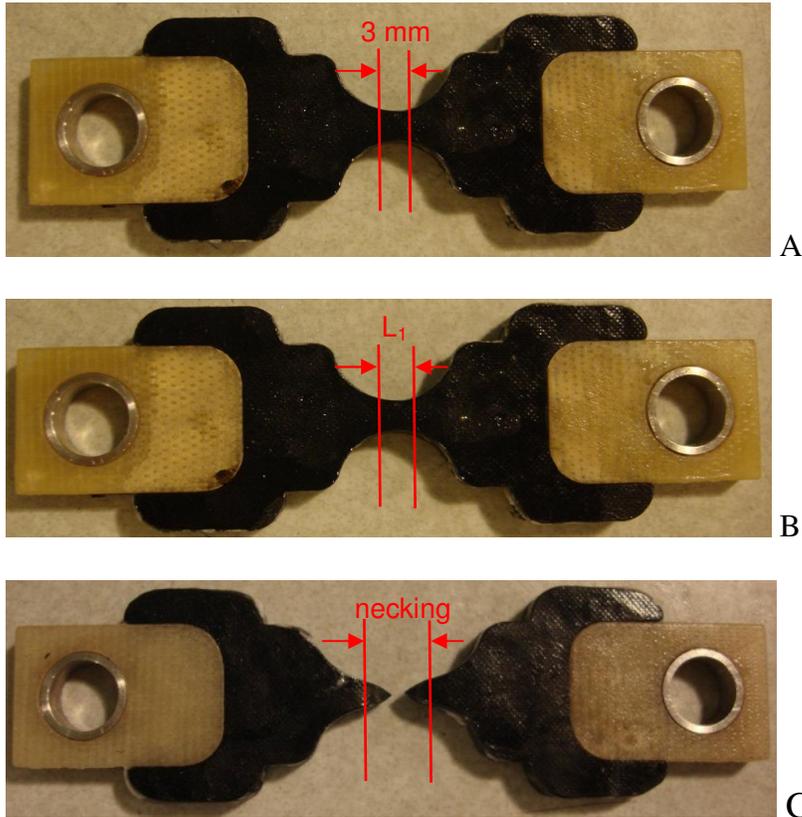
Figure 3-18 3mm necking section: A) 3mm before test, B) 3mm is elongated to L_1 at the first stress peak, and C) L_1 is further elongated and undergoes necking

At the first stress peak, the central cross-sectional area A_1 and length L_1 of the initial 3mm middle part can be obtained using nonlinear FEA with large strain formulation (see Figures 3-19 and 3-20).

Length of 3mm Middle Part vs. Extension

$y = -0.40296955x^6 + 0.50107221x^5 - 0.06773753x^4 + 0.08619530x^3 + 0.15119509x^2 + 0.14159203x + 0.11811010$

$R^2 = 0.99999997$
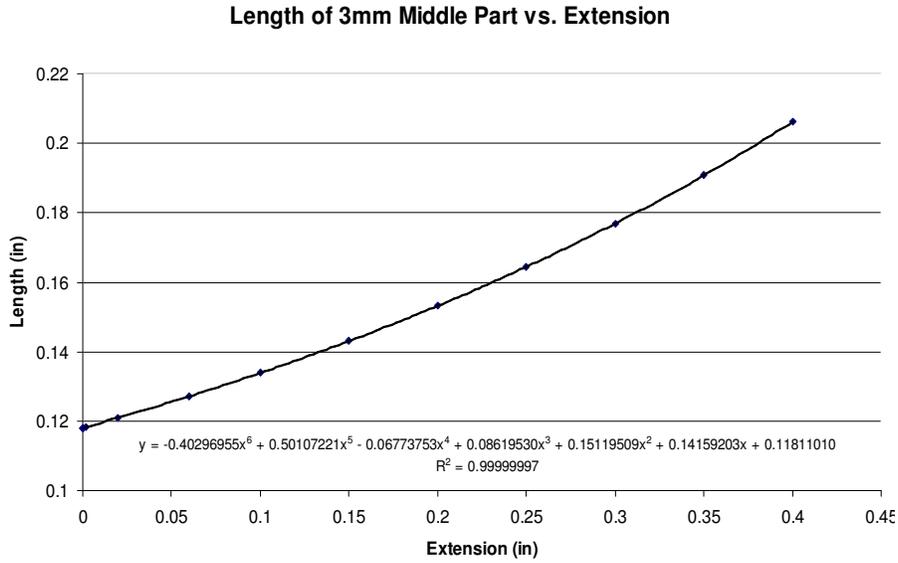
Figure 3-19 FEA results for calculating length L_1 of the initial 3 mm middle part at the first stress peak

Area of Middle Cross-Section vs. Extension

$y = -9.73348713x^6 + 12.42876978x^5 - 6.10014164x^4 + 1.43623070x^3 - 0.15211610x^2 - 0.03141237x + 0.03739017$

$R^2 = 0.99979994$
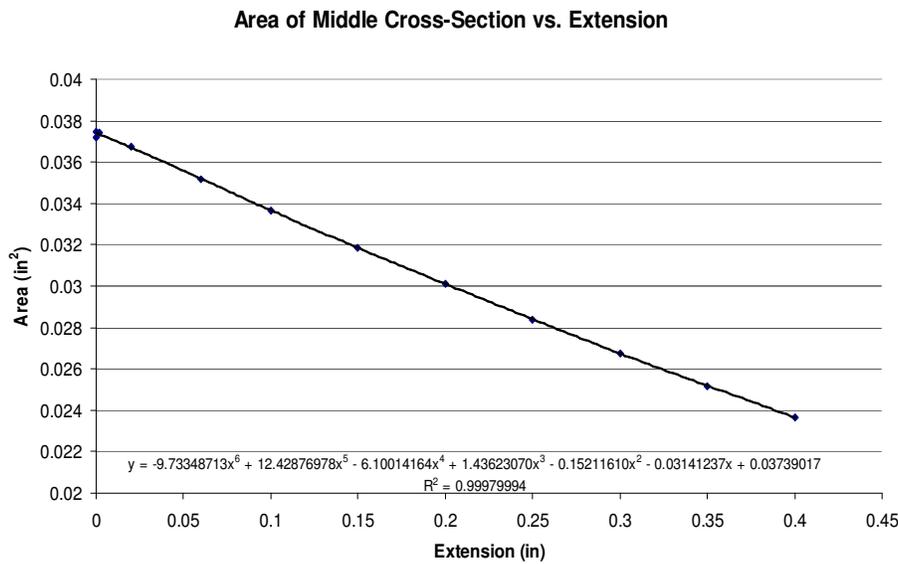
Figure 3-20 FEA results for calculating central cross-sectional area A_1 at the first stress peak

Then we take out the middle part and calculate its deformation after the first stress peak (Figure 3-21).
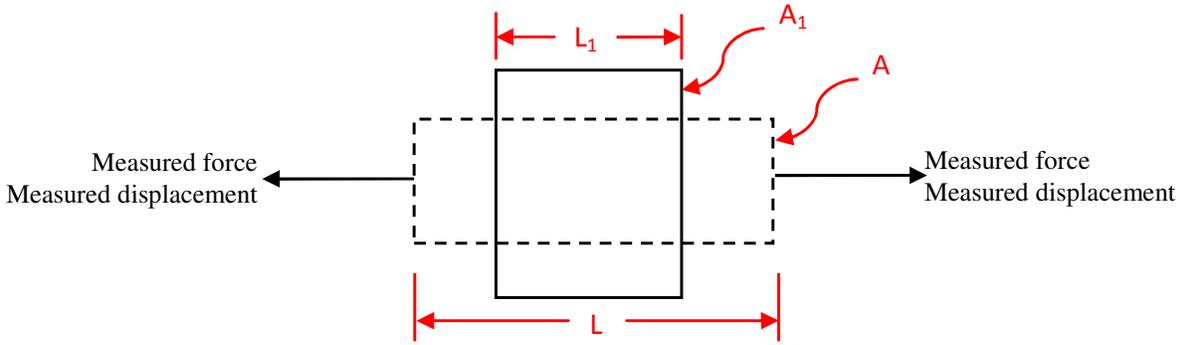
Figure 3-21 Deformation of the middle part after the first stress peak

Since poisson's ratio of asphalt binder is usually very high, we can assume that the volume of middle part is a constant during extension. So, Equation (3-1) is obtained by which we can calculate cross-sectional area A after the first stress peak.

$$A \cdot L = A_1 \cdot L_1$$
$$\Rightarrow A = A_1 \cdot \frac{L_1}{L} \tag{3-1}$$

Where:

A_1 – central cross-sectional area at the first stress peak
A – central cross-sectional area after the first stress peak
L_1 – length of initial 3 mm middle part at the first stress peak
L – length of initial 3 mm middle part after the first stress peak

Now we can calculate true stress after the first stress peak with the equation below,

$$\sigma = \frac{F}{A}$$
$$= \frac{F}{A_1 \cdot \frac{L_1}{L}} \tag{3-2}$$

Where:

σ – average true stress on central cross-sectional area after the first stress peak
F – measured force
A_1, A, L_1, and L are the same as defined previously

22

The true strain after the first stress peak can be calculated with the large strain formulation below.

$$\varepsilon = \ln\frac{L}{L_1} \tag{3-3}$$

Where:

ε – true strain after the first stress peak
L_1 and L are the same as defined previously

As shown in Figure 3-22, after applying the new calculation method, the point of initial fracture is very clear. The post-peak energy after the point of initial fracture should not be considered when calculating fracture energy, as this is the energy required to split the specimen in half, rather than the energy to initiate fracture in the binder. Fracture energy should be calculated from the beginning of true stress-true strain curve to the last stress peak which is the point of initial fracture. We will discuss this issue further in Chapter 5 "Characteristic True Stress-True Strain Curves".

A   B
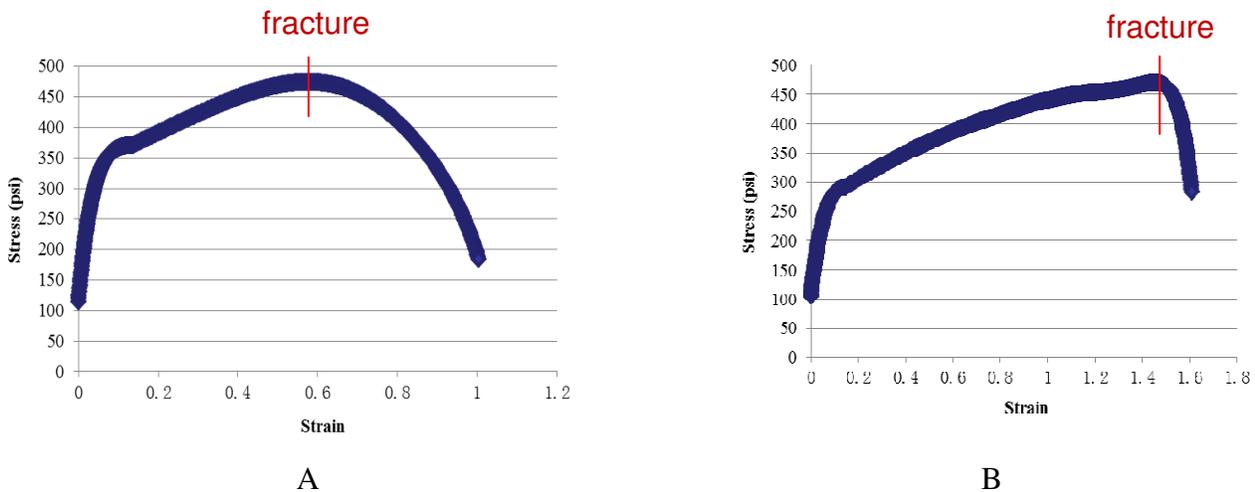
Figure 3-22 True stress-true strain curve by new calculation procedure. A) PG 67-22, 10°C, 400 mm/min, B) PG 76-22, 10°C, 400mm/min

CHAPTER 4
TESTS AND ANALYSES ON A RANGE OF BINDERS

4.1 Materials

The primary purpose of this research is to develop a test to accurately measure fracture energy of binders at intermediate temperatures. Therefore, a wide range of binders was selected to verify the effectiveness of a new direct tension test developed for this purpose. A total of twelve types of binder, including unmodified binders, SBS-modified binders, rubber-modified binders and hybrid binders were tested and analyzed. Both pressure aging vessel (PAV) residue and recovered binders were prepared. The binders and their components, as provided to the research team, are listed in Table 4-1.

Table 4-1 Binders and the constituents/formulations

Binder	Modifying Components
PG 67-22	None (graded as a PG 69.78-26.50)
PG 64-22	None
AC-30	None
AC-20	None
PG 76-22	4.25% SBS (graded as a PG 76.7-27.16)
PG 82-22	8.5% SBS
Geotech	1% SBS (approximately 30 mesh, incorporated dry), 8% of Type B ground tire rubber (GTR), and 1% hydrocarbon
Hudson	3.5% crumb rubber, 2.5% SBS, and 0.4%-plus Link PT-743 cross-linking agent
Wright	GTR (digested rubber) and SBS. Unknown contents.
Marianni	Unclear. Maybe 13% GTR. Its true stress-true strain curve indicated that it may contain polymer.
ARB-5	5% Type B rubber
ARB-12	12% Type B rubber

<center>**4.2 Preliminary Tests**</center>

Preliminary tests were performed in order to evaluate the new direct tension test and identify optimal test conditions and appropriate test procedures.

4.2.1 Binders and Testing Conditions

Binder types. All the binders were PAV residues: one type of SBS polymer-modified binder, PG 76-22 (4.25% SBS), and one type of unmodified binder, PG 67-22.

Test temperatures. The following test temperatures were used: 0, 5, 10, 15, and 20°C. At 20°C, specimens became too soft to obtain fracture energy accurately.

Loading rates. Various loading rates were used depending on test temperature in order to avoid premature fracture.

4.2.2 Test Results and Analysis

Test results are shown in Figures 4-1 through 4-6.

4.2.2.1 15°C

As shown in Figure 4-1, the fracture energy density was very consistent for the same binder at different loading rates, and the difference between modified and unmodified binder was very clear. Although, as indicated below, similar trends were observed at other intermediate test temperatures, the least variability and least number of premature failures were observed at 15°C. Therefore, this appeared to be the optimal temperature for determination of fracture energy of the majority of binders and conditions evaluated.

<center>25</center>
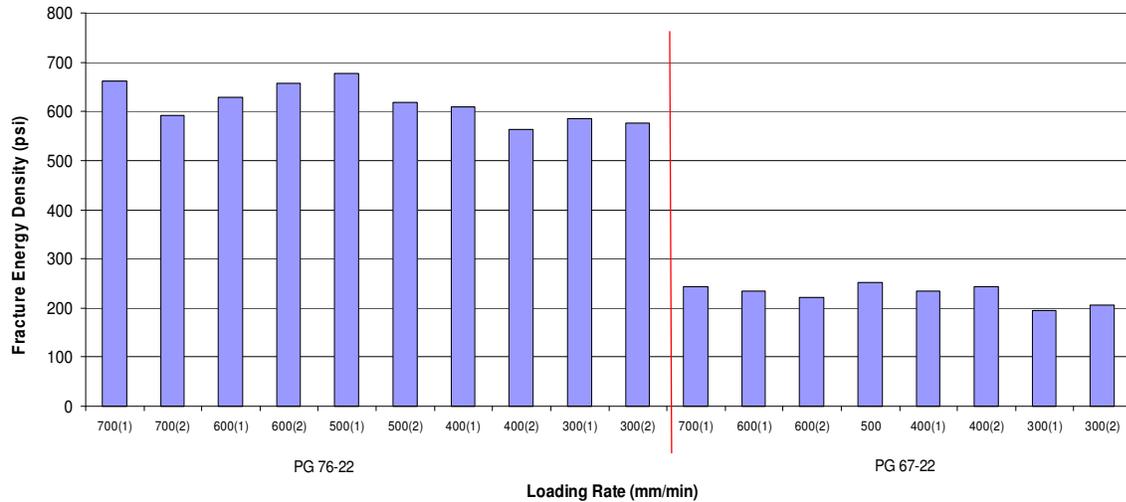
Figure 4-1 Fracture energy (FE) density at 15°C

4.2.2.2 10°C

As shown in Figure 4-2, greater variability in test results was observed at 10°C than at 15°C. As discussed earlier, premature failure is more likely to occur at lower temperatures. However, the fracture energy density was still relatively consistent at different loading rates, and its magnitude was very close that determined at other temperatures. The difference between modified and unmodified binder remained very clear.
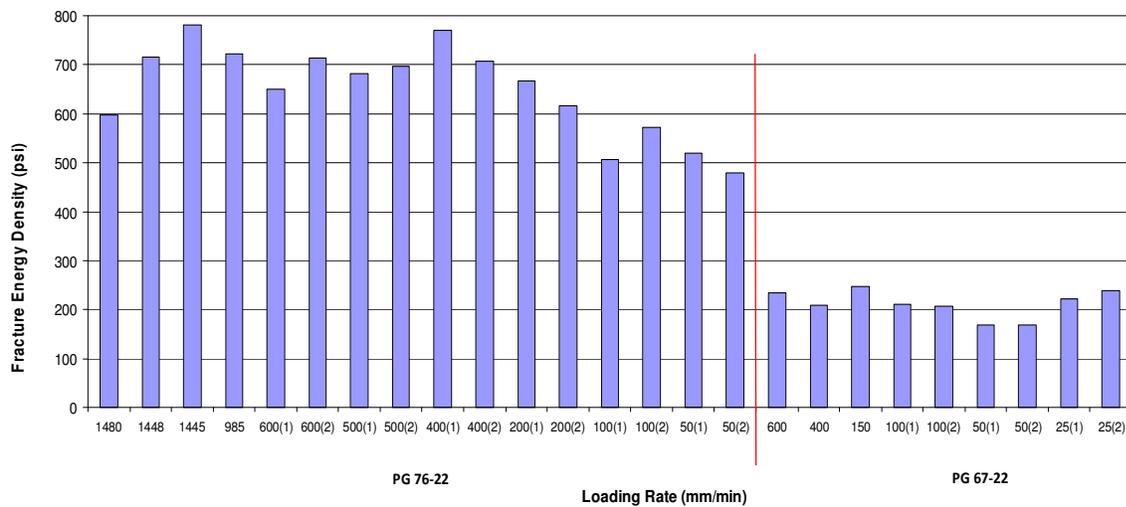
Figure 4-2 Fracture energy density at 10°C

4.2.2.3 5°C

As shown in Figure 4-3, greater variability in test results was also observed at 5°C than at 15°C. Once again, premature failure is more likely to occur at lower temperatures. However, the fracture energy density was still relatively consistent at different loading rates, and its magnitude was very close that determined at other temperatures. Also, the difference between modified and unmodified binder remained very clear. Figure 4-3 also illustrates how excessively slow loading rates (e.g., lower than 10 mm/min for unmodified binder) results in under-prediction of fracture energy. These tests clearly exhibited excessive deformation where the cross-section became needle-like prior to fracture. Figure 4-4, which shows the results at 5°C without these loading rates, illustrates how the fracture energy values are very consistent with results obtained at 10 and 15°C.
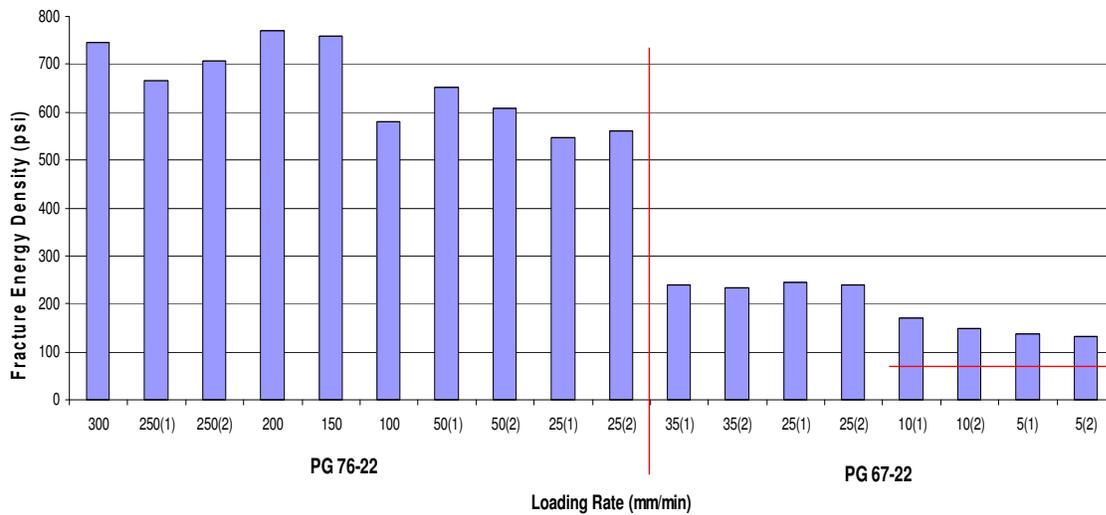
Figure 4-3 Fracture energy density at 5°C
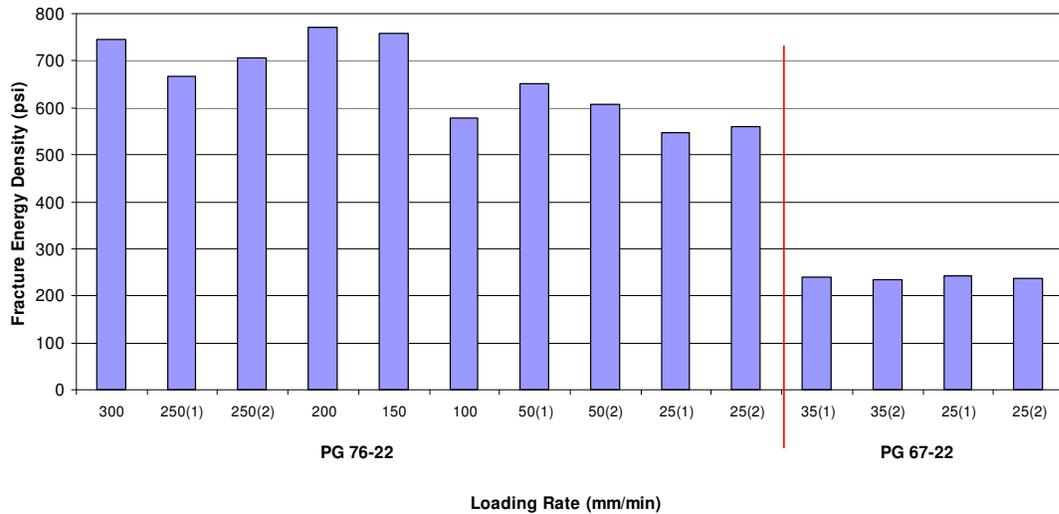
Figure 4-4 Fracture energy density at 5°C (without loading rates ≤ 10 mm/min)

4.2.2.4 0°C

At 0°C, all PG 67-22 specimens failed prematurely. Therefore, only PG 76-22 results are presented in Figure 4-5 for 0°C.

As shown in Figure 4-5, under-prediction of fracture energy was also observed at loading rates of 10 mm/min or less at 0°C. Figure 4-6, which shows the results at 0°C without 10 mm/min, the fracture energy density was consistent at different loading rates, and was also consistent with those tested at other temperatures. Figure 4-6 illustrates that the fracture energy density can also be over-predicted if excessively high loading rates are used (in this case, 100 mm/min). This may be a result of differences in cross-sectional area and length of specimens at failure and how these differences affect the calculation of true stress-true strain.
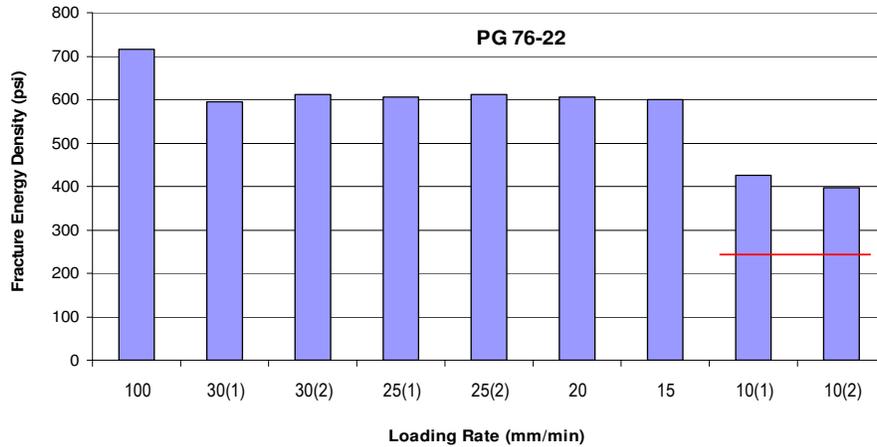
Figure 4-5 Fracture energy density at 0°C
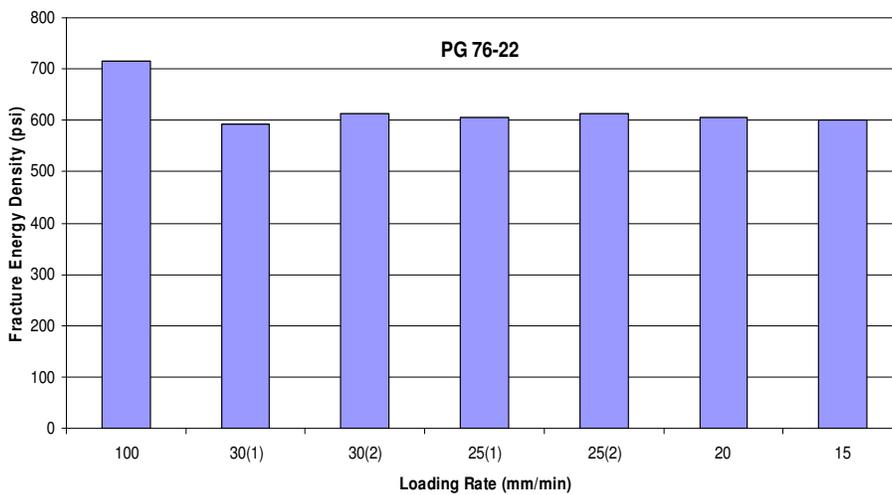
Figure 4-6 Fracture energy density at 0°C (without loading rates ≤ 10 mm/min)

To summarize all results, the average fracture energy density of the same binder at each temperature was plotted in Figure 4-7, which shows the average fracture energy at each temperature is very consistent for PG 76-22 and PG 67-22. Also, the difference between PG 76-22 and PG 67-22 is very clear. These results indicate that binder fracture energy is independent of temperature, and the proposed new DT test is able to capture the expected trend of fracture

29

energy between unmodified and SBS-modified binders. A detailed statistical analysis to support these findings is provided in Appendix D.
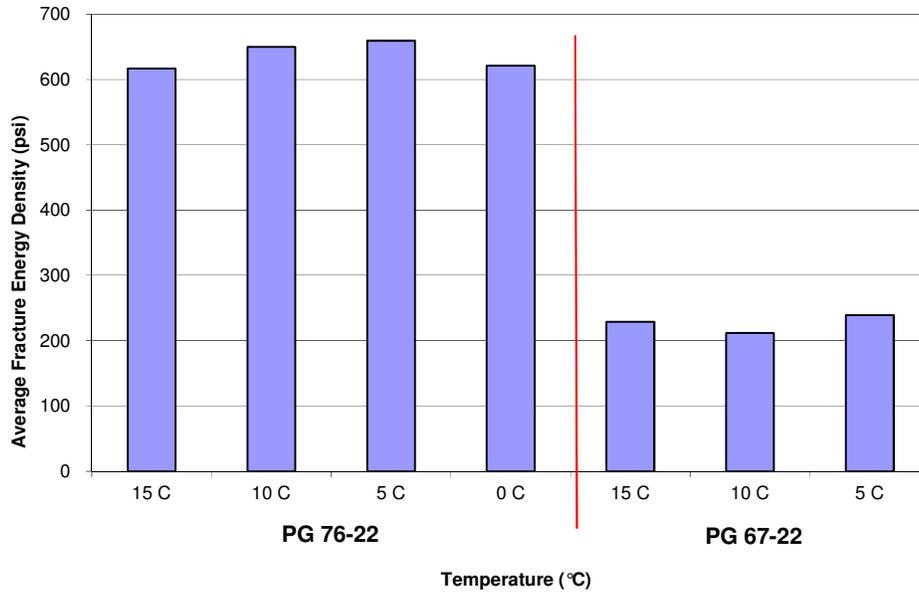
Figure 4-7 Average fracture energy density at each temperature

Figure 4-8 shows that the lower the loading rate, the higher the deformation at fracture. The significant difference in deformation at fracture indicates that the shape of the deformed section may be different at different loading rates, which may in turn affect the accuracy of the large strain formula used to determine true strain. The initial length subjected to large deformation is always taken to be 3 mm, but the actual length may be different depending on total deformation to failure. This implies that there is an optimal or acceptable loading rate range within which tests should be performed to obtain fracture energy consistently and accurately.

In summary, the new direct tension test can differentiate between the polymer-modified PG 76-22 and the neat binder PG 67-22 clearly. At 15°C, the measured fracture energy is very consistent for the same binder at different loading rates. Thus, 15°C appears to be the optimal test temperature for these types of binder. The appropriate loading rate should not allow

specimens to deform excessively or to fracture prematurely, which may result in inaccurate

fracture energy. Further results will be shown later regarding the other binders tested.
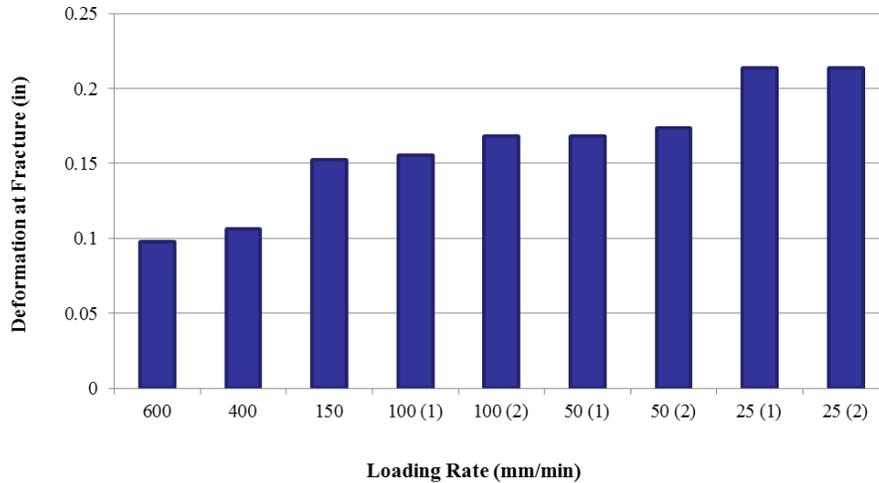
Figure 4-8 PG 67-22 at 10°C, deformation at fracture vs. loading rate.

4.3 Tests on Binders Recovered from Superpave Sections

The new direct tension test system was performed on a range of binders recovered from the

Superpave Monitoring Project (BDK 75-977-06). These 12 Superpave Monitoring Projects each

included two layers of asphalt mixture encompassing a broad range of binders. All binders were

recovered by FDOT. In total, more than 200 out of the several hundred tests were successful

(i.e., they resulted in proper fracture as opposed to premature fracture and excessive

deformation).

4.3.1 Binders and Testing Conditions

Binder types. As mentioned above, all binders were recovered from asphalt mixture of 12

Superpave Monitoring Projects. These included:

3 types of unmodified binders: AC-30, AC-20, PG 64-22

1 type of SBS polymer-modified binder: PG 76-22

1 type of rubber-modified binder: ARB-5

31

Test temperature. All tests were conducted at 15°C since prior work indicated that this was the optimal temperature to obtain fracture energy consistently.

Loading rates. Various loading rates were used depending on the property of individual binders in order to avoid both premature fracture, which results in erroneous results, and excessive deformation at fracture, which results in the underestimation of fracture energy.

4.3.2 Test Results and Analysis

Test results for two locations for one Superpave test section (i.e., Project One) are shown in Tables 4-2 and 4-3, respectively. A complete set of test results for the Superpave Projects are presented in Appendix B.

Each type of binder was tested at multiple loading rates. For binders with replicate specimens, the tested fracture energy of the same type of binder was averaged at the same loading rate. Then, the fracture energy vs. loading rate was plotted for each type of binder to show the influence of loading rate on fracture energy.

4.3.2.1 Recovered PG 76-22

Since recovered PG 76-22 had replicate specimens, its averaged fracture energy density at each loading rate is shown in Figure 4-9. From Figure 4-9, we can see that generally, the fracture energy of PG 76-22 is consistent at various loading rates. The loading rate didn't influence the fracture energy significantly. A further statistical analysis to prove this point is provided in Appendix D.1.2.

On the other hand, the values presented in Tables 4-2 and 4-3 indicate that for binders recovered from Superpave sections, the variance of tested fracture energy of the same binder in different conditions (location, layer, etc.) is greater than that of PAV residues. This makes sense because age-hardening of binder in mixtures in the field is a much more complex phenomenon

32

than age-hardening in the laboratory, i.e., the same binder type will age differently in different

mixtures and at different depths within the pavement.
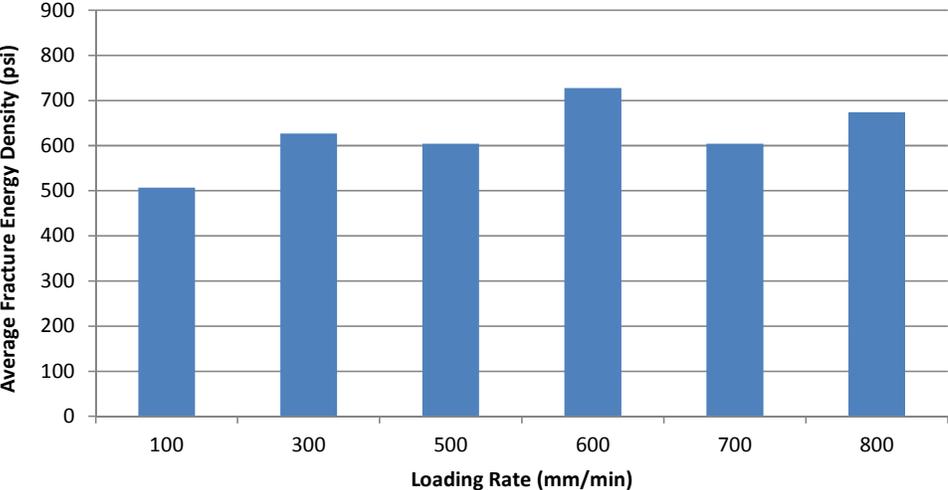
Figure 4-9 PG 76-22 recovered, fracture energy vs. loading rate

Table 4-2 Test results of binders recovered from Superpave Project 1 at Location 5 (box 1)

| Box No. 1 | | | | SMO Lab No. | Binder Type | Fracture Energy Density @ 15°C | | |
Project	Location	Layer	Source			Loading Rate (mm/min)	FE Density (psi)	Extension (in)
1	5	A	WP	19234	AC-30	300	354.82	0.1827
					AC-30	500	373.63	0.1693
			BWP	19235	AC-30	500	374.21	0.1530
					AC-30	500	345.66	0.1507
		B	WP	19236	AC-30	500	313.02	0.1877
					AC-30	500	316.01	0.1828
			BWP	19237	AC-30	500	341.04	0.1871
					AC-30	500	324.73	0.1856

Note: WP and BWP denote wheel path and between wheel path, respectively.

Table 4-3 Test results of binders recovered from Superpave Project 1 at Location 15 (box 2)

| Box No. 2 | | | | SMO Lab No. | Binder Type | Fracture Energy Density @ 15°C | | |
Project	Location	Layer	Source			Loading Rate (mm/min)	FE Density (psi)	Extension (in)
1	15	A	WP	19238	AC-30	500	406.01	0.1615
					AC-30	500	400.87	0.1499
			BWP	19239	AC-30	500	371.94	0.1658
					AC-30	500	376.52	0.1745
		B	WP	19240	AC-30	500	321.51	0.1908
					AC-30	500	283.12	0.1762
			BWP	19241	AC-30	500	348.64	0.1815
					AC-30	500	331.02	0.1903

4.3.2.2 Recovered AC-20

Test results of AC-20 are listed in Table 4-4. Because of the various aging levels resulting from the complicated field conditions such as different locations, mixtures and depths, etc., the engineering characteristics of AC-20 specimens is quite different. For example, some were soft and ductile, while others were stiff and brittle. Therefore, the appropriate loading rate for different AC-20 specimens varied greatly (Table 4-4). For the same reason, the extension to fracture was also variable. For different AC-20 specimens, a lower loading rate didn't necessarily result in a longer extension to fracture.

However, the fracture energy of different AC-20 specimens remained close regardless of the loading rate and extension to fracture. This can be seen in both Table 4-4 and Figure 4-10.

Table 4-4 Test results of AC-20

SMO Lab No.	Binder	Loading Rate (mm/min)	Fracture Energy Density (psi)	Extension to Fracture (in)
19242	AC-20	500	275.85	0.1686
	AC-20	700	306.48	0.1712
19243	AC-20	500	249.98	0.1896
	AC-20	500	271.33	0.2074
19244	AC-20	500	268.67	0.2014
	AC-20	500	272.02	0.1999
19245	AC-20	500	288.01	0.2084
	AC-20	500	284.45	0.2001
19246	AC-20	500	337.11	0.1978
	AC-20	500	316.71	0.1819
19247	AC-20	500	266.64	0.1952
	AC-20	500	297.24	0.1994
19248	AC-20	500	256.31	0.2171
	AC-20	500	234.13	0.2153
19249	AC-20	500	231.44	0.2223
	AC-20	500	243.92	0.2134
19250	AC-20	500	249.17	0.2214
	AC-20	500	253.2	0.2169

Table 4-4 (Continued)

SMO Lab No.	Binder	Loading Rate (mm/min)	Fracture Energy Density (psi)	Extension to Fracture (in)
19251	AC-20	500	274.9	0.2184
	AC-20	500	244.38	0.2175
19252	AC-20	500	220.76	0.2131
	AC-20	500	228.14	0.2122
19253	AC-20	500	258.22	0.2138
	AC-20	500	233.79	0.2123
20368	AC-20	800	284.93	0.1488
	AC-20	800	300.4	0.1507
20369	AC-20	800	283.07	0.1318
	AC-20	800	302.73	0.1332
20370	AC-20	800	276.92	0.1483
	AC-20	1000	263.34	0.1424
20371	AC-20	1000	256.69	0.1457
	AC-20	–	–	–
20372	AC-20	1000	290.47	0.1293
	AC-20	1000	288.45	0.1289
20373	AC-20	1000	277.09	0.1133
	AC-20	1000	275.36	0.1137
20374	AC-20	1000	263.55	0.1436
	AC-20	1000	253.29	0.1482
20375	AC-20	1000	330.95	0.095
	AC-20	1000	301.99	0.0966
20468	AC-20	600	265.22	0.1311
	AC-20	500	264.7	0.147
20469	AC-20	500	282.02	0.1184
	AC-20	–	–	–
20470	AC-20	600	240.69	0.1529
	AC-20	800	252.1	0.1411
20471	AC-20	900	267.07	0.1374
	AC-20	1200	247.42	0.1273
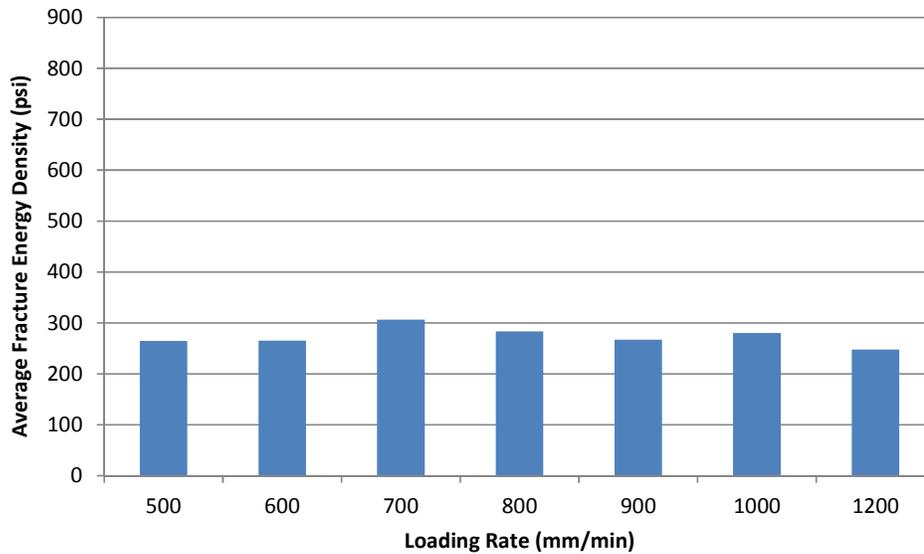
Figure 4-10 AC-20 recovered, fracture energy vs. loading rate

The recovered AC-20 also had replicate specimens. The averaged fracture energy density at each loading rate level was plotted in Figure 4-10, which shows that fracture energy of AC-20 was very consistent at different loading rates. The loading rate had no influence on the fracture energy. A further statistical analysis (see Appendix D.1.2) was performed to verify the effect of loading rate on fracture energy for AC-20.

The variance of AC-20 is clearly less than that of recovered PG 76-22. Actually, we will repeatedly see the relatively low variance of unmodified binders compared to some modified binders. This makes sense since the environment in field is complicated, and may have much influence on modifiers such as polymer and rubber by aging or other effects, which will affect the fracture resistance performance of modified binders. In different locations and layers, this influence on modifiers may be different, which results in the variance in fracture energy.

However, it is clear that fracture energy of AC-20 was lower than that of recovered PG 76-22, which means the new direct tension test effectively distinguished between these two types of binder.

37

4.3.2.3 Recovered AC-30

The appropriate loading rate for different AC-30 specimens did not vary as greatly as that of AC-20. Only three loading rate levels were used for numerous AC-30 specimens.
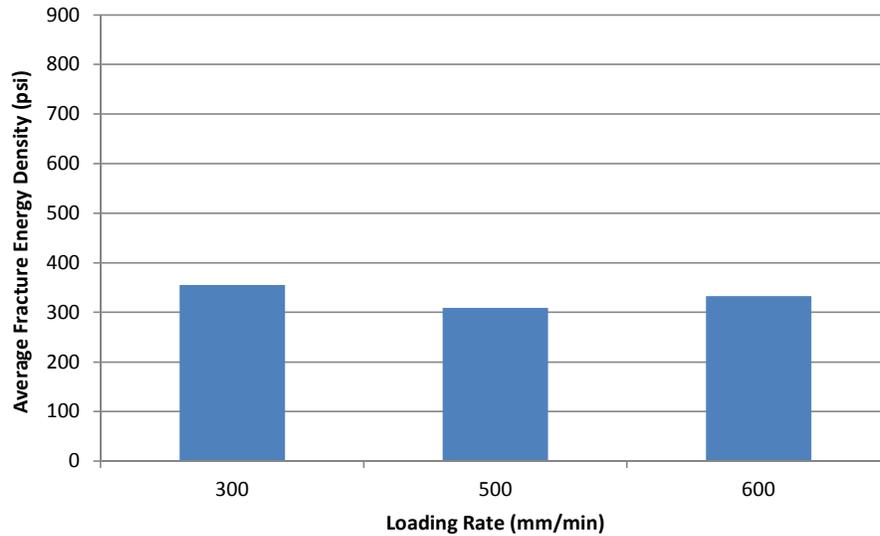
Figure 4-11 AC-30 recovered, fracture energy vs. loading rate

The average fracture energy density at each loading rate level was plotted in Figure 4-11, which shows the fracture energy of AC-30 is very consistent at different loading rates. A further statistical analysis proved that the loading rate has no effect on the fracture energy for AC-30 (see Appendix D.1.2).

4.3.2.4 Recovered PG 64-22

As for the AC-20, the appropriate loading rate range for PG 64-22 was relatively large (from 50 to 600 mm/min). However, the fracture energy of different PG 64-22 specimens was very similar regardless of loading rate. This can be seen in Figure 4-12.
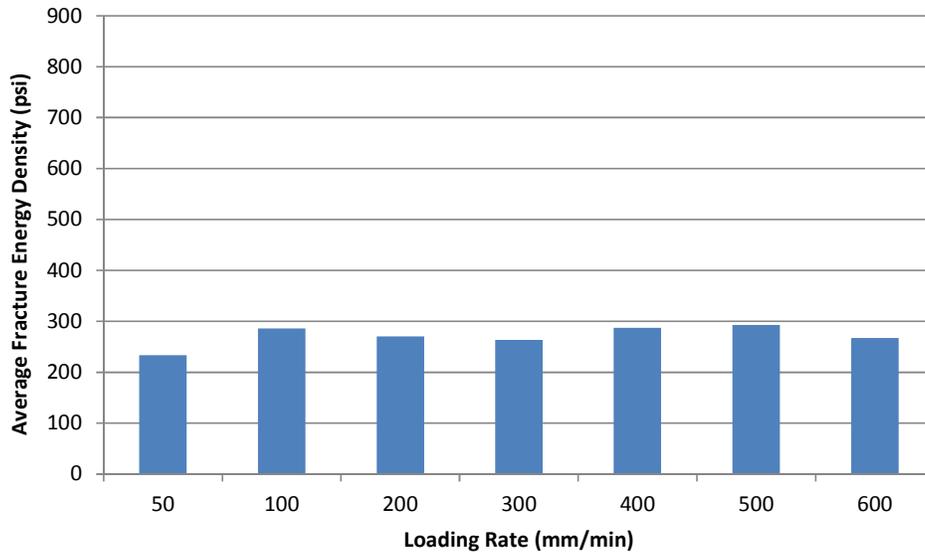
Figure 4-12 PG 64-22 recovered, fracture energy vs. loading rate

The fracture energy density at each loading rate level was averaged and plotted in Figure 4-12. We can see that the fracture energy of PG 64-22 is very consistent at different loading rates. A further statistical analysis was performed to prove it (see Appendix D.1.2).

From above figures and Figure 4-17, we can also see that the fracture energy of recovered PG 76-22 is clearly higher than that of unmodified binders, which is similar to test results of PAV residue of PG 76-22 and PG 67-22. Furthermore, binder fracture energies of different unmodified binders were close to each other. Statistical analysis was conducted to test the difference between them (see Appendix D.2.2).

Tests performed on both laboratory specimens (PAV residue) and specimens recovered from field (Superpave) indicated the same results:

1.   The new direct tension test system clearly distinguished between unmodified binders and SBS-modified binder.

2.   The tested fracture energy was independent of loading rate.

From the test results, we can see that the fracture energy of recovered rubber-modified binder ARB-5 was close to that of recovered unmodified binders (Figure 4-17). However, it is

very interesting that the true stress-true strain curve of recovered rubber-modified binder ARB-5 (Figure 4-15) was also similar to that of recovered unmodified binders AC-20, AC-30, PG 64-22 (Figure 4-14), where only one stress peak occurred.

In contrast, the true stress vs. true strain curve of SBS polymer-modified PG 76-22 has the second stress peak (Figure 4-13).
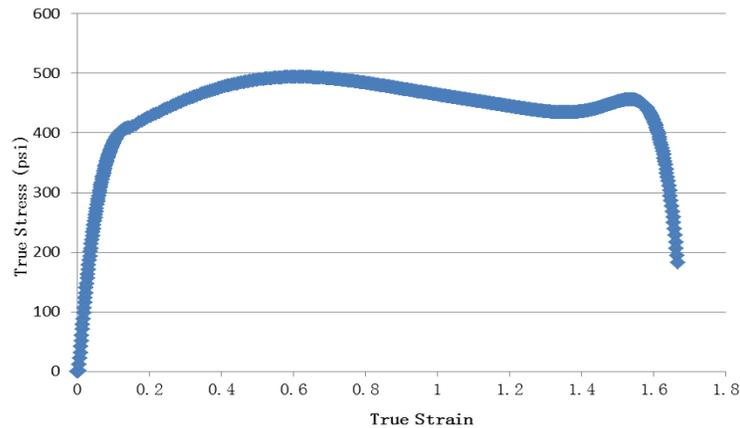
Figure 4-13 PG 76-22 recovered from field (Superpave #19278), true stress vs. true strain
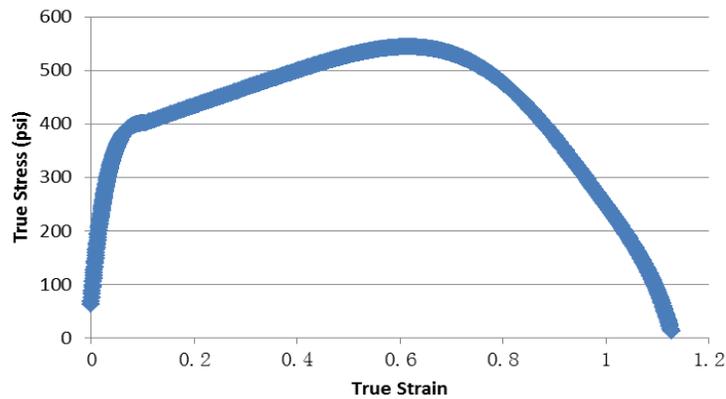
Figure 4-14 PG 64-22 recovered from field (Superpave #19312), true stress vs. true strain
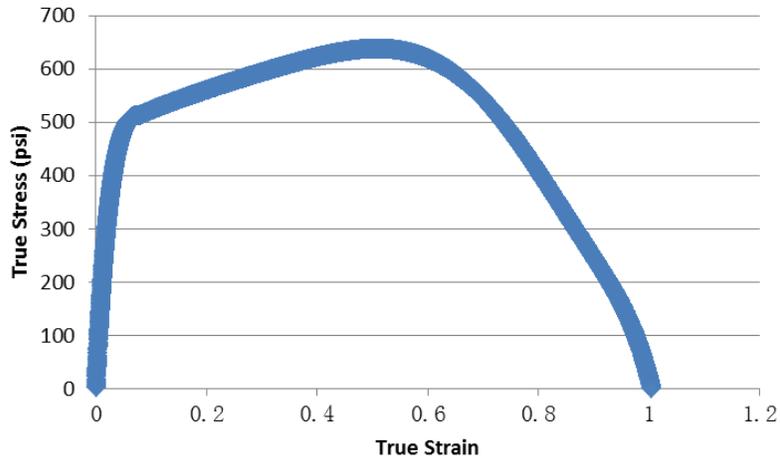
Figure 4-15 ARB-5 recovered from field (Superpave #19298), true stress vs. true strain
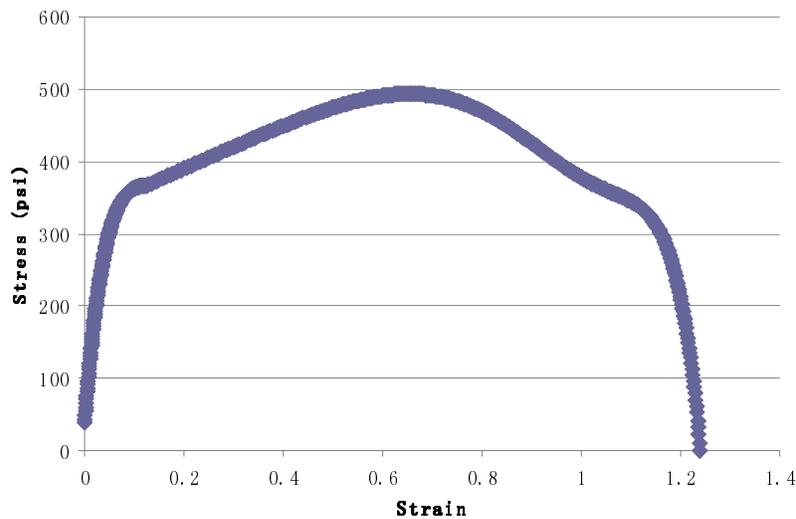
Figure 4-16 ARB-5 PAV residue, true stress vs. true strain

It was found that during the recovery process, the rubber particles not soluble in the binder were caught in the filter paper, and therefore there was no rubber in binder after recovery. This is the reason why the fracture energy of recovered rubber-modified binder ARB-5 was so close to that of unmodified binders, and their true stress-true strain curves were also so similar.

In order to clarify this issue, PAV residue of rubber-modified ARB-5 and ARB-12 was produced and tested by the research team. Because of the existence of rubber, the true stress-true strain curve has an inflection (Figure 4-16) instead of the second stress peak of SBS-modified

PG 76-22. From Figure 4-17 also shows that fracture energy of PAV residue of rubber-modified binder is higher than that of recovered rubber-modified binders and unmodified binders. Both the fracture energy and the shape of true stress-true strain curve of PAV residue of rubber-modified binders are between those of polymer-modified binder and unmodified binders.
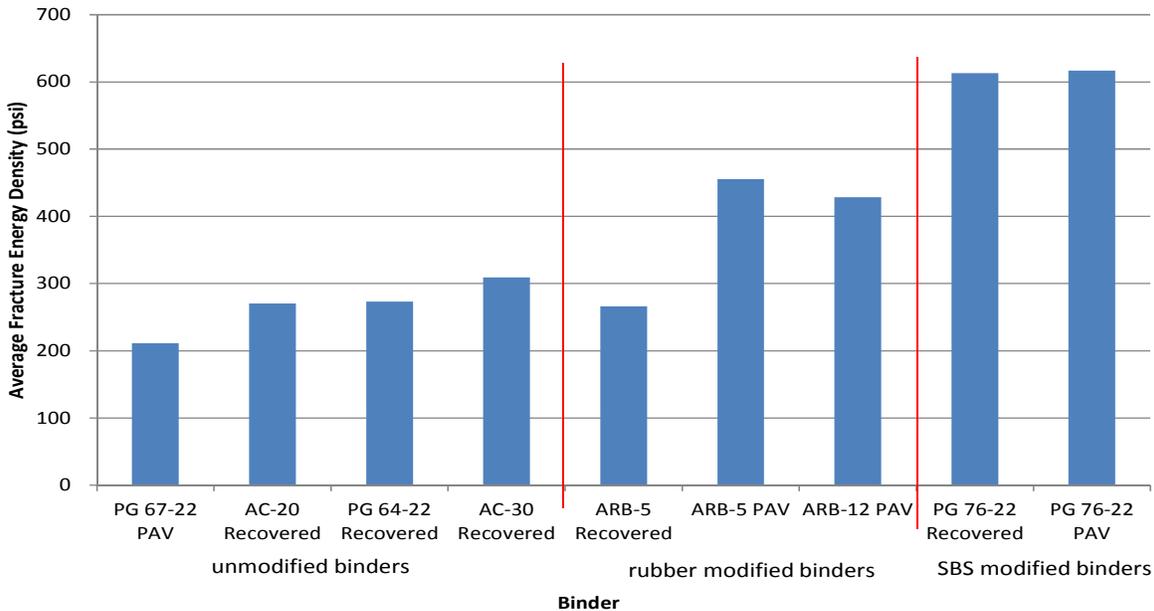
Figure 4-17 PG 76-22, rubber-modified and unmodified binder, fracture energy vs. loading rate

The clear difference of fracture energy and true stress-true strain curve between PAV residue of rubber-modified binders and recovered rubber-modified binders showed the capability of the new direct tension test to identify the component of binders.

For polymer-modified binders, the polymer completely soluble in the binder was not caught in the filter paper in recovery process. The true stress-true strain curve of recovered polymer-modified binder PG 76-22 was similar to that of PAV residue made in lab, where a second stress peak was present, except the recovered PG 76-22 had more variance.

Both recovered polymer-modified binder PG 76-22 and PAV residue's fracture energies were high compared to unmodified binders and rubber-modified binders (Figure 4-17). The second stress peak and high fracture energy identifies the existence of polymer in binder.

Even for the same type of recovered binder, in different conditions (location, mixture, layer, etc.), its engineering characteristics could be different (e.g., stiffness and brittleness). Therefore, the appropriate loading rate range was also different. This difference sometimes is so huge that it is impossible to define an appropriate loading rate range for a certain type of recovered binder. On the other hand, for each type of binder in a specific condition, there is an appropriate loading rate range which results in consistent fracture energies. In order to properly determine fracture energy, it is necessary to find out this appropriate loading rate range. A detailed protocol will be presented later.

4.4 Tests on Hybrid Binders and Highly Polymer-Modified Binder

The previous tests showed that the new DT test and interpretation system was able to clearly differentiate between unmodified binders, polymer-modified binder and rubber-modified binder. In order to further verify and evaluate the capability of the new DT test to distinguish between relatively complicated modified binders in terms of fracture resistance, 3 types of hybrid binders (Wright, Hudson, Geotech), one type of highly polymer-modified binder PG 82-22, and one type of rubber-modified binder (Marianni) were tested and analyzed.

It should be noted that the components of Marianni were unclear. It was thought that Marianni contained 13% rubber modifier. However, its true stress-true strain curve showed that it may contain polymer modifier. Please see Chapter 5 "Characteristic True Stress-True Strain Curves" for more detailed information.

The original binders were supplied by FDOT. They were subjected to PAV aging (including RTFO) before being tested. In other words, all PAV residues were used in the DT tests.

The properties of hybrid binders and highly polymer-modified binder are different from those of ordinary modified binders. It has been found that it is difficult for all test methods in

current specifications to effectively distinguish between hybrid binders and other modified binders in terms of fracture resistance, particularly when the difference is small. Therefore, whether or not the new DT test can differentiate between them would provide convincing evidence of its capability to identify fracture resistance.

4.4.1 Binders and Testing Conditions

Binder types. All the binders were PAV residues.

3 types of hybrid binders:

Wright (GTR and SBS. Unknown contents)

Hudson (3.5%crumb rubber+2.5%SBS+0.4%-plus Link PT-743-Cross Linking)

Geotech (1% SBS (approximately 30 mesh, incorporated dry) +8% of Type B

GTR+1% hydrocarbon)

1 type of rubber-modified binder:

Marianni (Components are unclear. Maybe 13% Tire Rubber. The true stress-true

strain curve shows that it may contain polymer.)

1 type of highly polymer-modified binder:

PG 82-22 (8.5% SBS)

Test temperatures. 10°C and 15°C were used.

Hybrid binders and Marianni: all tests were conducted at 15°C because it is the optimal temperature for most types of binder to get consistent fracture energies.

PG 82-22: a PG 82-22 binder was tested at both 15°C and 10°C. Due to the very ductile nature of this highly polymer-modified binder, it was impossible to perform the new DT test successfully at 15°C, where the deformations to failure were excessive even at very fast loading rates. The excessively ductile specimen shape may make the interpretation inaccurate.

Loading rates. Various loading rates were used depending on the property of individual binders in order to avoid both premature fracture, which results in erroneous results, and excessive deformation, which results in the underestimation of fracture energy.

For hybrid binders and Marianni, we applied the loading rates up to the possible fastest rate, which resulted in good test results.

For highly polymer-modified binder PG 82-22, the situation of premature fracture was uncommon: excessive deformation was the main problem. A broad range of loading rates was applied to PG 82-22 in order to identify an approach to deal with this problem.

4.4.2 Test Results and Analysis

The average test results of all types of binder were calculated and plotted in Figure 4-18. We will also analyze binders individually.
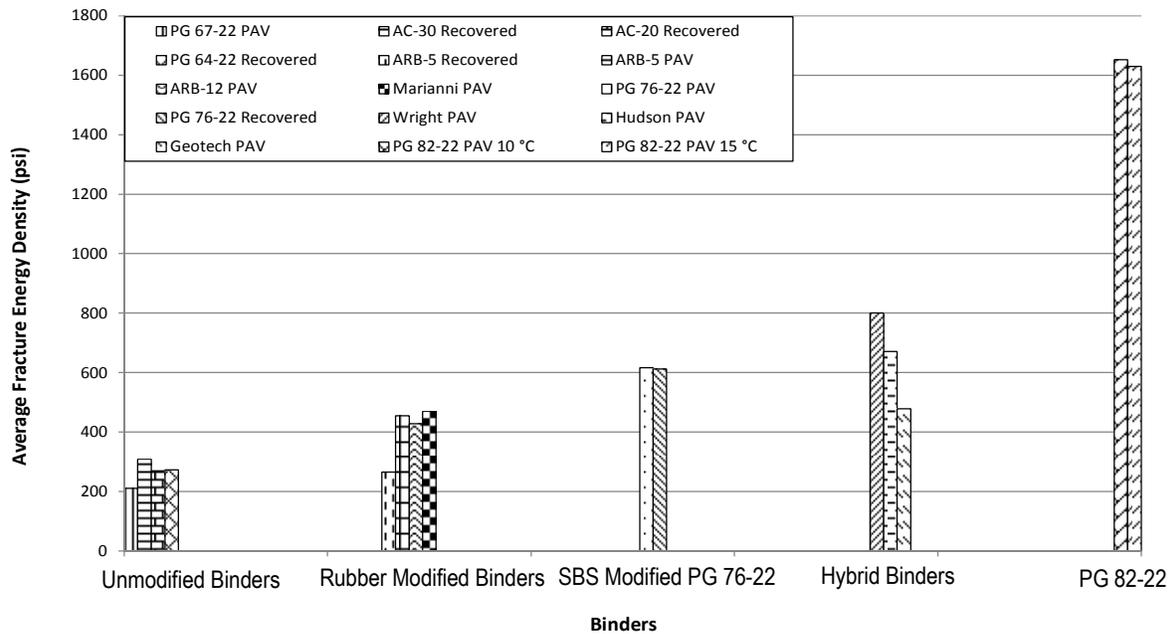
Figure 4-18 All binders' fracture energy

4.4.2.1 Hybrid binders

Figure 4-18 shows that all hybrid binders had fracture energy higher than that of unmodified binders and comparable to SBS polymer-modified binder PG 76-22. Two hybrid

binders, Wright and Hudson, exhibited higher fracture energy than that of SBS-modified binder PG 76-22.

The fracture energy versus loading rate is shown in Figure 4-19 (complete results of fracture energy, loading rate, and extension are presented in Appendix C). Figure 4-19 shows that for each type of hybrid binder, the fracture energy is independent of loading rate. The difference between different hybrid binders is clear. Statistical analysis was performed to further prove these points (see Appendix D.2.2).
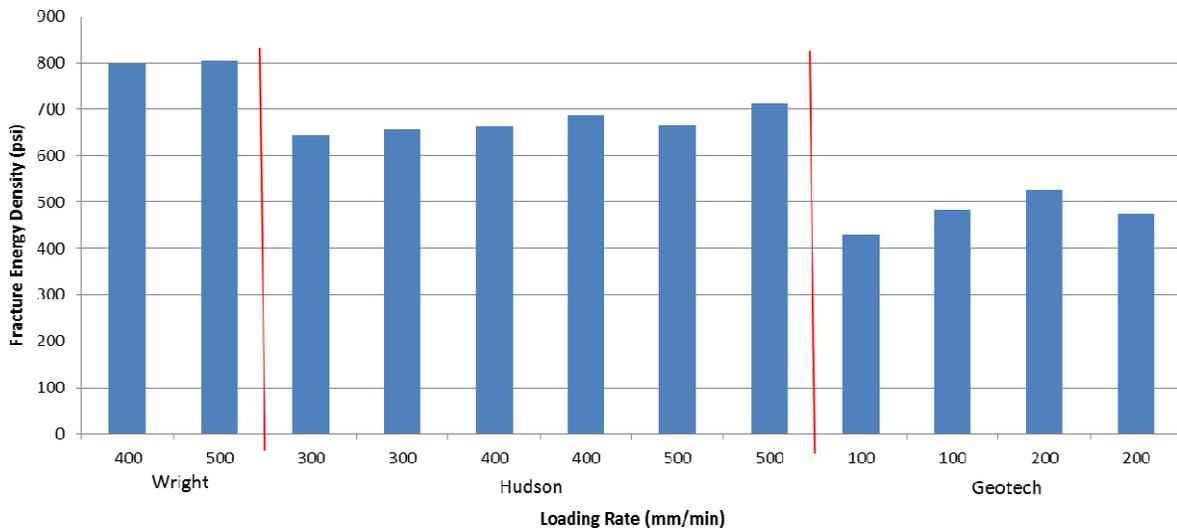
Figure 4-19 Hybrid binders, fracture energy vs. loading rate

It is interesting to analyze the true stress-true strain curve of hybrid binders because they include both polymer and rubber. Although the true stress-true strain curve of some types of hybrid binder is sometimes complicated, certain trends are still evident.

In previous tests, we have found that the second stress peak and high fracture energy identify the existence of polymer in binder. This can also be seen in hybrid binders. Figure 4-21 shows that the second stress peak of Geotech, tested at a loading rate of 200 mm/min, was very clear.
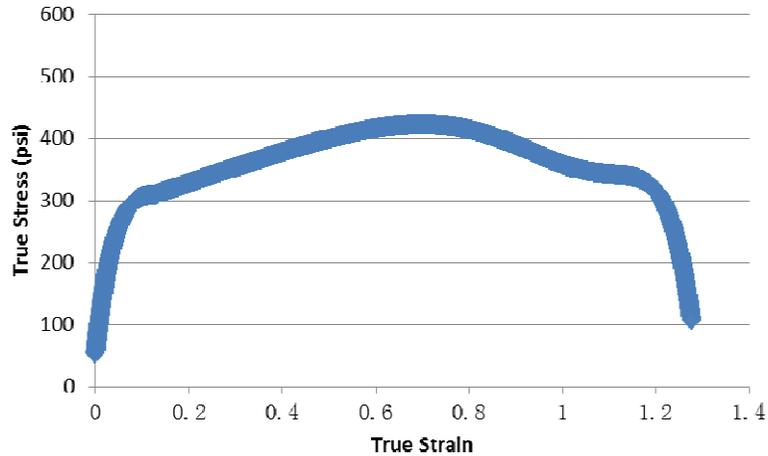
Figure 4-20 Geotech hybrid binder at 100 mm/min, true stress vs. true strain
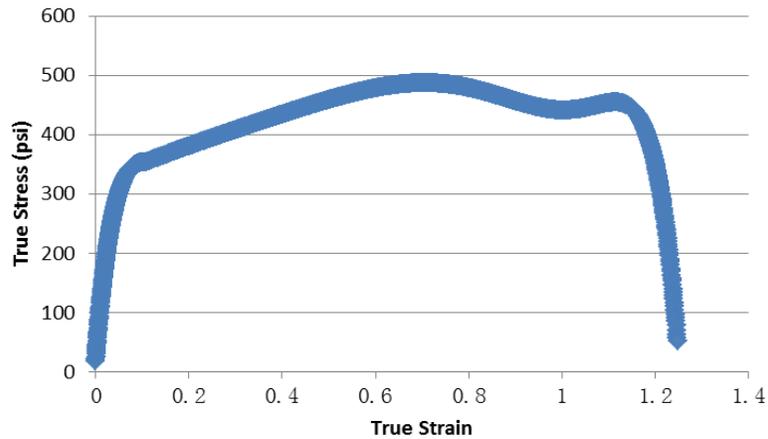
Figure 4-21 Geotech hybrid binder at 200 mm/min, true stress vs. true strain

Some types of hybrid binder may not exhibit a second stress peak at slow loading rates. But when we increase the loading rate, the second stress peak was present. Figure 4-20 shows the true stress-true strain curve of Geotech hybrid binder tested at 100 mm/min. There is only an inflection instead of the second stress peak, which looks similar to that of rubber-modified binders. When we increased the loading rate to 200 mm/min, i.e., the fastest loading rate creating satisfactory test results, the second stress peak became clear (Figure 4-21), which indicated the existence of polymer.

Therefore, it should be noted that some types of hybrid binder may exhibit a more complicated true stress-true strain curve than that of polymer-modified binders since they also include rubber.

Figure 4-22 shows the true stress-true strain curve of Wright hybrid binder at 500 mm/min. There are some waves on the curve, which is different from other binders. However, the second stress peak is clear, which reveals the presence of polymer in binder.
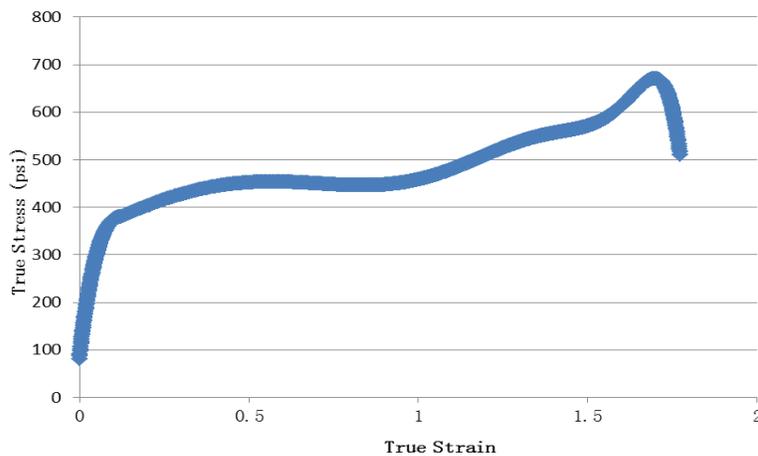
Figure 4-22 Wright hybrid binder at 500 mm/min, true stress vs. true strain

Figure 4-23 shows the true stress-true strain curve of Hudson hybrid binder at 500 mm/min. It exhibited a significantly lower second stress peak than the first peak, but the second stress peak was still clear, once again indicating the presence of polymer.
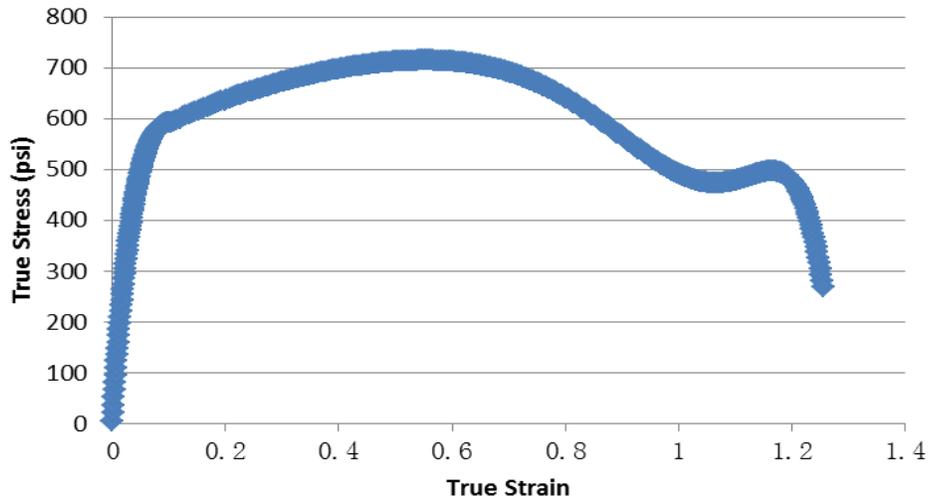
Figure 4-23 Hudson hybrid binder at 500 mm/min, true stress vs. true strain

4.4.2.2 Marianni

Figure 4-24 shows test results of Marianni. In order to compare to rubber-modified binders,

ARB-5 and ARB-12 PAV residues are also plotted.
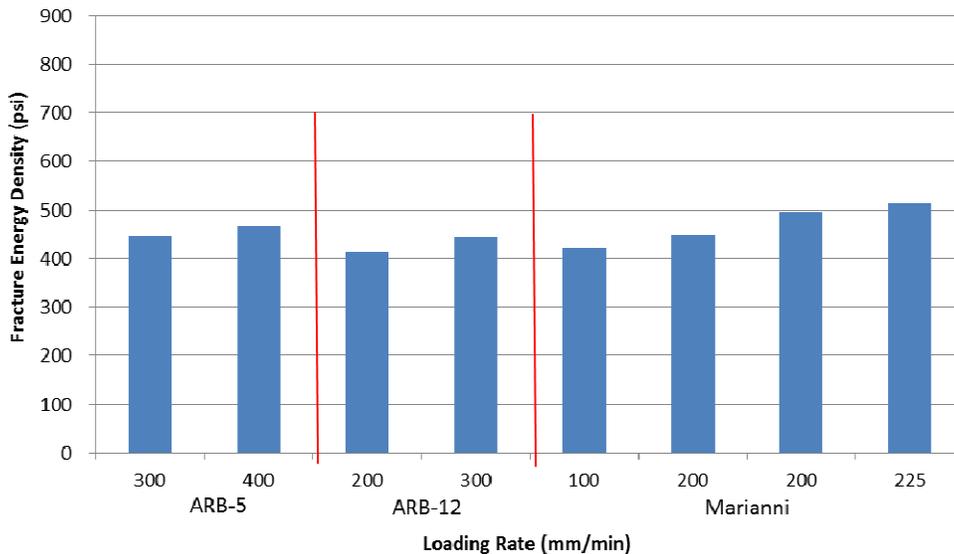
Figure 4-24 Rubber-modified binders, true stress vs. true strain

Figure 4-24 shows that fracture energy of Marianni was similar to that of ARB-5 and

ARB-12, which was lower than SBS-modified and hybrid binder, but higher than unmodified

binders. The fracture energy was consistent at different loading rates.

49

Figure 4-25 shows the clear second stress peak of Marianni hybrid binder at 100 mm/min. At the fastest loading rate of 225 mm/min that created satisfactory test results, the first stress peak was extended, while the second stress peak was more evident (Figure 4-26).

The clear second stress peak usually indicates the existence of polymer, which is inconsistent with the information indicating that only rubber was used to modify this binder.
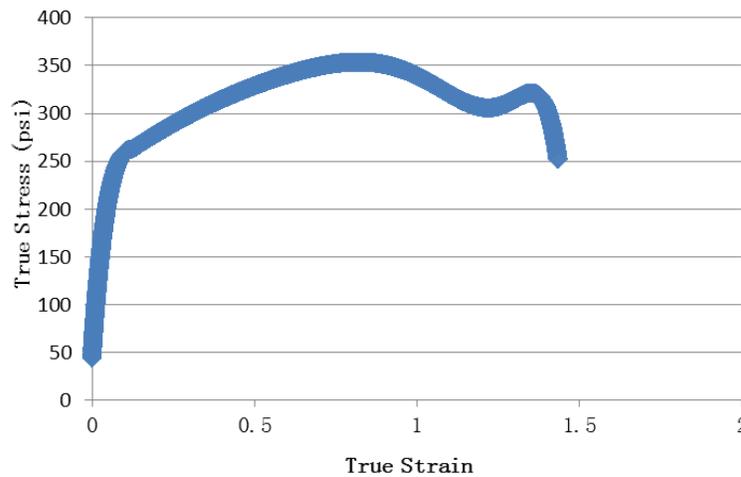
Figure 4-25 Marianni hybrid binder at 100 mm/min, true stress vs. true strain
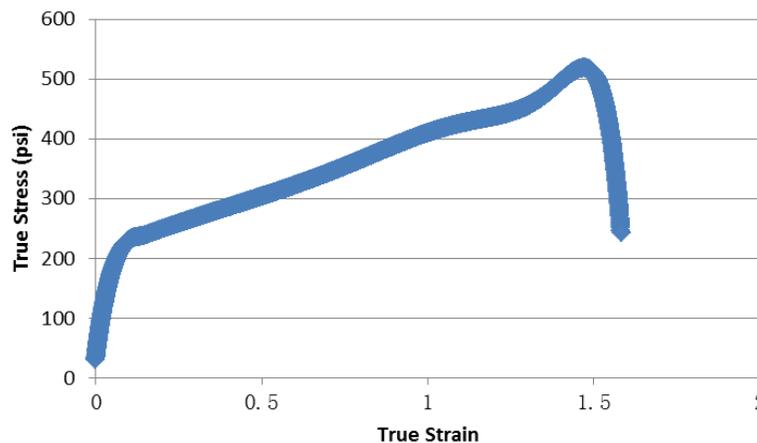
Figure 4-26 Marianni hybrid binder at 225 mm/min, true stress vs. true strain

4.4.2.3 Highly polymer-modified binder PG 82-22

The properties of highly polymer-modified binder PG 82-22 are very special and quite different from other binders. Consequently, analysis of PG 82-22 helped to clarify some

important concepts such as "premature fracture" for viscoelastic polymer materials, determine the appropriate test protocol and improve the interpretation method.

Initially, PG 82-22 binder was tested at 15 °C which was the same temperature used for all other binders. However, deformations to failure were excessive, even at very fast loading rates. For all three specimens (at 500 mm/min, 700 mm/min, 900 mm/min) with complete true stress-true strain curves, the extension exceeded 1.2 inch without fracture (Figure 4-27). However, the fracture point (i.e., the second stress peak) was reached. Thus the true stress-true strain curve was complete (Figure 4-28), indicating that premature fracture did not occur.

For all other specimens (at 800 mm/min, 1000 mm/min through 1400 mm/min), the second stress peak was not reached, even though failure did occur. Thus, the true stress-true strain curve was incomplete (Figure 4-29), indicating that premature fracture did occur.

Figure 4-27 PG 82-22 at 15°C, extension greater than 1.2 in without fracture
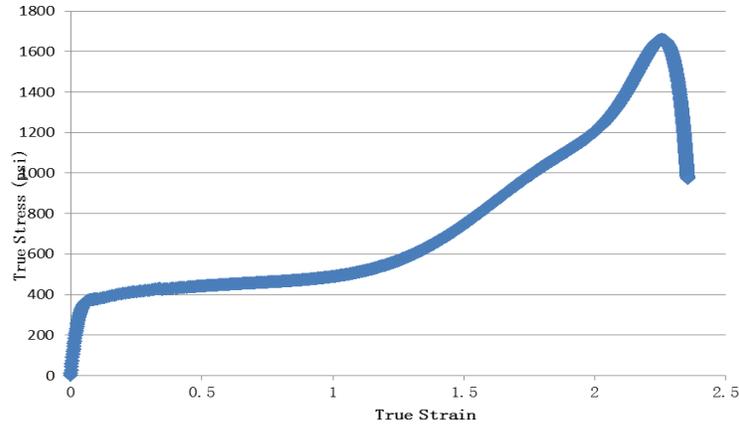
Figure 4-28 PG 82-22 at 15°C, 900 mm/min, true stress vs. true strain
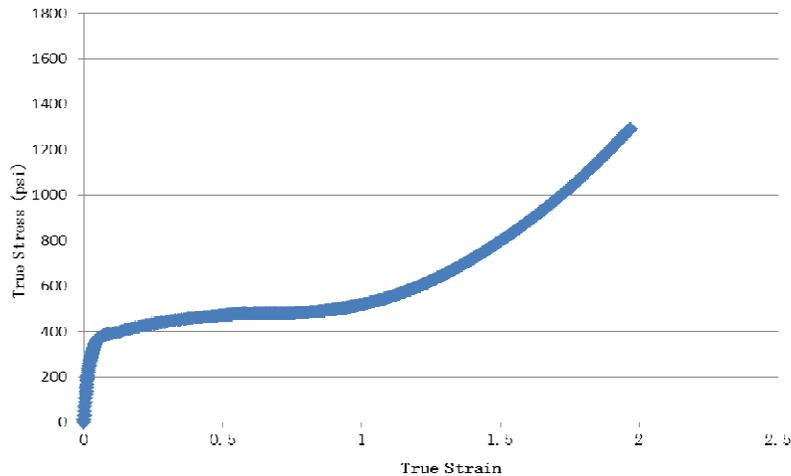
Figure 4-29 PG 82-22 at 15°C, 800 mm/min, true stress vs. true strain

Table 4-5 presents only the test results from complete true stress-true strain curves at 15°C. All extensions to fracture exceeded 1 inch, which is excessive because it is impossible to accurately determine stress and strain. However, as shown in Figure 4-30, the fracture energy was consistent for these tests, even though the actual value may be inaccurate. The excessively ductile specimen shape very likely makes the interpretation inaccurate. Due to the very ductile nature of this highly polymer-modified binder PG 82-22, test temperature was then reduced to 10°C.

Table 4-6 presents only the test results with complete true stress-true strain curves at 10°C. The fracture energy was independent of loading rate (Figure 4-30). The extension to fracture point was more reasonable compared to that at 15°C. Therefore, 10 °C was considered a more appropriate test temperature for highly polymer-modified binder PG 82-22. Interestingly, the fracture energy values determined at both temperatures was about the same, indicating that the error associated with excessive deformation may not be critical.

Table 4-5 Test results of PG 82-22 at 15°C

Loading Rate (mm/min)	Fracture Energy Density (psi)	Extension (in)
500	1620.86	1.0912
700	1696.07	1.0698
900	1574.74	1.0600

Table 4-6 Test results of PG 82-22 at 10°C

Loading Rate (mm/min)	Fracture Energy Density (psi)	Extension (in)
100	1670.18	1.1140
200	1621.59	0.9118
300	1602.03	0.7564
400	1641.40	0.7509
500	1714.18	0.7421
700	1665.19	0.6684
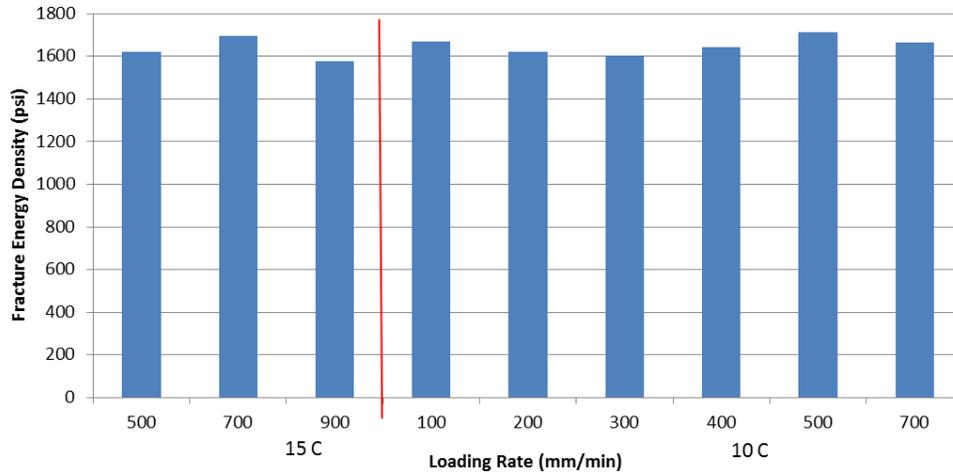
Figure 4-30 PG 82-22, fracture energy vs. loading rate

Figure 4-18 clearly shows that the highly polymer-modified binder PG 82-22 had significantly higher fracture energy than unmodified, rubber-modified, SBS polymer-modified, and hybrid binders.

It is interesting that even at a very low loading rate, with a complete true stress-true strain curve, the fracture section of PG 82-22 always looked like that of specimens exhibiting premature fracture (Figure 4-31 A, B, D) for the other binder types. It never looked like that typically observed in failed specimens of other binder types when tests were performed successfully (i.e., premature fracture had not occurred: Figure 4-31 C). This phenomenon helped to clarify the concept premature fracture.
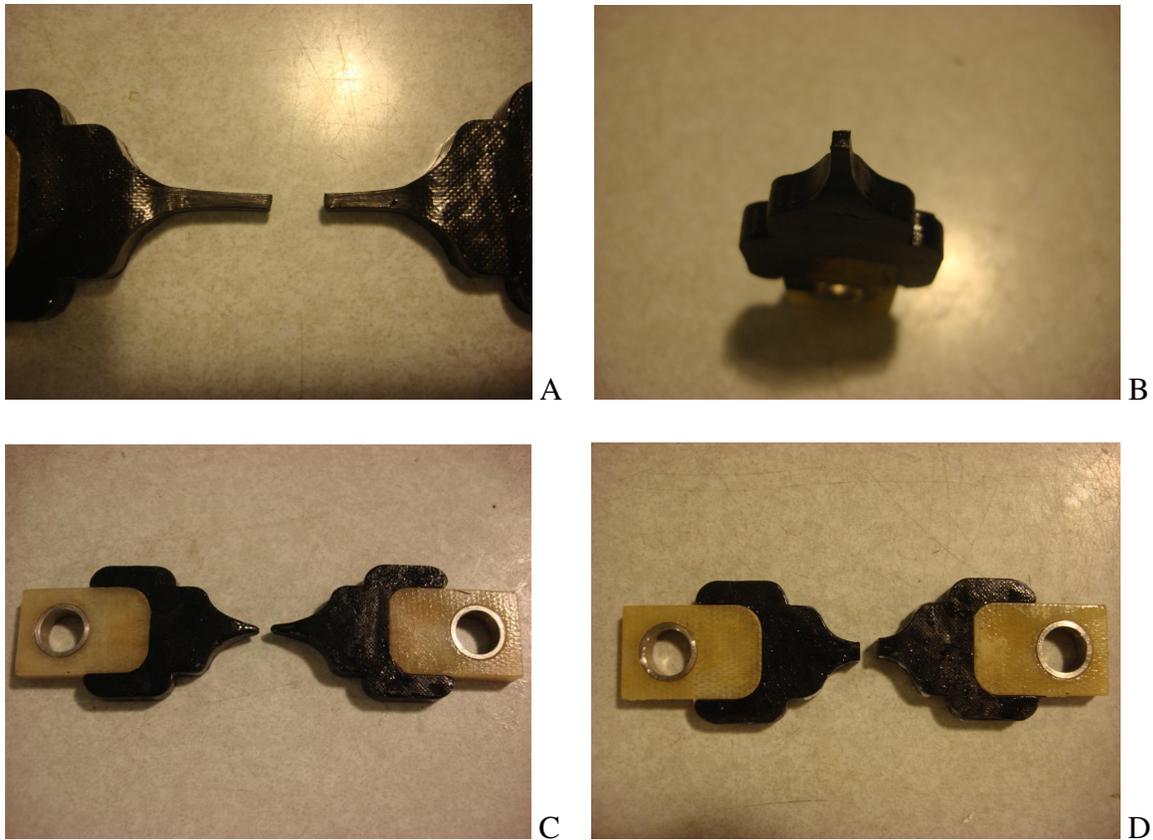
Figure 4-31 Comparison of fracture section between PG 82-22 and other binders. A) PG 82-22, complete stress-strain curve. B) fracture section of PG 82-22, complete stress-strain curve. C) a typical fracture section of other binders (PG 76-22 in picture), complete stress-strain curve. D) a typical premature fracture section of other binders (PG 76-22 in picture).

Therefore, it appears that premature fracture can only be identified by determining whether a complete true stress-true strain curve was reached; in other words the characteristic shape of the failed specimen is not a reliable indicator of premature fracture. Only data from tests resulting in complete true stress-true strain curves should be used for determination of fracture energy.

Characteristics of complete true stress-true strain curve are summarized below. More detailed principles will be shown in the Chapter 5 "Characteristic True Stress-True Strain Curves".

1.   For unmodified binder, a single stress peak should be reached prior to fracture.

2.   For rubber-modified binder, a single stress peak followed by an inflection (instead of the second stress peak of polymer-modified binder) should be reached prior to fracture.

3.   For polymer-modified or hybrid binder, a second stress peak should be reached prior to fracture. Sometimes the first stress peak is extended, so it may not be very distinct, but the second stress peak always exists. Sometimes at low loading rate, the second stress peak is hidden like the inflection of rubber-modified binder, and a higher loading rate can make it clearer. The second stress peak and high fracture energy identify the existence of polymer in binder.

Accurate and complete true stress-true strain curves usually results from an acceptable range of extension and loading rate. Based on tests performed on a wide range of binders, it appears that a reasonable extension range is between 0.05 to 1 inch. Also, the loading rate should not be greater than 900 mm/min. This may have to be achieved by reducing the test temperature.

4.5 Summary

The new direct tension test clearly distinguished between fracture energy of various modified binders and unmodified binders. Figure 4-18 shows that the highly polymer-modified binder PG 82-22 had significantly greater fracture energy than unmodified, SBS-modified, rubber-modified and hybrid binders. All hybrid binders had fracture energy higher than that of unmodified binders and comparable to SBS-modified binder PG 76-22. Two hybrid binders, Wright and Hudson, exhibited higher fracture energy than that of SBS-modified binder PG 76-22. The rubber-modified binders had fracture energy greater than that of unmodified binders, but lower than that of other modified binders. For each type of binder, the fracture energy was independent of loading rate.

CHARACTERISTIC TRUE STRESS-TRUE STRAIN CURVES

Another important finding in this research project was that characteristics of true stress-true strain curves of binders were closely related to modifier type and content. Each binder type had its own characteristic true stress-true strain curve. Therefore, it appears that in most cases, the true stress-true strain curve can be used to identify the presence of modifier or rubber and their relative content.

Typical characteristic true stress-true strain curves of various types of binder were introduced in Chapter 4. In this chapter, all true stress-true strain curves of each type of binder will be investigated and compared to identify specific trends related to the modifier type and relative content.

5.1 Typical True Stress-True Strain Curve of Each Type of Binder

In order to evaluate true stress-true strain curves for each type of binder, the true stress-true strain curves were plotted for different loading rates. These plots led to identification of patterns and shapes that could be uniquely associated with binder type and relative content. Most types of binder were tested at 15°C. So if not mentioned, the figures refer to the tests at 15°C.

5.1.1 Unmodified Binders

Four types of unmodified binder were tested in this study, including AC-20, AC-30, PG 64-22 recovered from field, and PG 67-22 PAV residue. All unmodified binders' true stress-true strain curves exhibited only one stress peak, followed by a relatively steep drop in the true stress-true strain curve (see Figure 5-1). As will be discussed later, this is distinctly different from polymer-modified binder, which exhibits a second stress peak, and rubber-modified binder, which exhibits an inflection after the first peak.
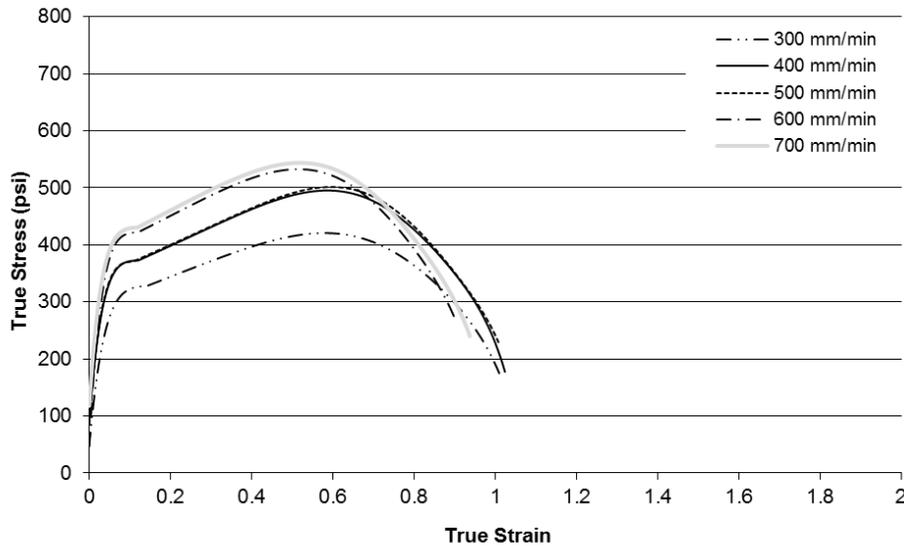
Figure 5-1 PG 67-22 PAV residue, true stress vs. true strain, 15°C

5.1.1.1 PG 67-22 PAV residue

PG 67-22 was tested at multiple temperatures. Only the true stress-true strain curves at 15°C were plotted in Figure 5-1, because 15 °C was selected as the most appropriate test temperature for fracture energy testing of most binder. Although higher loading rates resulted in higher peak stress, the characteristics of the curves were the same, exhibiting a single peak.

5.1.1.2 Recovered AC-30

A large number of AC-30 specimens were tested. True stress-true strain curves for all specimens had a similar shape, so only a few representative results of tests performed at different loading rates were plotted in Figure 5-2. As shown in the figure, all curves exhibited a single stress peak, which was characteristic for unmodified binder.
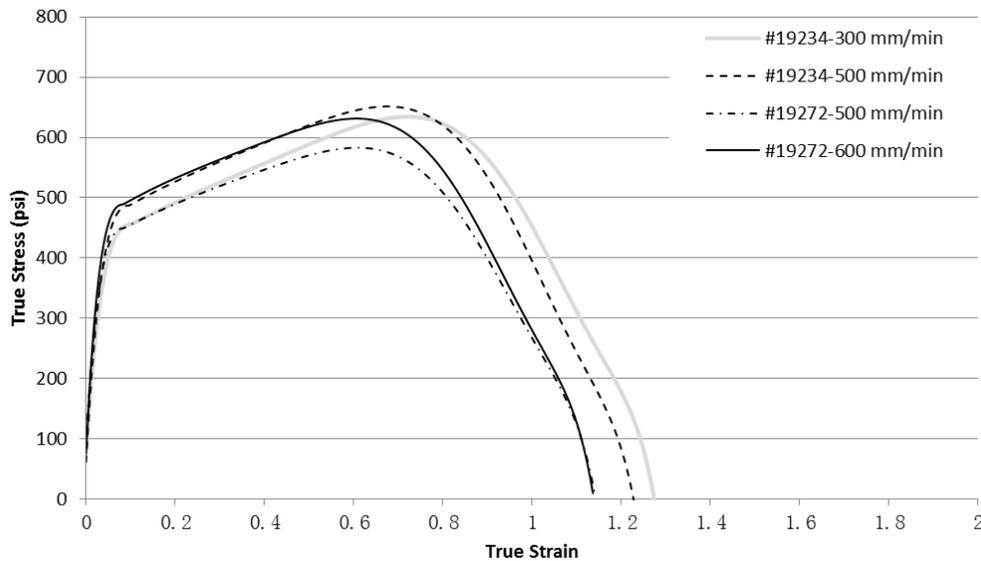
Figure 5-2 AC-30 recovered, true stress vs. true strain

Actually, this single stress peak shape was observed for all unmodified AC-30 binder regardless of where the specimen was obtained. In addition, the fracture energy of all unmodified AC-30 binder from a particular section was very similar, even though the magnitude of the stress peak varied.

5.1.1.3 Recovered AC-20

A large number of AC-30 specimens were tested (Figure 5-2). As shown in the figure, all curves exhibited a single stress peak, which was characteristic for unmodified binder.

Similarly, numerous AC-20 specimens were tested. True stress-true strain curves for all specimens had a similar shape, so only a few representative results of tests performed at different loading rates were plotted in Figure 5-3. Again, all these curves had only one stress peak, which is characteristic of unmodified binder. As for the AC-30 binder, the single stress peak shape was observed for all unmodified AC-20 binder regardless of where the specimen was obtained. In addition, the fracture energy of all unmodified AC-20 binder from a particular section was very similar, even though the magnitude of the stress peak varied.
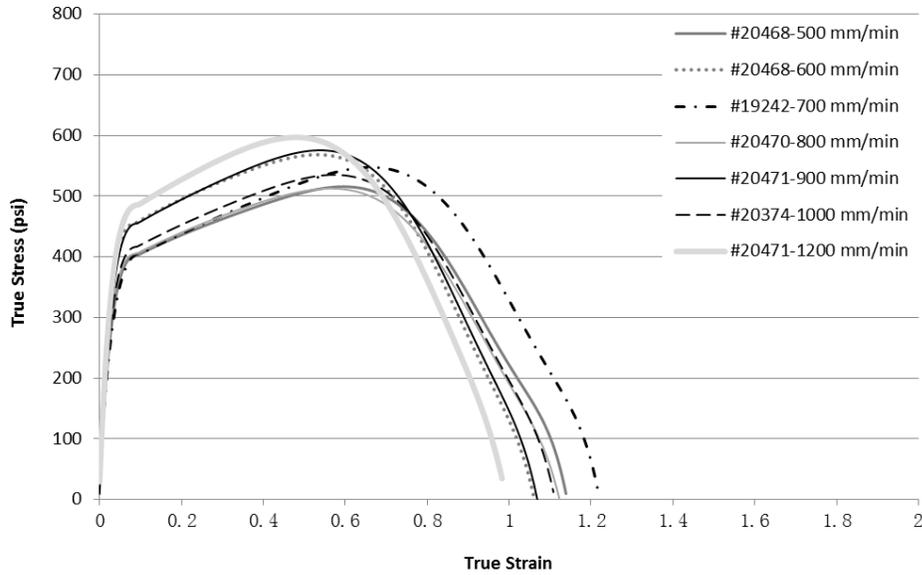
Figure 5-3 AC-20 recovered, true stress vs. true strain

5.1.1.4 Recovered PG 64-22
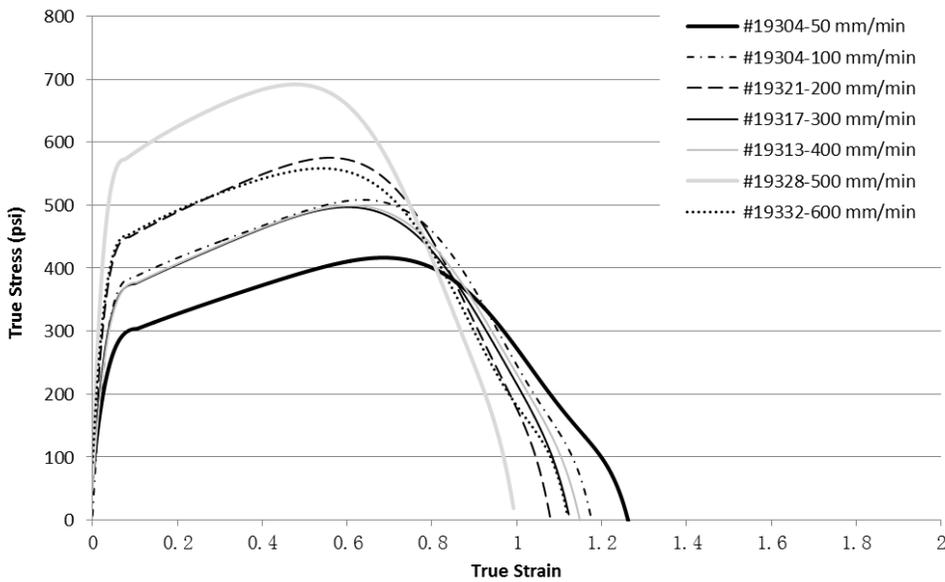
Figure 5-4 PG 64-22 recovered, true stress vs. true strain

Results for recovered unmodified PG 64-22 (Figure 5-4) were similar to those obtained for

AC-30 and AC-20 binder. Again, all these curves exhibited only one stress peak, which is

characteristic of unmodified binder. Also, although peak stress varied with loading rate and

ductility of individual binder specimens, the fracture energy was about the same for all specimens.

5.1.1.5 Comparison between unmodified binders
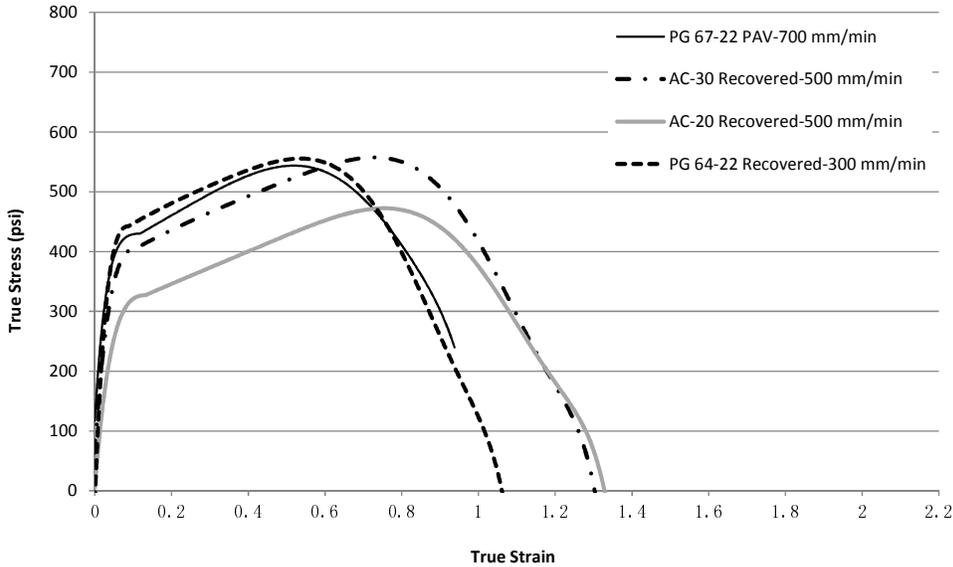
Figure 5-5 Unmodified binders, true stress vs. true strain

Typical true stress-true strain curves of each type of unmodified binder were plotted in Figure 5-5. It is clear that all unmodified binders had similar characteristic true stress-true strain curves where only one stress peak is present. A single stress peak and low fracture energy are characteristic of unmodified binders.

5.1.2 SBS Polymer-Modified Binders

Three types of SBS-modified binder were tested: PG 76-22 recovered from field; and PG 76-22 and PG 82-22 PAV residue. Although a few anomalies were encountered, the typical true stress-true strain curve of SBS-modified binder exhibited a second stress peak with high fracture energy.

5.1.2.1 Recovered PG 76-22

Typical true stress-true strain curves of most SBS-modified PG 76-22 recovered from field are shown in Figures 5-6 and 5-7. The difference in shapes between the two figures is probably

due to complicating factors associated with specimens recovered from the field (cores from different locations and different aging levels) and the fact that multiple PG 76-22 binders were sampled. Although, the second stress peak was sometimes lower than the first (Figure 5-7), a second stress peak was always observed for SBS-modified binder. In addition, the fracture energy for most SBS-modified PG 76-22 binder was similar and consistently higher than for unmodified binder.
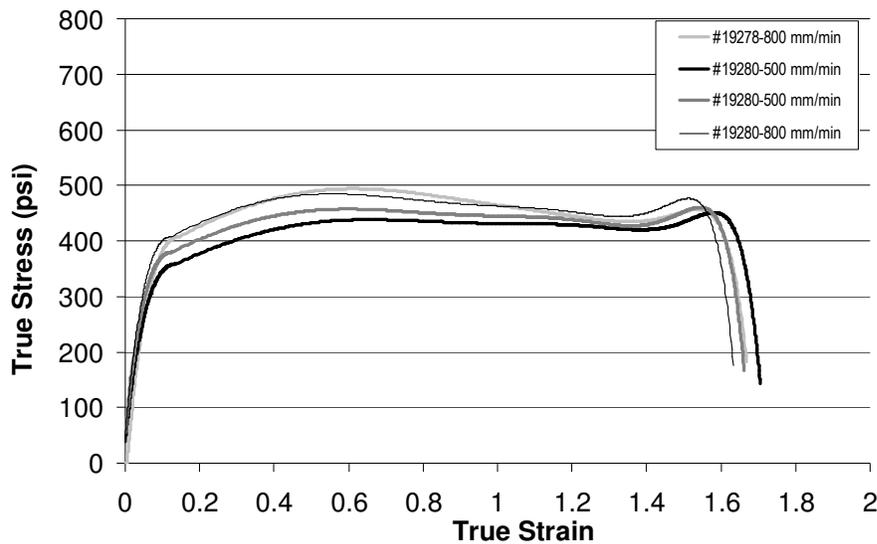
Figure 5-6 PG 76-22 recovered, true stress vs. true strain (1)
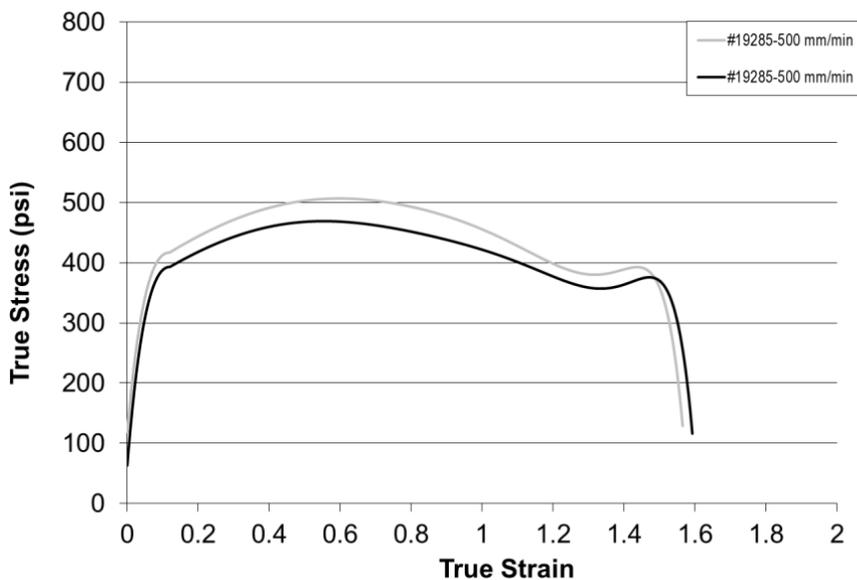
Figure 5-7 PG 76-22 recovered, true stress vs. true strain (2)
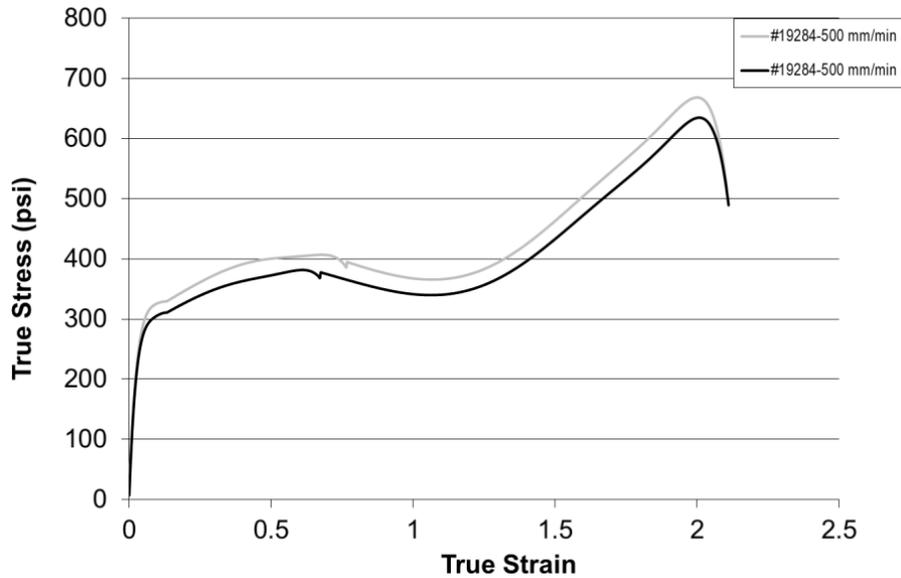
Figure 5-8 PG 76-22 recovered, true stress vs. true strain (3)

A few recovered SBS-modified PG 76-22 binders exhibited a significant higher second stress peak and a greater strain to fracture (Figure 5-8). Consequently, their fracture energy was higher. The specific make-up of these field binders was unknown, so one can only speculate on the reason for the difference, which could be a difference in polymer type or content.

As mentioned earlier, a few anomalies were encountered. As shown in Figure 5-9, two of the SBS-modified PG 76-22 binders recovered from the field did not exhibit a clear second peak, but only and inflection in the true-stress-true strain curve after the first peak. Again, one can only speculate as to the reason, but there is no question that field specimens introduce complicating factors, including the fact that the actual make-up and grade of the original binder used was unknown. However, the fact that the specimens presented in Figure 5-9 had higher fracture energy than unmodified and rubber-modified binders, which typically exhibit an inflection instead of the second stress peak (see below), indicates that these binders were SBS-modified.
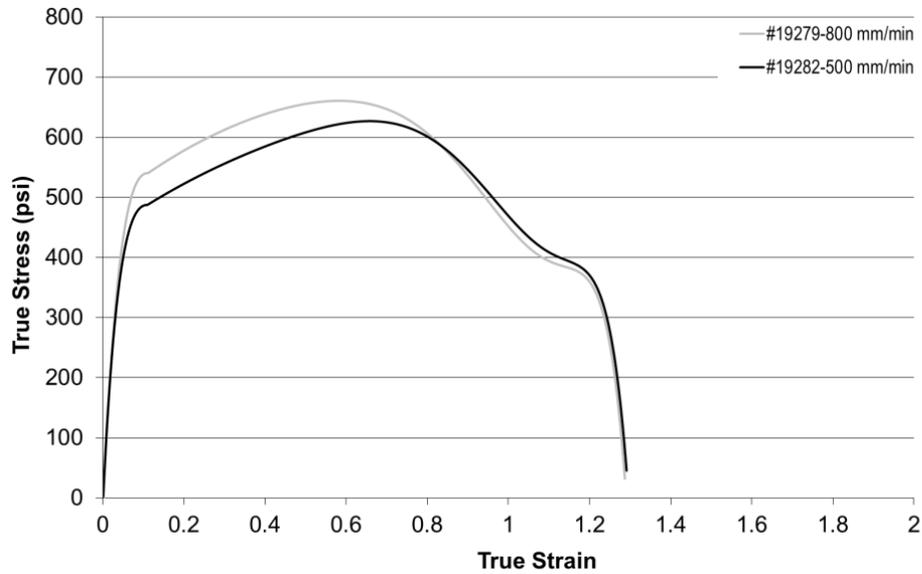
Figure 5-9 PG 76-22 recovered, true stress vs. true strain (4)

5.1.2.2 PG 76-22 PAV residue

Binders were tested at multiple temperatures. However, only the true stress-true strain curves at 15°C were plotted in Figure 5-10, because 15 °C was selected as the most appropriate test temperature for fracture energy testing of most binder. Figure 5-10 clearly shows that compared to SBS-modified PG 76-22 recovered from field, the shape of the true stress-true strain curve SBS-modified PG 76-22 PAV residue very similar for all binders tested. In addition, their fracture energy was very similar. Figure 5-10 also shows that the first stress peak was not as clearly defined, while the second stress peak was very clear. Fracture energy of the laboratory PAV specimens was high and similar to the average fracture energy of SBS-modified PG 76-22 binder recovered from field.
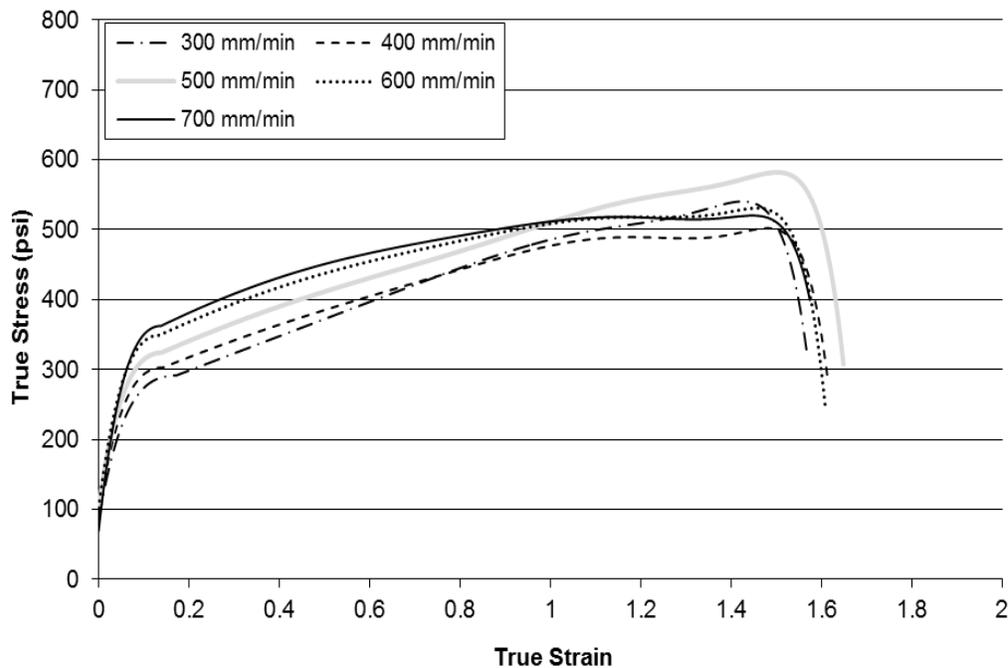
Figure 5-10 PG 76-22 PAV residue, true stress vs. true strain

5.1.2.3 PG 82-22 PAV residue

The SBS content of PG 82-22 used in this study was double that of the SBS-modified PG 76-22. Figure 5-11 shows the true stress-true strain curve of PG 82-22 exhibits much greater peak stress and strain than that of PG 76-22. Therefore, its fracture energy is much greater than that of PG 76-22. Like PG 76-22 PAV residue, the true stress-true strain curves of PG 82-22 exhibit a very clear second stress peak, while the first stress peak levels out and becomes an upward slope. At 10°C, the true stress-true strain curves of PG 82-22 greater peak stress and lower strain than those at 15°C. However, their shape is similar, and the fracture energy for both temperatures were the same.
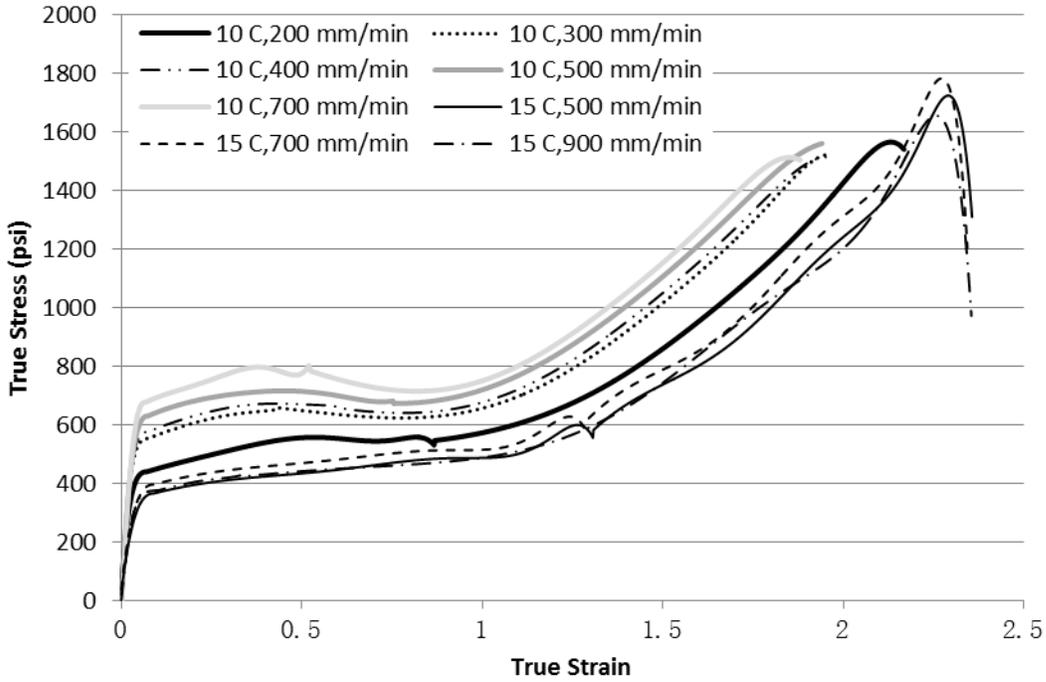
Figure 5-11 PG 82-22 PAV residue, true stress vs. true strain

5.1.2.4 Comparison between polymer-modified binders
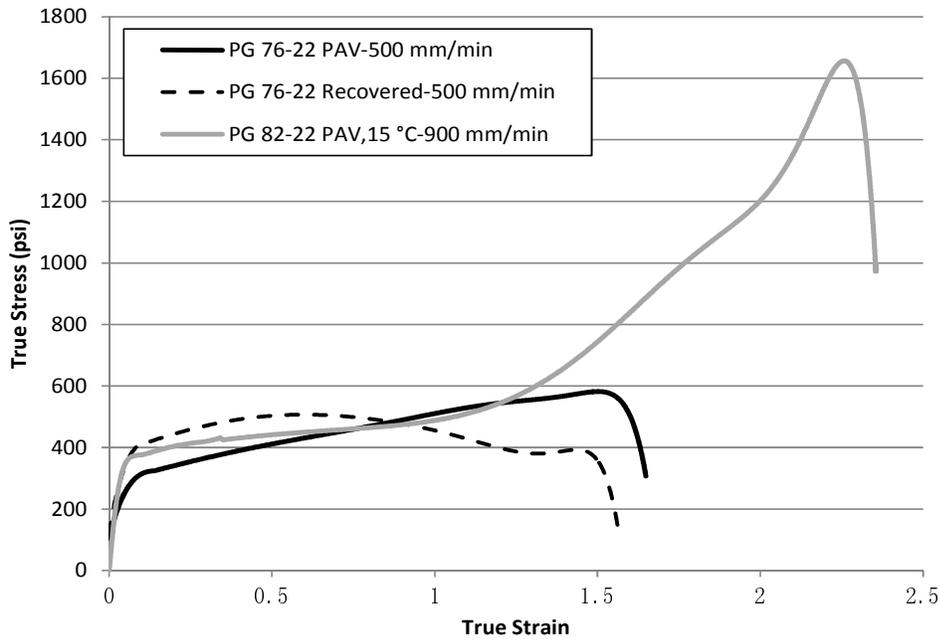
Figure 5-12 Polymer-modified binders, true stress vs. true strain

Typical true stress-true strain curves of each type of polymer-modified binder were plotted in Figure 5-12, which clearly shows the true stress-true strain curve of PG 82-22 exhibited significantly higher peak stress and greater strain than PG 76-22.

5.1.3 Rubber Modified Binders

The following rubber-modified binders were tested: ARB-5 recovered from field cores, ARB-5 and ARB-12 prepared in the laboratory, and Marianni PAV residue, which was reported to have 13% rubber content. As stated previously in Chapter 4, ARB-5 recovered from field cores lost its rubber during the recovery process, and became a neat binder. Also, the true stress-true strain curves for the Marianni binder exhibited a clear second stress peak which indicated that there may be polymer modifier in the Marianni binder. As shown in the section, the characteristic true stress-true strain curve of rubber-modified binders have the first stress peak followed by an inflection instead of the second stress peak.

5.1.3.1 ARB-5 and ARB-12 PAV residue

Figure 5-13 shows that true stress-true strain curves for ARB-5 and ARB-12 exhibited and initial stress peak followed by an inflection, instead of the second stress peak. This was the typical shape observed for true stress-true strain curves of rubber-modified binder. The peak following the inflection was taken as the fracture point to calculate fracture energy, which was not as high as those with a clear second stress peak (i.e., SBS polymer-modified binder). This is consistent with findings of previous FDOT/UF research indicating that rubber-modified binder only slightly improved fracture energy of mixtures, if at all, whereas SBS polymer-modified binder had a much greater benefit on mixture fracture energy. Figure 5-13 also shows that fracture energy is consistent although the curves exhibited higher peak stress and shorter strain at at higher loading rate.
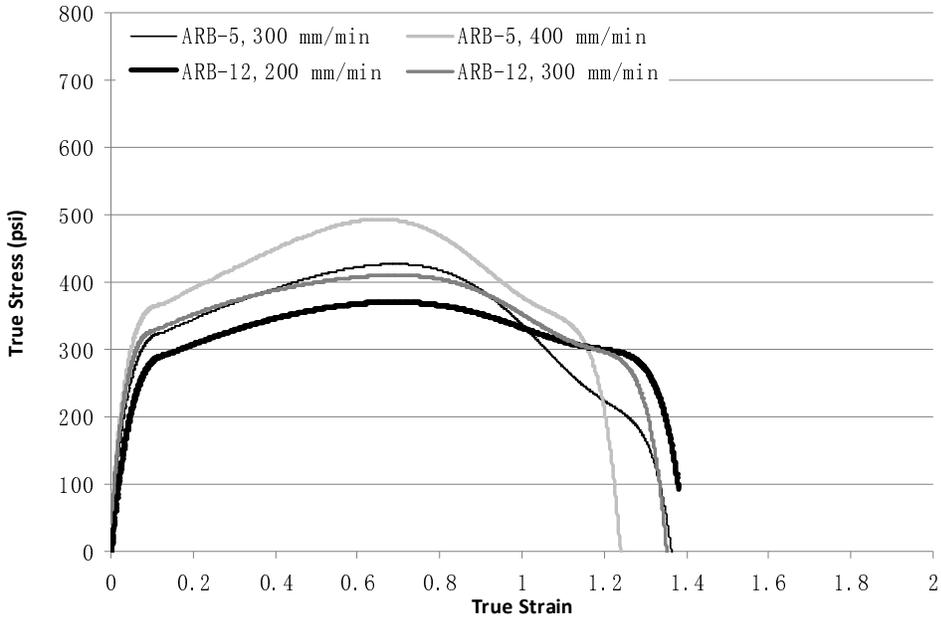
Figure 5-13 ARB-5 and ARB-12 PAV residue, true stress vs. true strain

It is interesting that a specimen of ARB-12, which was heated many times, also exhibited a second peak (Figure 5-14). However, its peak stress was low, and its fracture energy was much lower than that of normal ARB-12 specimens. Therefore, although a second stress peak was observed, the very low fracture energy clearly distinguished it from SBS-polymer-modified binder, which typically exhibited a second stress peak.
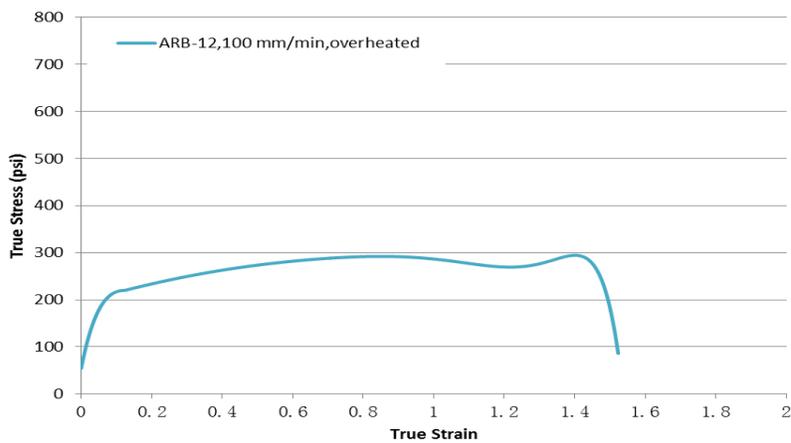
Figure 5-14 Overheated ARB-12 PAV residue, true stress vs. true strain

68

5.1.3.2 Recovered ARB-5

Many ARB-5 specimens were tested. Because all true-stress-true strain exhibited similar characteristic shapes, only one true stress-true strain curve at each loading rate was plotted in Figure 5-15. Because the rubber in these binders was lost during extraction (it could not pass through the filters), these curves exhibited only one stress peak, which is characteristic of unmodified binder.
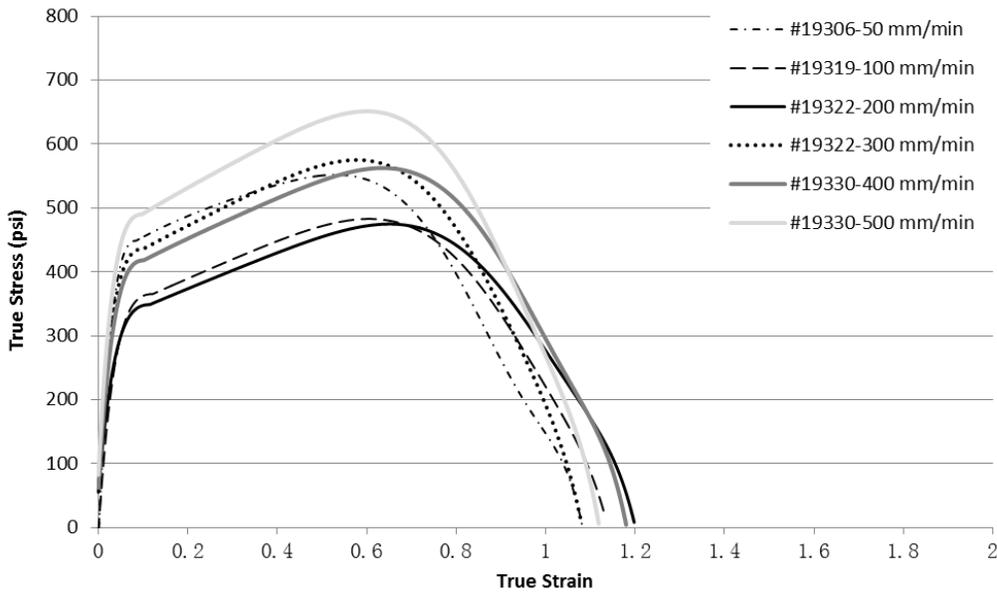
Figure 5-15 ARB-5 recovered, true stress vs. true strain

5.1.3.3 Marianni PAV residue

It was reported that Marianni was modified with 13% rubber. However, its true stress-true strain curves exhibited a second stress peak (Figure 5-16) indicating that it may contain polymer modifier. Figure 5-16, also shows that a higher loading rate can make the second stress peak more evident.
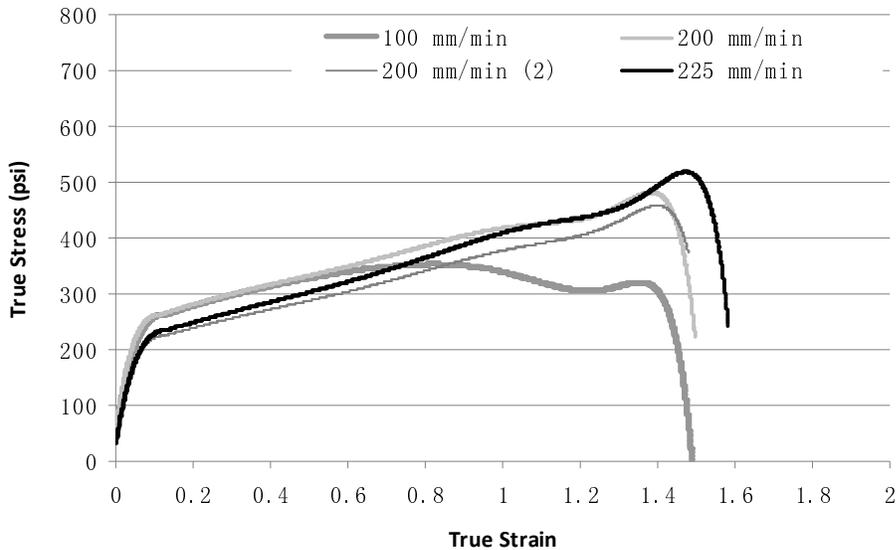
Figure 5-16 Marianni PAV residue, true stress vs. true strain

5.1.3.4 Comparison between rubber-modified binders

Typical true stress-true strain curves of each type of rubber-modified binder were plotted in Figure 5-17. In summary, for rubber-modified binders like ARB-5 and ARB-12 PAV residues, there is a first stress peak followed by an inflection instead of the second stress peak, while for recovered ARB-5, which lost its rubber during recovery, there was only the first stress peak. This result showed that the new direct tension test is able to identify rubber modifier by characteristic true stress-true strain curves.
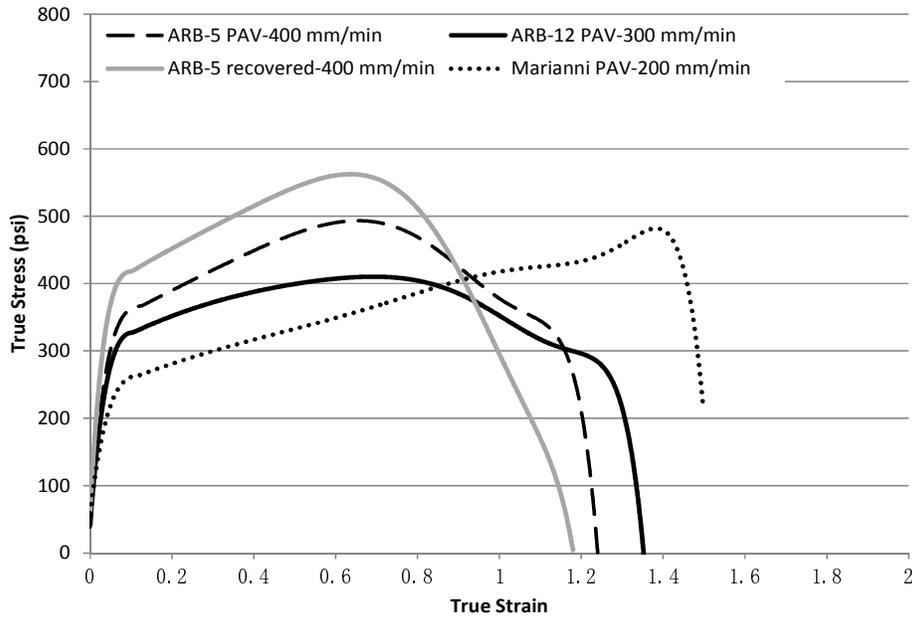
Figure 5-17 Rubber-modified binders, true stress vs. true strain

5.1.4 Hybrid Binders

Hybrid binders are modified with both polymer and rubber. Consequently, their true stress-true strain curve exhibited a second stress peak due to the existence of polymer. Differences were observed between true stress-true strain curves of different hybrid binders, depending on polymer and rubber content. However, each type of hybrid binder has similar true stress-true strain curve shapes.

5.1.4.1 Wright PAV residue

The polymer and rubber contents of Wright were not known. However, its true stress-true strain curve exhibited a very pronounced second stress peak (Figure 5-18), and its fracture energy was very high, which iindicates that it may contain relatively high polymer content. Its true stress-true strain curve shapes and fracture energy values were similar for tests performed at different loading rates.
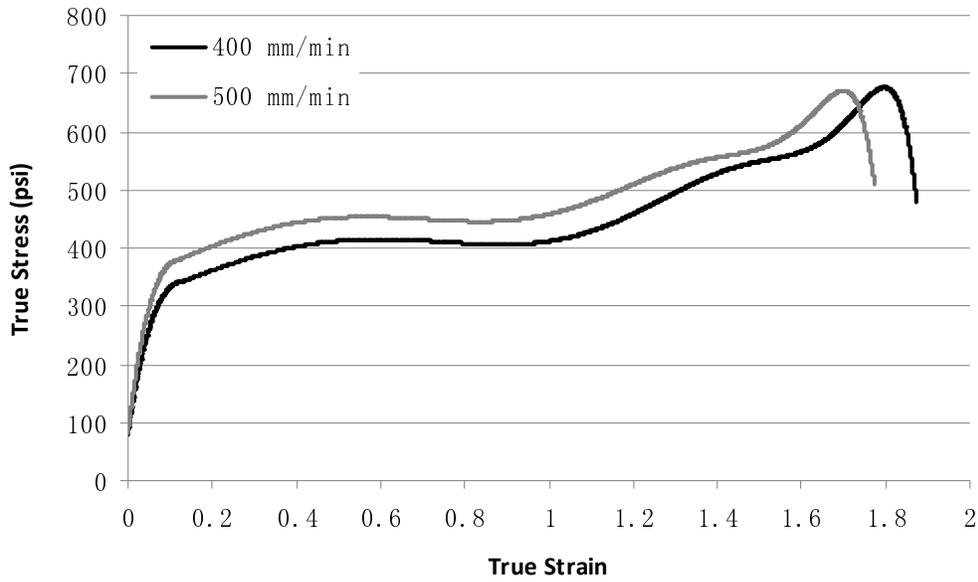
Figure 5-18 Wright PAV residue, true stress vs. true strain

5.1.4.2 Hudson PAV residue

As shown in Figure 5-19, Hudson also exhibited a clear second stress peak, due to the existence of polymer. (Hudson had 3.5% rubber and 2.5% SBS). It was interesting to note that even though its second stress peak was not as that of SBS-modified PG 76-22 (4.25% SBS), this particular combination of rubber and SBS resulted in higher fracture energy than that of the SBS-modified PG 76-22. Its true stress-true strain curve shapes were similar and fracture energy values was independent of loading rate.
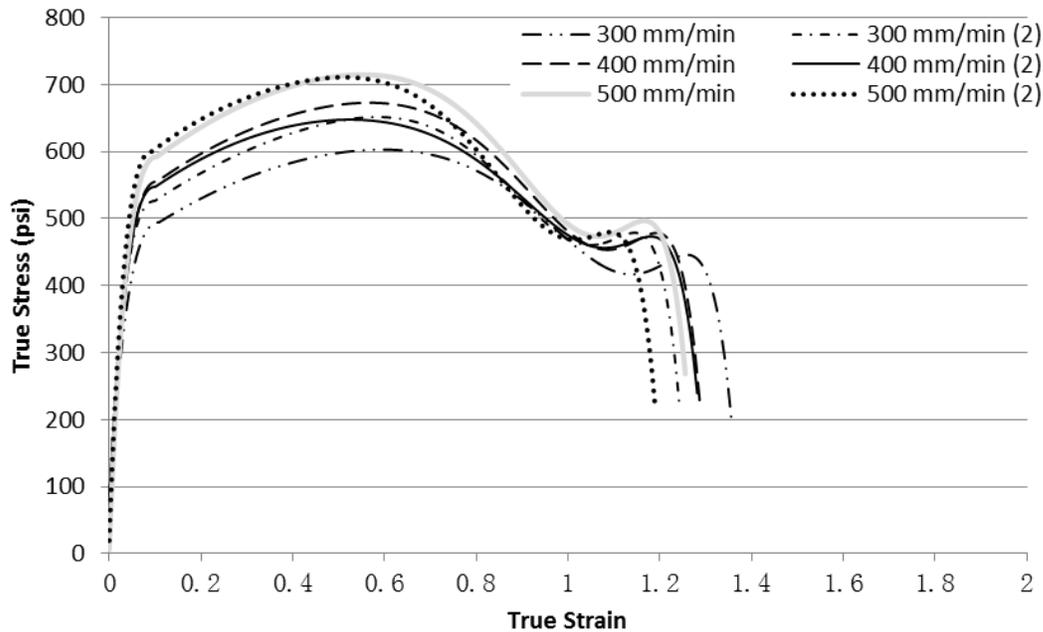
Figure 5-19 Hudson PAV residue, true stress vs. true strain

5.1.4.3 Geotech PAV residue

Geotech has 8% rubber and 1% SBS. Its second stress peak (Figure 5-20) was not as pronounced as that of PG 76-22 (4.25% SBS). Also, its fracture energy was less than that of other hybrid binders and SBS-modified binders. Figure 5-20 also illustrates that at lower loading rates, an inflection rather than a second stress peak was observed after the initial stress peak. It appears that the SBS content was insufficient, and this binder behaved more like a simple rubber-modified binder both in terms of true stress-true strain curve characteristics and fracture energy.
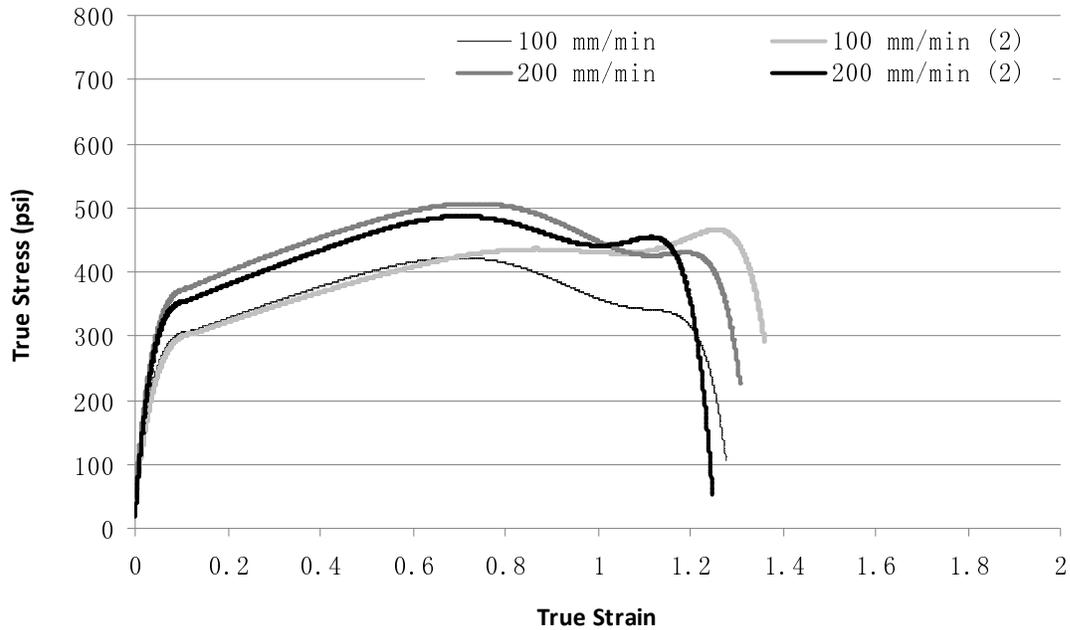
Figure 5-20 Geotech PAV residue, true stress vs. true strain

5.1.4.4 Comparison between hybrid binders

The typical true stress-true strain curves of hybrid binders shown in Figure 5-21 shows that all hybrid binders exhibited a second stress peak, which is characteristic of the presence of polymer in binder. However, due to different polymer and rubber contents, the true stress-true strain curves of hybrid binders exhibited different characteristics. It appears that hybrid binders with higher polymer content resulted in a more pronounced second stress peak, greater strain to fracture and higher fracture energy.
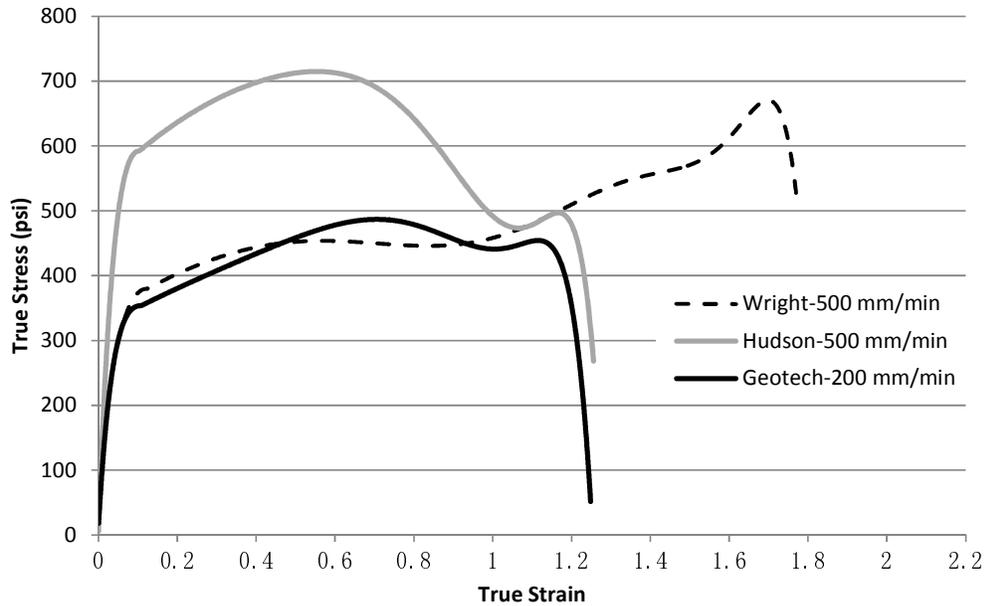
Figure 5-21 Hybrid binders, true stress vs. true strain

5.2 Comparison of True Stress-True Strain Curve between Binders

Since each type of binder has its own characteristic true stress-true strain curve, we can compare between them to reveal the differences. Figure 5-22 compares SBS-modified PG 76-22 to unmodified binders. Only PG 76-22 PAV residue was used, since its true stress-true strain curves were more consistent than those of recovered PG 76-22. PG 64-22 was selected as representative of unmodified binder for this comparison. Figure 5-22, clearly shows the true stress-true strain curve of SBS-modified PG 76-22 exhibits much greater strain to failure and a second stress peak. These differences result in the much higher fracture energy of SBS-modified PG 76-22.
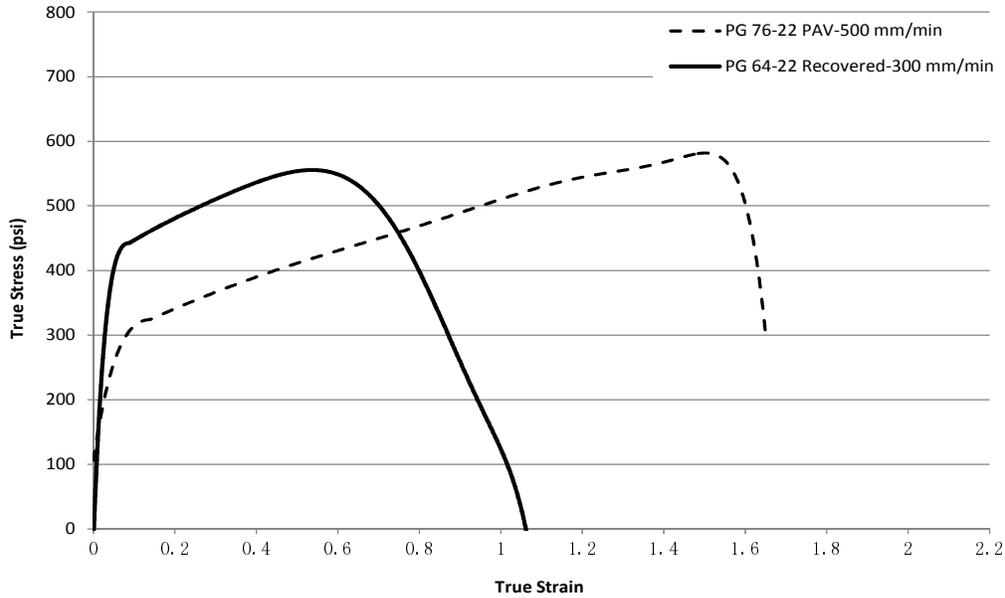
Figure 5-22 PG 76-22 and unmodified binder, true stress vs. true strain

Figure 5-23, includes the Hudson hybrid binder. The true stress-true strain curve of

Hudson (2.5% SBS, 3.5% rubber) exhibits lower failure strain than that of the SBS-modified PG

76-22 (4.25% SBS). However, it appears that the introduction of rubber in the Hudson binder

resulted in a higher peak stress. Thus, the fracture energy of Hudson was significantly higher

than that of unmodified binder, and slightly higher than that of SBS-modified PG 76-22.
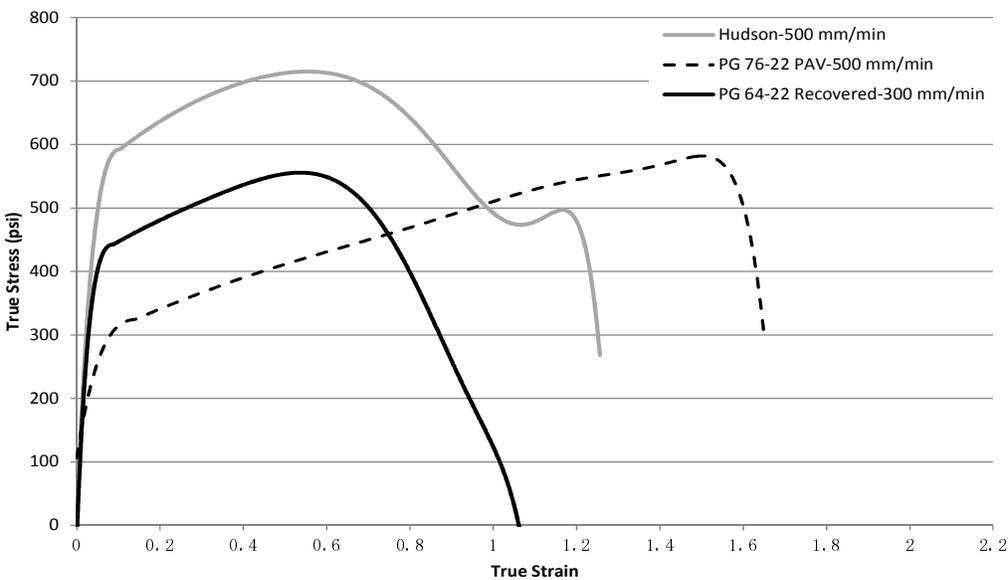
Figure 5-23 Comparison with Hudson, true stress vs. true strain
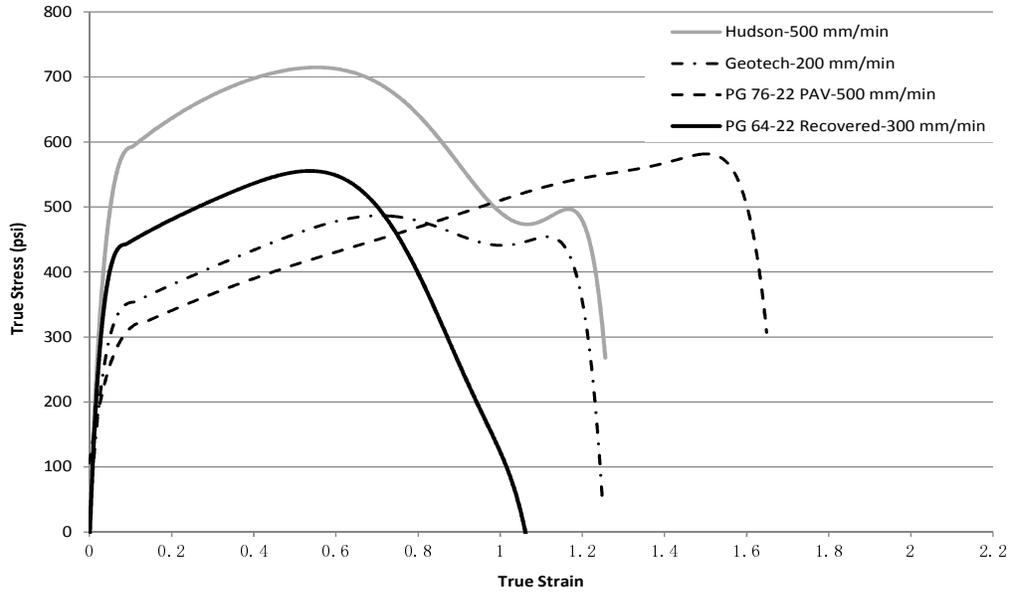
Figure 5-24 Comparison with Geotech, true stress vs. true strain

Figure 5-24 includes the Geotech hybrid binder (1% SBS, 8% rubber) for comparison. Due to the lower SBS content, the second stress peak of Geotech is not as pronounced as that of SBS-modified PG 76-22 or Hudson. Its peak stress was also lower (actually lower than the unmodified binder. Therefore, its fracture energy was less than that of SBS-modified PG 76-22 and Hudson.
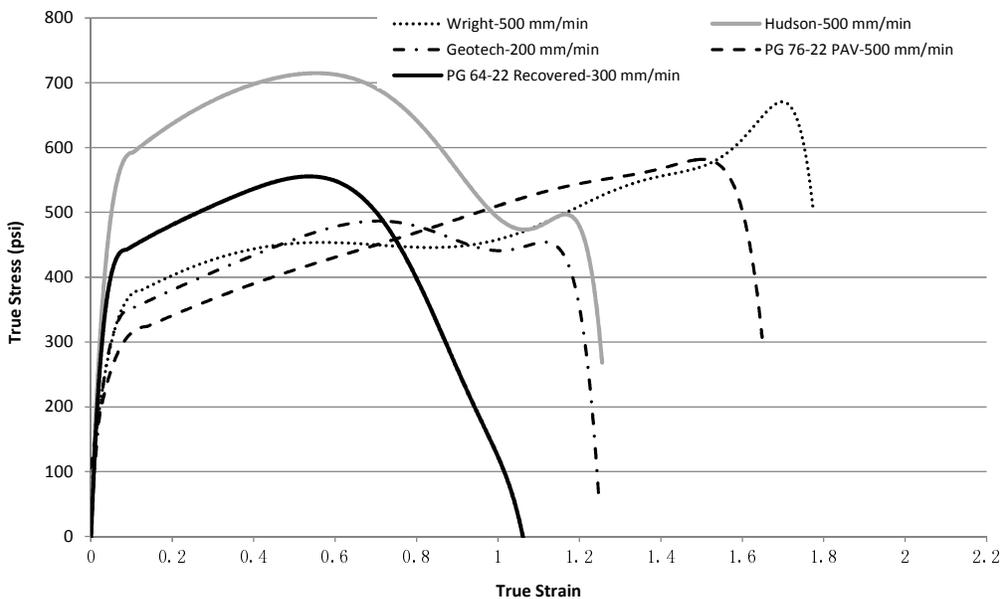
Figure 5-25 Comparison with Wright, true stress vs. true strain

Wright hybrid binder was included in Figure 5-25. Its second stress peak is most pronounced, and it exhibited the largest strain to failure of all binders. Although the actual contents are unknown, these results appear to clearly indicate that the Wright hybrid binder had a relatively high polymer content.

Since the true stress-true strain curves of ARB-5 and ARB-12 are very similar, only ARB-12 was introduced in Figure 5-26. The rubber in ARB-12 resulted in an inflection after the initial stress peak, instead of the second stress peak. In addition, its peak stress and failure strain were lower than for the hybrid binders and the SBS-modified PG 76-22, which resulted in the relatively low fracture energy of rubber-modified binder. It is clear that rubber alone cannot significantly increase fracture energy; it must be combined with polymer modifier to obtain a significant increase in fracture energy.
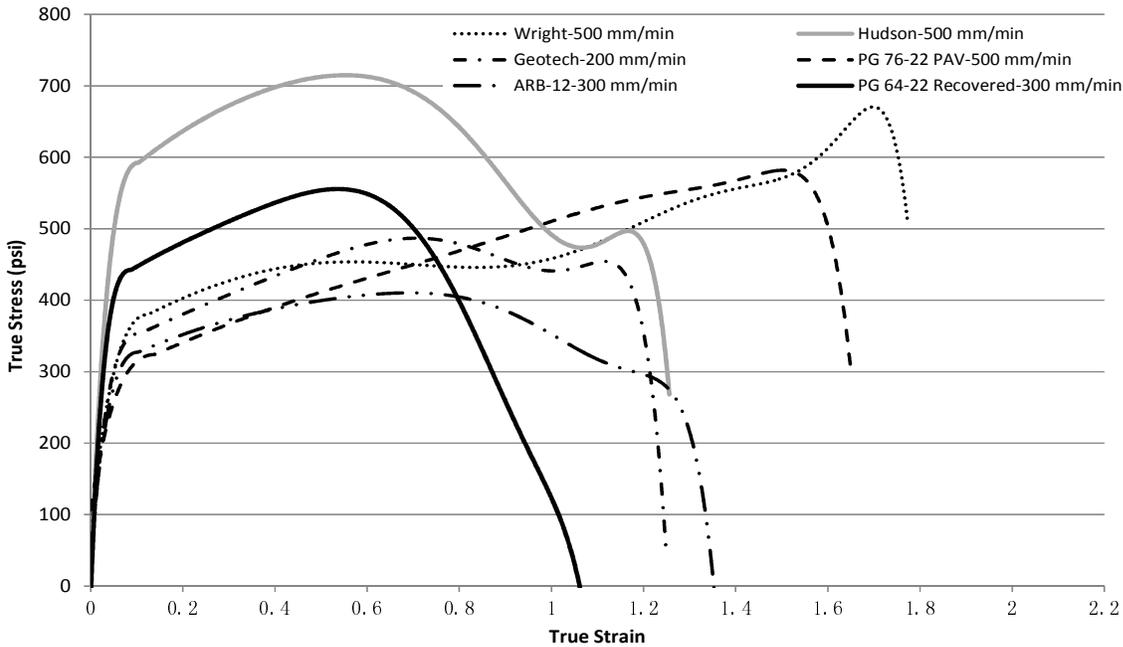
Figure 5-26 Comparison with ARB-12, true stress vs. true strain
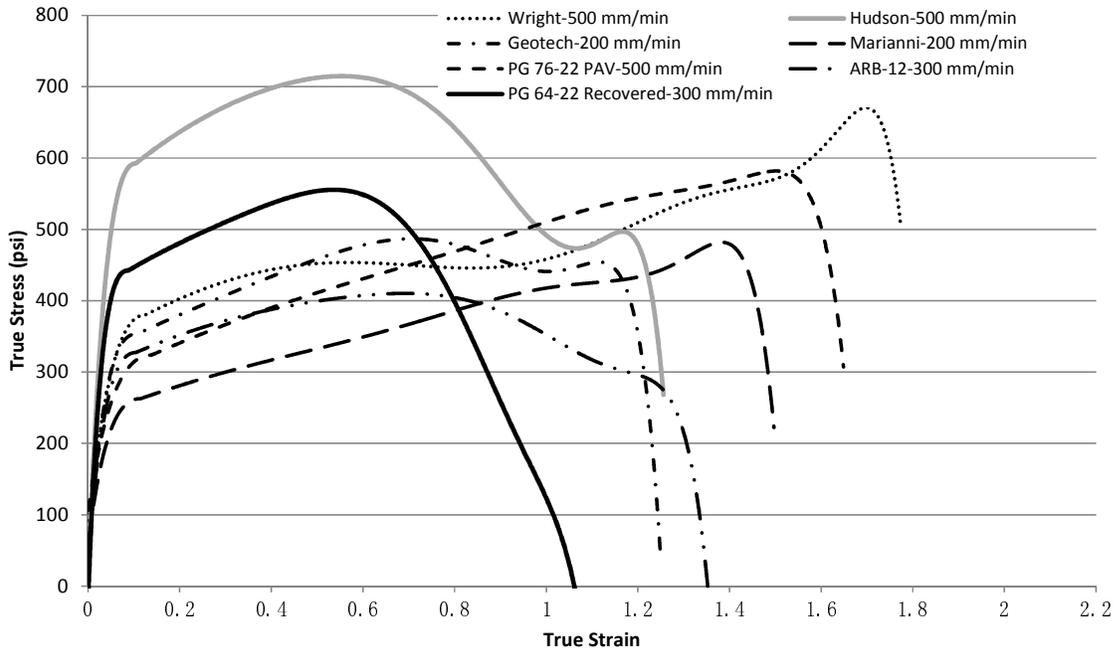
Figure 5-27 Comparison with Marianni, true stress vs. true strain

As shown in Figure 5-27, the true stress-true strain curve of the Marianni binder, which was reported to be modified with rubber only, exhibited characteristics of SBS-polymer-modified binder (i.e., a second stress peak and high failure strain). Therefore, it was suspected that this binder included polymer modifier. Its failure strain was less than that of SBS-modified PG 76-22, which may imply a lower polymer content.
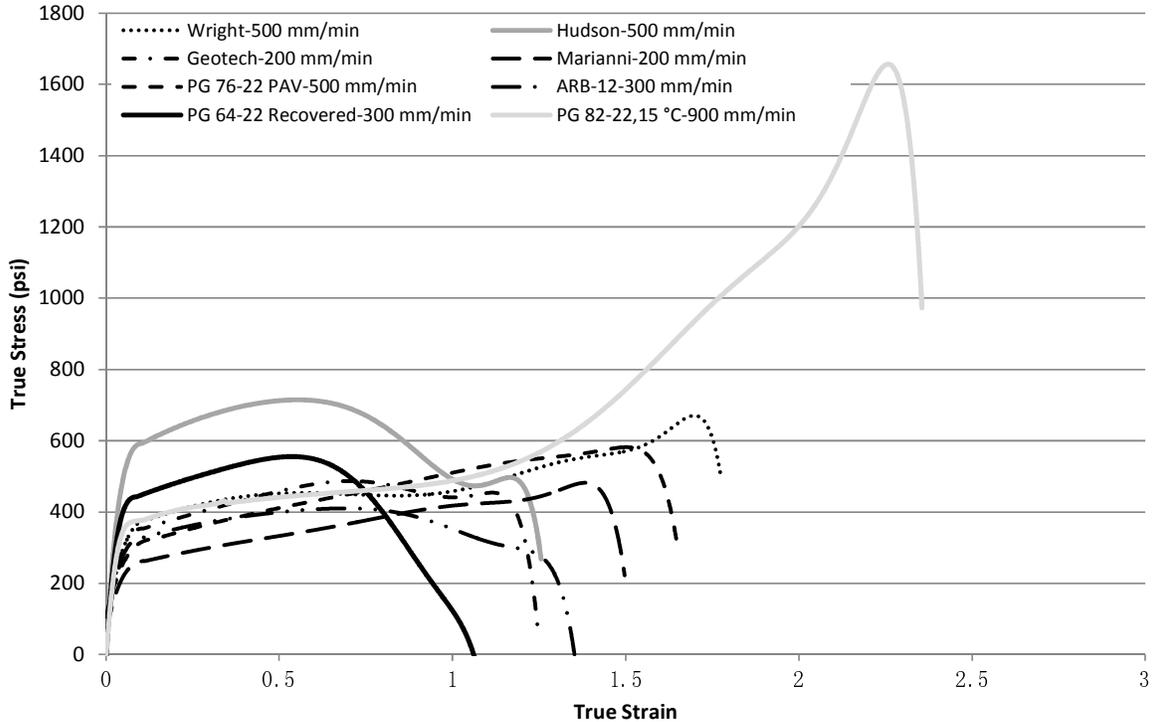
Figure 5-28 Comparison with PG 82-22, true stress vs. true strain

Finally, the true stress-true strain curve of PG 82-22 at 15°C was introduced in Figure 5-28.
The effect of the much higher SBS polymer content (8.5%) was clear, exhibiting much higher
peak stress, strain to failure and fracture energy than all other binders.

5.3 Summary of Characteristic True Stress-True Strain Curves

The principles listed below may be used to identify the binder type, modifier type and
relative content.

1.   Each type of binder has its own characteristic true stress-true strain curve.

2.   Generally, there are two stress peaks on the true stress-true strain curve of SBS polymer-
      modified binder. The first stress peak is within a strain of 1 (usually around 0.5), while the
      second stress peak occurs at a strain greater than 1 (usually between 1.2 and 1.8)

3.   Unmodified binders only have the first stress peak.

4.   At lower polymer contents, the second stress peak may not be present at low loading rates
      and only an inflection is present after the first stress peak. Although a second stress peak
      may be observed at higher loading rates, the peak stress, failure strain, and fracture energy
      of low polymer content binder is low (not much greater than for unmodified binder).

80

5. Some polymer-modified binders do not exhibit a very pronounced initial stress peak, but rather a continuously increasing stress to failure at high strain levels.

6. Polymer-modified binders' true stress-true strain curve typically exhibit higher strain to failure that that of unmodified and rubber-modified binders. Higher polymer content increases the failure strain and the makes the second stress peak more pronounced, which leads to a higher fracture energy.

7. The existence of both a second stress peak (or continuously increasing stress) and high fracture energy appear to identify the existence of polymer in binder.

8. Rubber-modified binders exhibit only an inflection after the first stress peak instead of a second stress peak.

9. The rubber-modified binders' fracture energy is usually lower than those with polymer modifier. The polymer modifier is needed to obtain high fracture energy.

10. Some hybrid binders (e.g., Hudson) exhibit higher fracture energy with a lower polymer content compared to conventional SBS polymer-modified binder (e.g., PG 76-22).

11. Sometimes the specimen of rubber-modified binder which has been heated many times also exhibits a second peak. However, its peak stress is very low, and its fracture energy is far smaller than that of normal specimens. Therefore, it is very easy to identify it, and would not be confused with binders comprising SBS polymer.

12. There appears to be a typical range of fracture energy associated with each type of binder, which can assist to identify binders in case the curve shape is abnormal or confusing. A typical

The use of characteristic true stress-true strain curves to distinguish polymer-modified binder from unmodified binder is another accomplishment resulted from development of a test to measure fracture energy. The characteristic curve may be used as a potential supplement or substitute for MSCR test.

Table 5-1 Typical ranges of FE density values and features of characteristic stress-strain curves associated with each type of the binders

Binders	% SBS	% Rubber	FE Density (psi)	First stress peak	Second stress peak	Inflection point
Unmodified	0	0	200-300	YES	NO	NO
Rubber-modified	0	5-13	400-500	YES	NO	YES
SBS-modified	4.25	0	600-700	YES[1]	YES	NO
	8.5	0	1600-1700	YES	YES	NO
Hybrid	1-2.5 or higher	3.5-8	400-800	YES	YES[2]	NO[2]

Note: (1) Some polymer-modified binders do not exhibit a pronounced initial stress peak, but rather a continuously increasing stress to failure at high strain levels. (2) At lower polymer contents, an inflection may be present instead of a second stress peak. Higher loading rates are usually required to make the second stress peak present.

5.4 Fracture Energy Determination

In Chapter 3.2 "Data Interpretation", it was mentioned that fracture energy should be calculated from the beginning of true stress-true strain curve to the last stress peak, which is the point of initial fracture. Now with the knowledge of characteristic true stress-true strain curves, this issue can now be discussed in further detail.

Some researchers calculate fracture energy based on the area under the whole true stress-true strain curve from beginning to end. Theoretically, this may be correct. However, in actual testing, this may not be appropriate. During extension to failure, localized fracture occurs somewhere in the cross-section first, before the specimen completely ruptures or splits into two pieces. Therefore, the energy beyond the point of first fracture, which usually occurs at peak stress in a direct tension specimen, is energy associated with breaking the remainder of the specimen cross-section after fracture has already occurred. Therefore, it is meaningless to include the energy beyond first fracture as part of the energy required to induce fracture (i.e., the fracture energy).
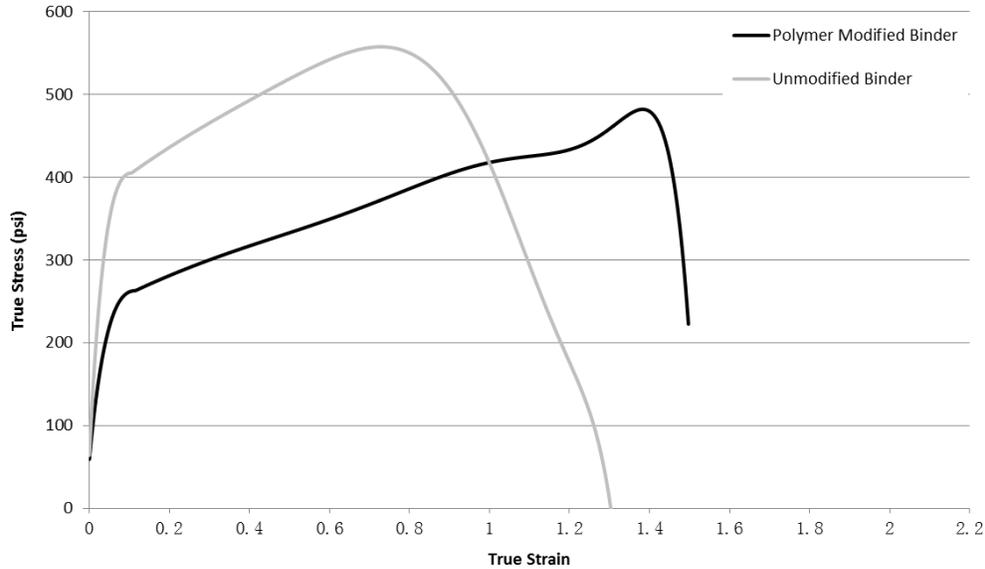
Figure 5-29 True stress vs. true strain, polymer-modified (reduced size) and unmodified binder

Figure 5-29 shows the typical shape of true stress-true strain curves of polymer-modified

and unmodified binders, except that stress and strain values were intentionally artificially

reduced for the case of the polymer-modified binder. Now, assume the areas below these two

curves are exactly the same. Would their fracture energy be the same? The answer is absolutely

not. For the unmodified binder, a large part of fracture energy is from the area after stress peak

associated with initial fracture. Because fracture has already occurred, the stresses and strain

beyond this peak are impossible to determine accurately, and are associated with crack growth.

Therefore, calculating the fracture energy using the entire area under the stress-strain curve

would significantly overestimate the fracture energy of the unmodified binder. For the polymer-

modified binder, the fracture energy is from the area up to the second stress peak, before which

fracture had not been initiated.

CHAPTER 6
RECOMMENDED TESTING PROTOCOL

The general testing protocol outlined below is recommended based on all binder tests

performed in this research project.

6.1 Preparation

1. At least six specimens should be prepared for each binder type using molds and loading
    heads with specimen geometry developed in this study.

    •   Binder should be heated to allow it to be easily poured into mold with de-bonding
        agent. Great care must be taken to prevent bubbles from developing within
        specimens.

    •   The lowest temperature and heating time possible should be used, which will of
        course, depend on binder type and age.

    •   Each specimen should remain in mold until immediately prior to testing.

2. Specimens in molds should be placed in a temperature controlled chamber set to the
    desired test temperature (usually 15°C). This should preferably be the same chamber
    containing the loading frame to be used for testing.

3. Immediately prior to testing, carefully de-mold specimen. Great care must be taken in
    order not to deform, even slightly, the specimen during de-molding.

    •   Specimen should easily release from molds or should be discarded if it sticks to the
        mold during de-molding.

    •   Specimens must be de-molded with the specimen suspended in a vertical position to
        ensure that no bending is induced prior to testing. This is accomplished by holding
        the specimen by one of the loading heads.

4. This loading head should then be carefully inserted into the upper loading head slot on the
    load frame. The specimen is now suspended vertically on the upper fixture of the load
    frame.

5. The suspended specimen should then be very carefully lowered so that the lower loading
    head on the specimen is inserted into the lower loading head slot on the load frame.

6.2 Testing and Analysis

1. Allow the test chamber to equilibrate at the test temperature (usually 15°C).

2. Perform the first test using a loading rate of 500 mm/min. If the test results in a complete
    stress-strain curve, then the results are acceptable. If an incomplete stress-strain curve or

excessively low fracture energy density is observed, then the specimen fractured prematurely, and the loading rate should be reduced until acceptable results are obtained.

3. The test should then be repeated using the above procedures on a different test specimen at the same loading rate (two replicates should be performed at each loading rate). The difference in fracture energy density between the two specimens should be less than 15% based on the lower of the two fracture energy density values. If greater than 15%, then additional should be tested until the difference between two specimens is within 15%.

4. If premature fracture still occurs at 50 mm/min, then increase test temperature to 20°C. Conversely, if the specimen does not fracture, then the loading rate should be increased until fracture is observed. If the specimen still does not fracture at 700 mm/min, then decrease the temperature to 10°C.

CHAPTER 7
CLOSURE

7.1 Summary and Findings

This study was conducted to develop a binder direct tension test and associated data interpretation methods that allow for accurate determination of binder fracture energy at intermediate temperatures. The work involved three main tasks: 1) Developing a binder testing system; 2) Evaluating the new system; 3) Exploring other uses for the new system. The work conducted and associated findings are summarized below.

A new binder fracture energy test was developed based on nonlinear 3-D FEA to identify and optimize an appropriate specimen geometry that assures accurate determination of stress and strain on the fracture plane, which in turn assures accurate determination of fracture energy. The feasibility and validity of different specimen geometries identified were evaluated by conducting prototype direct tension tests using a servo-hydraulic loading frame in a temperature-controlled environment.

A data interpretation system was established based on both nonlinear FEA and large strain formulation. A set of diagrams were proposed based on nonlinear FEA results for convenience of performing the calculation procedure. In preliminary evaluations, the new fracture energy test and data interpretation system were shown to provide consistent and repeatable fracture energy of binder at intermediate temperatures.

Then, the new fracture energy test and data interpretation system were applied to a range of binders for a more comprehensive evaluation, including unmodified binders, SBS-modified binder, rubber-modified binders, hybrid binders, highly SBS-modified binder from PAV residue, as well as binders recovered from field test sections. For each binder, tests were performed at

multiple loading rates and temperatures. Findings for this phase of the work are summarized below.

- Statistical analysis showed the new fracture energy test and data interpretation system significantly distinguished between different binders by fracture energy values. Expected trends in fracture energy between binders were observed.

- Statistical analysis also showed that for a given binder, fracture energy was independent of loading rates evaluated in this study and test temperatures from 0 to 15°C. Thus, fracture energy appears to be a fundamental property of binder, which does not depend on test condition, and can be determined by tests performed at a single temperature and loading rate.

- It was also determined that erroneous results may occur if excessively high or low loading rates are used. A detailed testing protocol was recommended that helps assure tests are performed at appropriate loading rate ranges within which accurate fracture energy is obtained. In addition, it was determined that erroneous tests resulting from inappropriate loading rates can be identified by way of the characteristics of the resulting true stress-true strain curve.

- The characteristic shape of the true stress-true strain curve from the fracture energy test was found to be closely related to binder type, including presence of modifier or rubber and relative content. Therefore, the true stress-true strain curve can be used to identify the binder type, modifier type and relative content. Basic principles for interpretation of the true stress-true strain curves were proposed for this purpose.

- Finally, the fracture energies of all binders tested may be ranked as described below:

  - The highly polymer-modified binder PG 82-22 had significantly greater fracture energy than all other binders tested.

- All hybrid binders had fracture energy higher than that of unmodified binders, and they either exhibited fracture energy higher than (i.e., Wright and Hudson) or comparable to that of the SBS-modified binder (PG 76-22). Some hybrid binders (e.g., Hudson) exhibited higher fracture energy with a lower polymer content compared to the SBS-modified binder.
- The rubber-modified binders had fracture energy slightly greater than unmodified binders, but lower than other modified binders. Therefore, it appeared that polymer modifier is necessary to substantially increase binder fracture energy.

7.2 Conclusions

The following key conclusions were drawn based on findings of this study:

- The new binder fracture energy test and data interpretation system developed appears to suitably measure fracture energy of unmodified and modified binders.

- It appears that the presence and relative content of modifier or rubber may be detectable from the test results.

7.3 Recommendations and Future Work

Based on extensive evaluations performed in this study, recommendations for further implementation of this work are summarized below:

- The retrofit of existing binder direct tension test devices to perform the test developed.

- Further use and evaluation of the test to determine binder damage rates and fracture properties of mastic.

- Further use of the test to develop relationships to predict fracture resistance of mixture, and to identify and develop binder guideline/specifications that optimize fracture resistance of mixture.

LIST OF REFERENCES

Anderson, D. A., Lapalu, L., Marasteanu, M.O., Hir, Y. M. L, Planche, J. P., and Martin, D. , "Low-temperature thermal cracking of asphalt binders as ranked by strength and fracture properties" Journal of the Transportation Research Board, Volume 1766, page 1-6, 2001.

Anderson, T.L., Fracture mechanics: fundamentals and applications, 3rd Ed., CRC Press, 2005.

Andriescu, A., Hesp, S.A., and Youtcheff, J.S., "Essential and plastic works of ductile fracture in asphalt binders" Journal of the Transportation Research Board, Volume 1875, page 1-7, 2004.

ASTM D 6521, "Standard practice for accelerated aging of asphalt binder using a pressurized aging vessel (PAV)" Annual Book of ASTM Standards 04.03, ASTM International, West Conshohocken, PA, 2004.

ASTM D 6723, "Standard method of test for determining the fracture properties of asphalt binder in direct tension (DT)" Annual Book of ASTM Standards 04.03, ASTM International, West Conshohocken, PA, 2001.

Bahia, H., Wen, H., and Johnson, C.M., "Developments in intermediate-temperature binder specifications" Transportation Research Circular, E-C147, December, 25-33, 2010.

Hoare, T. R., and Hesp, S.A., "Low-temperature fracture testing of asphalt binders" Journal of the Transportation Research Board, Volume 1728 /2000, page 36-42, 2000.

Janssen, M., Zuidema, J., and Wanhill, R.J.H., Fracture Mechanics, 2nd Ed., VSSD, The Netherlands, 2002-2006.

Ponniah, J.E., Cullen, R.A., and Hesp, S.A., "Fracture energy specifications for modified asphalts" Preprints of Papers, Journal Volume 41, Journal Issue 4, Conference 212, National meeting of the American Chemical Society (ACS), Orlando, FL, USA, 25-30 August 1996.

Roque, R., Birgisson, B., Drakos, C., and Dietrich, B., "Development and Field Evaluation of Energy-Based Criteria for Top-down Cracking Performance of Hot Mix Asphalt" Journal of the Association of Asphalt Paving Technologists, Volume 73, page 229-260, 2004.

Roque, R., Lopp, G., Li, W., and Niu, T., "Evaluation of hybrid binder use in surface mixtures in Florida" Final report for FDOT BD-545 Contract, University of Florida, Gainesville, FL, 2009.

Rosales, Alejandro, "Fracture energy method for determining stiffness in polymer modified asphalt binders using the single edge notched beam," *McNair Scholars Research Journal:* Vol. 7: Iss. 1, Article 15, 2011.

SAS Institute Inc., SAS 9.3 Help and Documentation, Cary, NC, USA, 2002-2011

APPENDIX A
PRELIMINARY TEST RESULTS

Table A-1 Fracture energy (FE) density at 15°C (PAV residue)

Binder	Loading Rate (mm/min)	Fracture Energy Density (psi)	Extension to Fracture (in)
PG 76-22	700	660.88	0.4590
PG 76-22	700	591.68	0.3984
PG 76-22	600	629.77	0.4433
PG 76-22	600	657.43	0.4616
PG 76-22	500	676.20	0.4873
PG 76-22	500	617.37	0.4654
PG 76-22	400	609.91	0.4776
PG 76-22	400	563.09	0.4663
PG 76-22	300	584.18	0.4663
PG 76-22	300	576.03	0.4823
PG 67-22	700	244.10	0.1489
PG 67-22	600	235.05	0.1489
PG 67-22	600	220.70	0.1449
PG 67-22	500	251.31	0.1579
PG 67-22	400	233.65	0.1706
PG 67-22	400	244.32	0.1632
PG 67-22	300	195.30	0.1733
PG 67-22	300	205.61	0.1736

Table A-2 Fracture energy density at 10°C (PAV residue)

Binder	Loading Rate (mm/min)	Fracture Energy Density (psi)	Extension to Fracture (in)
PG 76-22	1480	598.17	0.2025
PG 76-22	1448	714.78	0.2530
PG 76-22	1445	780.47	0.2448
PG 76-22	985	722.72	0.2900
PG 76-22	600	650.26	0.2565
PG 76-22	600	713.35	0.3028
PG 76-22	500	680.86	0.3214
PG 76-22	500	696.24	0.3302
PG 76-22	400	770.25	0.3579
PG 76-22	400	707.09	0.3284
PG 76-22	200	667.98	0.3911
PG 76-22	200	616.38	0.3454
PG 76-22	100	506.69	0.3976
PG 76-22	100	572.01	0.4408
PG 76-22	50	518.84	0.5033
PG 76-22	50	478.63	0.4659
PG 67-22	600	235.13	0.0981
PG 67-22	400	208.26	0.1065
PG 67-22	150	246.97	0.1522
PG 67-22	100	210.34	0.1552
PG 67-22	100	206.89	0.1679
PG 67-22	50	168.93	0.1679
PG 67-22	50	168.41	0.1737
PG 67-22	25	221.93	0.2138
PG 67-22	25	238.98	0.2134

Table A-3 Fracture energy density at 5°C (PAV residue)

Binder	Loading Rate (mm/min)	Fracture Energy Density (psi)	Extension to Fracture (in)
PG 76-22	300	745.88	0.2345
PG 76-22	250	666.28	0.1893
PG 76-22	250	707.36	0.2410
PG 76-22	200	770.40	0.2601
PG 76-22	150	757.41	0.2625
PG 76-22	100	579.69	0.3040
PG 76-22	50	651.57	0.3543
PG 76-22	50	608.14	0.3195
PG 76-22	25	546.49	0.3628
PG 76-22	25	560.17	0.3743
PG 67-22	35	238.61	0.1358
PG 67-22	35	234.91	0.1456
PG 67-22	25	243.48	0.1367
PG 67-22	25	238.41	0.1509
PG 67-22	10	171.07	0.1844
PG 67-22	10	147.88	0.1598
PG 67-22	5	138.76	0.1823
PG 67-22	5	131.05	0.1920

Table A-4 Fracture energy density at 0°C (PAV residue)

Binder	Loading Rate (mm/min)	Fracture Energy Density (psi)	Extension to Fracture (in)
PG 76-22	100	716.12	0.1884
PG 76-22	30	594.14	0.2461
PG 76-22	30	612.28	0.2455
PG 76-22	25	605.56	0.2535
PG 76-22	25	612.14	0.2408
PG 76-22	20	606.05	0.2619
PG 76-22	15	600.74	0.2699
PG 76-22	10	424.06	0.2852
PG 76-22	10	397.60	0.2747

TEST RESULTS OF BINDERS RECOVERED FROM SUPERPAVE SECTIONS

Table B-1 Test results of binders recovered from Superpave Project 1

Location	Layer	Source	SMO Lab No.	Binder Type	Fracture Energy Density @ 15°C (psi)		
					Loading Rate (mm/min)	FE Density	Extension (in)
5	A	WP	19234	AC-30	300	354.82	0.1827
				AC-30	500	373.63	0.1693
		BWP	19235	AC-30	500	374.21	0.1530
				AC-30	500	345.66	0.1507
	B	WP	19236	AC-30	500	313.02	0.1877
				AC-30	500	316.01	0.1828
		BWP	19237	AC-30	500	341.04	0.1871
				AC-30	500	324.73	0.1856
15	A	WP	19238	AC-30	500	406.01	0.1615
				AC-30	500	400.87	0.1499
		BWP	19239	AC-30	500	371.94	0.1658
				AC-30	500	376.52	0.1745
	B	WP	19240	AC-30	500	321.51	0.1908
				AC-30	500	283.12	0.1762
		BWP	19241	AC-30	500	348.64	0.1815
				AC-30	500	331.02	0.1903

Table B-2 Test results of binders recovered from Superpave Project 2

Location	Layer	Source	SMO Lab No.	Binder Type	Fracture Energy Density @ 15°C (psi)		
					Loading Rate (mm/min)	FE Density	Extension (in)
5	A	WP	19242	AC-20	500	275.85	0.1686
				AC-20	700	306.48	0.1712
		BWP	19243	AC-20	500	249.98	0.1896
				AC-20	500	271.33	0.2074
	B	WP	19244	AC-20	500	268.67	0.2014
				AC-20	500	272.02	0.1999
		BWP	19245	AC-20	500	288.01	0.2084
				AC-20	500	284.45	0.2001
15	A	WP	19246	AC-20	500	337.11	0.1978
				AC-20	500	316.71	0.1819
		BWP	19247	AC-20	500	266.64	0.1952
				AC-20	500	297.24	0.1994
	B	WP	19248	AC-20	500	256.31	0.2171
				AC-20	500	234.13	0.2153
		BWP	19249	AC-20	500	231.44	0.2223
				AC-20	500	243.92	0.2134
25	A	WP	19250	AC-20	500	249.17	0.2214
				AC-20	500	253.20	0.2169
		BWP	19251	AC-20	500	274.90	0.2184
				AC-20	500	244.38	0.2175
	B	WP	19252	AC-20	500	220.76	0.2131
				AC-20	500	228.14	0.2122
		BWP	19253	AC-20	500	258.22	0.2138
				AC-20	500	233.79	0.2123

Table B-3 Test results of binders recovered from Superpave Project 3

Location	Layer	Source	SMO Lab No.	Binder Type	Fracture Energy Density @ 15°C (psi)		
					Loading Rate (mm/min)	FE Density	Extension (in)
5	A	WP	19254	AC-30	500	348.12	0.1547
				AC-30	500	313.90	0.1443
		BWP	19255	AC-30	500	342.96	0.1540
				AC-30	500	350.69	0.1613
	B	WP	19256	AC-30	500	324.03	0.1460
				AC-30	500	341.37	0.1502
		BWP	19257	AC-30	500	264.98	0.1941
				AC-30	500	238.36	0.1953
25	A	WP	19258	AC-30	500	332.63	0.1599
				AC-30	500	324.34	0.1673
		BWP	19259	AC-30	500	292.97	0.1623
				AC-30	500	340.23	0.1643
	B	WP	19260	AC-30	500	317.27	0.1708
				AC-30	500	312.13	0.1718
		BWP	19261	AC-30	500	354.75	0.1740
				AC-30	500	346.96	0.1726

Table B-4 Test results of binders recovered from Superpave Project 4

Location	Layer	Source	SMO Lab No.	Binder Type	Fracture Energy Density @ 15°C (psi)		
					Loading Rate (mm/min)	FE Density	Extension (in)
5	A	WP	19262	AC-30	500	273.75	0.1629
				AC-30	500	260.33	0.1458
		BWP	19263	AC-30	500	275.65	0.1416
				AC-30	500	264.24	0.1407
	B	WP	19264	AC-30	500	315.70	0.1601
				AC-30	500	290.19	0.1567
		BWP	19265	AC-30	500	274.25	0.1842
				AC-30	500	283.35	0.1757
15	A	WP	19266	AC-30	500	276.64	0.1487
				AC-30	500	277.76	0.1630
		BWP	19267	AC-30	500	258.77	0.1741
				AC-30	500	220.85	0.1651
	B	WP	19268	AC-30	500	362.03	0.1584
				AC-30	500	340.02	0.1434
		BWP	19269	AC-30	500	315.42	0.1677
				AC-30	500	290.62	0.1610
18	A	WP	19270	AC-30	500	275.21	0.1632
				AC-30	500	263.98	0.1652
		BWP	19271	AC-30	500	286.17	0.1594
				AC-30	500	279.80	0.1559
	B	WP	19272	AC-30	500	307.07	0.1472
				AC-30	600	332.70	0.1466
		BWP	19273	AC-30	500	212.03	0.1863
				AC-30	500	247.83	0.1820
				AC-30	500	237.40	0.1898
25	A	WP	19274	AC-30	500	306.78	0.1362
				AC-30	500	312.64	0.1331
		BWP	19275	AC-30	500	267.82	0.1430
				AC-30	500	279.98	0.1460
	B	WP	19276	AC-30	500	320.08	0.1683
				AC-30	500	254.72	0.1587
		BWP	19277	AC-30	500	297.74	0.1762
				AC-30	500	303.20	0.1757

Table B-5 Test results of binders recovered from Superpave Project 6

Location	Layer	Source	SMO Lab No.	Binder Type	Fracture Energy Density @ 15°C (psi)		
					Loading Rate (mm/min)	FE Density	Extension (in)
5	A	WP	20366	AC-20	-	-	-
				AC-20	-	-	-
		BWP	20367	AC-20	-	-	-
				AC-20	-	-	-
15	A	WP	20368	AC-20	800	284.93	0.1488
				AC-20	800	300.40	0.1507
		BWP	20369	AC-20	800	283.07	0.1318
				AC-20	800	302.73	0.1332
25	A	WP	20370	AC-20	800	276.92	0.1483
				AC-20	1000	263.34	0.1424
		BWP	20371	AC-20	1000	256.69	0.1457
				AC-20	-	-	-

Table B-6 Test results of binders recovered from Superpave Project 7

Location	Layer	Source	SMO Lab No.	Binder Type	Fracture Energy Density @ 15°C (psi)		
					Loading Rate (mm/min)	FE Density	Extension (in)
5	A	WP	20372	AC-20	1000	290.47	0.1293
				AC-20	1000	288.45	0.1289
		BWP	20373	AC-20	1000	277.09	0.1133
				AC-20	1000	275.36	0.1137
	B	WP	20374	AC-20	1000	263.55	0.1436
				AC-20	1000	253.29	0.1482
		BWP	20375	AC-20	1000	330.95	0.0950
				AC-20	1000	301.99	0.0966
15	A	WP	20468	AC-20	600	265.22	0.1311
				AC-20	500	264.70	0.1470
		BWP	20469	AC-20	500	282.02	0.1184
				AC-20	-	-	-
	B	WP	20470	AC-20	600	240.69	0.1529
				AC-20	800	252.10	0.1411
		BWP	20471	AC-20	900	267.07	0.1374
				AC-20	1200	247.42	0.1273

Table B-7 Test results of binders recovered from Superpave Project 8

Location	Layer	Source	SMO Lab No.	Binder Type	Fracture Energy Density @ 15°C (psi)		
					Loading Rate (mm/min)	FE Density	Extension (in)
15	A	WP	19278	PG 76-22	500	525.79	0.5902
				PG 76-22	500	550.19	0.5981
				PG 76-22	800	683.74	0.5089
		BWP	19279	PG 76-22	500	511.65	0.3847
				PG 76-22	500	525.85	0.3632
				PG 76-22	800	657.45	0.3321
	B	WP	19280	PG 76-22	500	649.47	0.5277
				PG 76-22	500	659.97	0.5014
				PG 76-22	800	679.76	0.4836
		BWP	19281	PG 76-22	500	601.64	0.5232
				PG 76-22	500	590.34	0.5081
22	A	WP	19282	PG 76-22	500	575.93	0.3438
				PG 76-22	500	629.64	0.3316
		BWP	19283	PG 76-22	500	571.15	0.3358
				PG 76-22	500	544.56	0.4006
	B	WP	19284	PG 76-22	500	850.44	0.8202
				PG 76-22	500	799.50	0.8268
		BWP	19285	PG 76-22	500	641.59	0.4433
				PG 76-22	500	608.92	0.4611
25	A	WP	19286	PG 76-22	700	594.14	0.2696
				PG 76-22	500	520.96	0.2764
		BWP	19287	PG 76-22	500	600.92	0.3161
				PG 76-22	500	476.88	0.3786
	B	WP	19288	PG 76-22	500	527.96	0.3245
				PG 76-22	700	613.15	0.4026
		BWP	19289	PG 76-22	500	561.89	0.3315
				PG 76-22	500	581.31	0.3326

Table B-8 Test results of binders recovered from Superpave Project 9

Location	Layer	Source	SMO Lab No.	Binder Type	Fracture Energy Density @ 15°C (psi)		
					Loading Rate (mm/min)	FE Density	Extension (in)
15	A	WP	19290	ARB-5	500	296.03	0.0908
				ARB-5	300	285.54	0.1002
		BWP	19291	ARB-5	-	-	-
				ARB-5	-	-	-
	B	WP	19292	PG 64-22	300	245.60	0.1631
				PG 64-22	300	254.12	0.1510
		BWP	19293	PG 64-22	300	265.58	0.1390
				PG 64-22	300	278.33	0.1508
25	A	WP	19294	ARB-5	300	266.84	0.1038
				ARB-5	300	265.40	0.1028
		BWP	19295	ARB-5	300	219.77	0.1103
				ARB-5	300	253.30	0.1107
	B	WP	19296	PG 64-22	300	233.65	0.1471
				PG 64-22	300	237.91	0.1464
		BWP	19297	PG 64-22	300	247.32	0.1371
				PG 64-22	300	257.89	0.1346

Table B-9 Test results of binders recovered from Superpave Project 10

Location	Layer	Source	SMO Lab No.	Binder Type	Fracture Energy Density @ 15°C (psi)		
					Loading Rate (mm/min)	FE Density	Extension (in)
5	A	WP	19298	ARB-5	100	282.47	0.1246
				ARB-5	100	288.71	0.1097
				ARB-5	100	283.52	0.1176
		BWP	19299	ARB-5	50	202.48	0.1431
				ARB-5	100	248.56	0.1310
	B	WP	19300	PG 64-22	100	314.91	0.1045
				PG 64-22	100	279.50	0.1049
				PG 64-22	100	339.88	0.0944
		BWP	19301	PG 64-22	100	268.13	0.1383
				PG 64-22	100	232.96	0.1234
15	A	WP	19302	ARB-5	50	266.60	0.1396
				ARB-5	50	310.91	0.1372
		BWP	19303	ARB-5	100	265.36	0.1219
				ARB-5	100	251.41	0.1280
	B	WP	19304	PG 64-22	50	240.04	0.1762
				PG 64-22	100	274.72	0.1578
		BWP	19305	PG 64-22	100	277.08	0.1104
				PG 64-22	100	321.08	0.1272
25	A	WP	19306	ARB-5	50	284.18	0.1241
				ARB-5	50	256.14	0.1311
		BWP	19307	ARB-5	50	233.58	0.1382
				ARB-5	50	239.78	0.1381
	B	WP	19308	PG 64-22	50	226.02	0.1778
				PG 64-22	100	306.25	0.1573
		BWP	19309	PG 64-22	100	282.12	0.1386
				PG 64-22	100	289.48	0.1362

Table B-10 Test results of binders recovered from Superpave Project 11

Location	Layer	Source	SMO Lab No.	Binder Type	Fracture Energy Density @ 15°C (psi)		
					Loading Rate (mm/min)	FE Density	Extension (in)
15	A	WP	19310	PG 76-22	100	506.85	0.4490
				PG 76-22	500	695.70	0.3551
		BWP	19311	PG 76-22	500	692.23	0.3731
				PG 76-22	300	596.53	0.4216
	B	WP	19312	PG 64-22	300	281.03	0.1609
				PG 64-22	300	264.93	0.1633
		BWP	19313	PG 64-22	300	263.84	0.1714
				PG 64-22	400	256.81	0.1584
25	A	WP	19314	PG 76-22	300	525.92	0.5359
				PG 76-22	600	727.17	0.4494
		BWP	19315	PG 76-22	300	633.70	0.3661
				PG 76-22	300	750.84	0.3456
	B	WP	19316	PG 64-22	300	302.24	0.1599
				PG 64-22	300	282.96	0.1589
		BWP	19317	PG 64-22	300	253.51	0.1546
				PG 64-22	300	264.61	0.1600

Table B-11 Test results of binders recovered from Superpave Project 12

Location	Layer	Source	SMO Lab No.	Binder Type	Fracture Energy Density @ 15°C (psi)		
					Loading Rate (mm/min)	FE Density	Extension (in)
5	A	WP	19318	ARB-5	300	266.95	0.1529
				ARB-5	300	302.66	0.1524
		BWP	19319	ARB-5	100	235.51	0.1591
				ARB-5	100	243.76	0.1680
	B	WP	19320	PG 64-22	100	243.51	0.1410
				PG 64-22	200	294.75	0.1293
		BWP	19321	PG 64-22	200	277.57	0.1379
				PG 64-22	200	292.85	0.1314
10	A	WP	19322	ARB-5	200	258.34	0.1742
				ARB-5	300	281.65	0.1506
		BWP	19323	ARB-5	200	241.28	0.1624
				ARB-5	200	260.06	0.1462
	B	WP	19324	PG 64-22	200	233.55	0.1666
				PG 64-22	300	277.37	0.1564
		BWP	19325	PG 64-22	200	261.04	0.1422
				PG 64-22	200	262.64	0.1437
15	A	WP	19326	ARB-5	200	234.44	0.1726
				ARB-5	300	289.72	0.1665
		BWP	19327	ARB-5	200	223.25	0.1976
				ARB-5	400	213.27	0.1740
	B	WP	19328	PG 64-22	500	292.82	0.1163
				PG 64-22	400	302.22	0.1255
		BWP	19329	PG 64-22	400	299.07	0.1145
				PG 64-22	400	319.25	0.1118
25	A	WP	19330	ARB-5	400	301.93	0.1633
				ARB-5	500	330.76	0.1526
		BWP	19331	ARB-5	400	298.96	0.1361
				ARB-5	400	318.14	0.1333
	B	WP	19332	PG 64-22	400	256.08	0.1480
				PG 64-22	600	267.07	0.1323
		BWP	19333	PG 64-22	400	298.16	0.1208
				PG 64-22	400	276.36	0.1173

APPENDIX C
TEST RESULTS OF PG 82-22, MARIANNI AND HYBRID BINDERS

Table C-1 Test results of PG 82-22 at 15°C

Loading Rate (mm/min)	Fracture Energy Density (psi)	Extension (in)
500	1620.86	1.0912
700	1696.07	1.0698
900	1574.74	1.0600

Table C-2 Test results of PG 82-22 at 10°C

Loading Rate (mm/min)	Fracture Energy Density (psi)	Extension (in)
100	1670.18	1.1140
200	1621.59	0.9118
300	1602.03	0.7564
400	1641.40	0.7509
500	1714.18	0.7421
700	1665.19	0.6684

Table C-3 Test results of Marianni at 15°C

Loading Rate (mm/min)	Fracture Energy Density (psi)	Extension (in)
100	422.02	0.4071
200	448.17	0.4285
200	496.26	0.4154
225	513.27	0.4714

Table C-4 Test results of hybrid binders at 15°C

Binder	Loading Rate (mm/min)	Fracture Energy Density (psi)	Extension (in)
Wright	400	797.95	0.6618
	500	803.54	0.5925
	200	582.11	0.3576
	300	644.40	0.3080
	300	655.58	0.3578
Hudson	400	665.88	0.3224
	400	688.36	0.3289
	500	666.54	0.2852
	500	711.30	0.3185
	100	430.14	0.3375
	100	484.33	0.3659
Geotech	200	525.70	0.3331
	200	475.78	0.3030

APPENDIX D
STATISTICAL ANALYSIS

This part of the study was conducted to further test whether fracture energy is independent of loading rate and temperature for any binder tested, and whether the new direct tension test significantly differentiated between binders.

ANOVA is a statistical process to analyze the amount of variance contributed to a sample by different factors. There are commonly three approaches to calculate the sums of squares (SS) for ANOVA, i.e., Types I, II and III SS. When data is balanced and factors are orthogonal, Types I, II and III SS all give the same results. Types II and III SS are suitable for unbalanced data, while Type I SS is not. If interaction is present, Type II is inappropriate while Type III can still be used.

In the study, three main factors, i.e., binder type, loading rate, and temperatures that affect FE densities of the binders were considered. Since these factors are interrelated, interactions need to be considered in the analysis (which made Type II SS inappropriate). Furthermore, to avoid premature failure, only appropriate ranges of loading rates were used in our tests for different binders at different temperatures. These ranges of loading rates turned out to be very different for different binders. So, for several combinations of loading rate, temperature, and binder, the FE densities do not exist. In other words, our data is unbalanced (which made Type I SS inappropriate). As a result, Type III SS was selected to conduct the statistical analysis.

D.1 Consistency of Fracture Energy

We have seen the consistency of fracture energy in the previous chapter. In order to further test whether the fracture energy is independent of temperature and loading rate, the two-way analysis of variance was performed for the binders, which were tested at different temperatures and loading rates.

D.1.1 Two-way Analysis of Variance

D.1.1.1 PG 67-22 PAV residue

The statistical model used is a quadratic equation as shown below. Actually, a cubic regression model was also used, and the conclusion was the same.

$$e = \alpha + \beta_1 \cdot t + \gamma_1 \cdot l + \beta_2 \cdot t^2 + \gamma_2 \cdot l^2 + \delta \cdot t \cdot l + error \qquad \text{(D-1)}$$

Where:

e – fracture energy density
t – temperature
l – loading rate

The key statistical analysis results are in Table D-1.

Table D-1 Key statistical analysis results of PG 67-22

Source	DF	F Value	Pr > F
Model	5	1.65	0.2068

R-Square			
0.355116			

Type III sums of squares			
Source		F Value	Pr > F
t	1	0.24	0.6330
l	1	0.08	0.7747
$t*t$	1	0.00	0.9936
$l*l$	1	0.31	0.5886
$t*l$	1	0.56	0.4660

Note: DF denotes degree of freedom.

From Table D-1, we can see that according to a significance level of 5% ($\alpha=0.05$), the overall F test is not significant ($F=1.65$, $p=0.2068$), which means the whole model doesn't account for a significant amount of variation in e, i.e., fracture energy density. The model doesn't fit well ($R^2=0.36$). The $t*l$ interaction in the Type III sums of squares is not significant ($F=0.56$, $p=0.466$) indicating that the effects of t and l are independent from each other, which means the

tests for the individual effects are valid. The effects of t, l, t^2 and l^2 in the Type III sums of squares are not significant (t: $F=0.24$, $p=0.633$; l: $F=0.08$, $p=0.7747$; l^2: $F=0.24$, $p=0.633$; t^2: $F=0.24$, $p=0.633$).

In conclusion, for PG 67-22 PAV residue, the fracture energy is independent of temperature and loading rate in a certain range.

D.1.1.2 PG 82-22 PAV residue

The statistical model used is a quadratic equation as shown below. Because t has only two levels, the degree of freedom of t^2 is 0. Therefore, the quadratic term of t is not included in this regression model. Actually, a cubic regression model was also used, and the conclusion was the same.

$$e = \alpha + \beta_1 \cdot t + \gamma_1 \cdot l + \gamma_2 \cdot l^2 + \delta \cdot t \cdot l + error \qquad \text{(D-2)}$$

Where:

e – fracture energy density
t – temperature
l – loading rate

The key statistical analysis results are in Table D-2.

Table D-2 Key statistical analysis results of PG 82-22

Source	DF	F Value	Pr > F
Model	4	0.24	0.8999
R-Square			
0.195954			

Type III sums of squares

Source		F Value	Pr > F
t	1	0.04	0.8602
l	1	0.44	0.5413
$l*l$	1	0.03	0.8672
$t*l$	1	0.08	0.7909

From Table D-2, we can see that according to a significance level of 5% (α=0.05), the overall F test is not significant (F=0.24, p=0.8999), which means the whole model doesn't account for a significant amount of variation in e, i.e., fracture energy density. The model doesn't fit well (R^2=0.196). The $t*l$ interaction in the Type III sums of squares is not significant (F=0.08, p=0.7909) indicating that the effects of t and l are independent from each other, which means the tests for the individual effects are valid. The effects of t, l, t^2 and l^2 in the Type III sums of squares are not significant (t: F=0.04, p=0.8602; l: F=0.44, p=0.5413; l^2: F=0.03, p=0.8672).

In conclusion, for PG 82-22 PAV residue, the fracture energy is independent of temperature and loading rate in a certain range.

D.1.2 One-way Analysis of Variance

For the binders which were tested at only one temperature level 15°C, but have many specimens tested at multiple loading rates, we performed one-way analysis of variance to test the effect of loading rate on fracture energy.

D.1.2.1 Recovered AC-20

The statistical regression model used is shown in Equation (D-3). Actually, a cubic regression model was also used, and the conclusion was the same.

$$e = \alpha + \beta_1 \cdot l + \beta_2 \cdot l^2 + error \tag{D-3}$$

Where:

      e – fracture energy density
      l – loading rate

The key statistical analysis results are in Table D-3, from which, we can see that according to a significance level of 5% (α=0.05), the overall F test is not significant (F=2.7, p=0.0783), which means the whole model doesn't account for a significant amount of variation in e, i.e., fracture energy density. The model doesn't fit well (R^2=0.11). The effects of l and l^2 in the Type III sums of squares are not significant (l: F=3.44, p=0.0704; l^2: F=2.94, p=0.0934).

Table D-3 Key statistical analysis result of AC-20

Source	DF	F Value	Pr > F
Model	2	2.70	0.0783

R-Square
0.111741

Type III sums of squares

Source		F Value	Pr > F
l	1	3.44	0.0704
$l*l$	1	2.94	0.0934

In conclusion, for AC-20 recovered from field, the fracture energy is independent of loading rate in a certain range.

D.1.2.2 Recovered AC-30

The statistical regression model used is shown in Equation (D-4). Actually, a cubic regression model was also used, and the conclusion was the same.

$$e = \alpha + \beta_1 \cdot l + \beta_2 \cdot l^2 + error \qquad (D-4)$$

Where:

e – fracture energy density
l – loading rate

The key statistical analysis results are in Table D-4.

Table D-4 Key statistical analysis result of AC-30

Source	DF	F Value	Pr > F
Model	2	0.75	0.4773

R-Square
0.023574

Type III sums of squares

Source		F Value	Pr > F
l	1	1.17	0.2833
$l*l$	1	0.99	0.3238

From Table D-4, we can see that according to a significance level of 5% (α=0.05), the overall F test is not significant (F=0.75, p=0.4773), which means the whole model doesn't account for a significant amount of variation in e. The model doesn't fit well (R^2=0.023574). The effects of l and l^2 in the Type III sums of squares are not significant (l: F=1.17, p=0.2833; l^2: F=0.99, p=0.3238).

In conclusion, for AC-30 recovered from field, the fracture energy is independent of loading rate in a certain range.

D.1.2.3 Recovered PG 64-22

The statistical regression model used is shown below.

$$e = \alpha + \beta_1 \cdot l + \beta_2 \cdot l^2 + error \tag{D-5}$$

Where:

    e – fracture energy density
    l – loading rate

The key statistical analysis results are in Table D-5.

Table D-5 Key statistical analysis result of PG 64-22

Source	DF	F Value	Pr > F
Model	2	0.19	0.8243
R-Square 0.009161			
Type III sums of squares			
Source		F Value	Pr > F
l	1	0.29	0.5906
$l*l$	1	0.37	0.5474

From Table D-5, we can see that according to a significance level of 5% (α=0.05), the overall F test is not significant (F=0.19, p=0.8243), which means the whole model doesn't account for a significant amount of variation in e, i.e., fracture energy density. The model doesn't

fit well (R^2=0.009). The effects of l and l^2 in the Type III sums of squares are not significant (l: F=0.29, p=0.5906; l^2: F=0.37, p=0.5474).

In conclusion, for PG 64-22 recovered from field, the fracture energy is independent of loading rate in a certain range.

D.1.2.4 Recovered ARB-5

The statistical regression model used is shown below.

$$e = \alpha + \beta_1 \cdot l + \beta_2 \cdot l^2 + error \tag{D-6}$$

Where:

  e – fracture energy density
  l – loading rate

The key statistical analysis results are in Table D-6.

Table D-6 Key statistical analysis result of ARB-5 recovered from field

Source	DF	F Value	Pr > F
Model	2	1.80	0.1820
R-Square			
0.107384			
Type III sums of squares			
Source		F Value	Pr > F
l	1	0.63	0.4335
$l*l$	1	1.31	0.2618

From Table D-6, we can see that according to a significance level of 5% (α=0.05), the overall F test is not significant (F=1.8, p=0.182), which means the whole model doesn't account for a significant amount of variation in e, i.e., fracture energy density. The model doesn't fit well (R^2=0.107). The effects of l and l^2 in the Type III sums of squares are not significant (l: F=0.63, p=0.4335; l^2: F=1.31, p=0.2618).

In conclusion, for ARB-5 recovered from field, the fracture energy is independent of loading rate in a certain range.

D.1.2.5 Recovered PG 76-22

The statistical regression model used is shown below.

$$e = \alpha + \beta_1 \cdot l + \beta_2 \cdot l^2 + error \qquad \text{(D-7)}$$

Where:

e – fracture energy density
l – loading rate

The key statistical analysis results are in Table D-7.

Table D-7 Key statistical analysis result of PG 76-22 recovered from field

Source	DF	F Value	Pr > F
Model	2	0.89	0.4223
R-Square			
0.052458			

Type III sums of squares

Source		F Value	Pr > F
l	1	0.05	0.8214
$l*l$	1	0.01	0.9112

From Table D-7, we can see that according to a significance level of 5% (α=0.05), the overall F test is not significant (F=0.89, p=0.4223), which means the whole model doesn't account for a significant amount of variation in e. The model doesn't fit well (R^2=0.05). The effects of l and l^2 in the Type III sums of squares are not significant (l: F=0.05, p=0.8214; l^2: F=0.01, p=0.9112).

In conclusion, for PG 76-22 recovered from field, the fracture energy is independent of loading rate in a certain range.

D.1.2.6 PG 76-22 at 15°C (both recovered and PAV residue)

The statistical regression model used is shown below.

$$e = \alpha + \beta_1 \cdot l + \beta_2 \cdot l^2 + error \qquad \text{(D-8)}$$

112

Where:

       e – fracture energy density
       l – loading rate
The key statistical analysis results are in Table D-8.

Table D-8 Key statistical analysis result of all PG 76-22 at 15°C

Source	DF	F Value	Pr > F
Model	2	1.49	0.2375

R-Square
0.066167

Type III sums of squares

Source		F Value	Pr > F
l	1	0.16	0.6877
l*l	1	0.00	0.9944

From Table D-8, we can see that according to a significance level of 5% ($\alpha=0.05$), the overall *F* test is not significant ($F=1.49$, $p=0.2375$), which means the whole model doesn't account for a significant amount of variation in *e*. The model doesn't fit well ($R^2=0.066$). The effects of *l* and l^2 in the Type III sums of squares are not significant (*l*: $F=0.16$, $p=0.6877$; l^2: $F=0.00$, $p=0.9944$).

In conclusion, for all PG 76-22 at 15°C, the fracture energy is independent of loading rate in a certain range.

D.2 Statistical Significance of Differences of Fracture Energy among Binders

In the previous chapter, we have seen that the new direct tension test differentiated between binders clearly in terms of fracture energy. In order to further test it by statistical analysis, the three-way and two-way analyses of variance were performed for various types of binder.

D.2.1 Three-way Analysis of Variance

D.2.1.1 PG 67-22 and PG 76-22

According to our experiences, we have already known that the fracture resistance of PG 67-22 and PG 76-22 is quite different. Therefore, the difference between their test results should be statistically significant.

Both PG 67-22 and PG 76-22 specimens were tested at multiple temperatures and loading rates. Thus, a three-way (materials, temperatures and loading rates) analysis of variance was conducted for the two types of binder.

The statistical regression model used is shown below.

$$e = \mu + \alpha_i + \beta_j + \gamma_k + (\alpha\beta)_{ij} + (\beta\gamma)_{jk} + (\alpha\gamma)_{ik} + (\alpha\beta\gamma)_{ijk} + error \qquad \text{(D-9)}$$

Where:

e – fracture energy density
α_i – i th material
β_j – j th temperature
γ_k – k th loading rate
$(\alpha\beta)_{ij}$ – interaction between material and temperature
$(\beta\gamma)_{jk}$ – interaction between temperature and loading rate
$(\alpha\gamma)_{ik}$ – interaction between material and loading rate
$(\alpha\beta\gamma)_{ijk}$ – interaction between material, temperature and loading rate

i=1,…, number of levels of material
j=1,…, number of levels of temperature
k=1,…, number of levels of loading rate

The key statistical analysis results are in Table D-9.

Table D-9 Key statistical analysis results of PG 67-22 and PG 76-22

Source	DF	F Value	Pr > F
Model	7	90.95	<.0001
R-Square 0.867791			

Table D-9 (Continued)

Type III sums of squares			
Source		F Value	Pr > F
m	1	46.89	<.0001
t	1	0.12	0.7322
l	1	1.54	0.2172
$t*l$	1	0.78	0.3786
$l*m$	1	0.29	0.5914
$t*m$	1	0.01	0.9290
$t*l*m$	1	0.26	0.6139

From Table D-9, we can see that according to a significance level of 5% (α=0.05), the overall F test is significant (F=90.95, p<0.0001), which means the whole model accounts for a significant amount of variation in e. With R^2=0.87, the model fits well and accounts for 87% of variation in e. The m, l, t interactions in the Type III sums of squares are not significant ($t*l$: F=0.78, p=0.3786; $l*m$: F=0.29, p=0.5914; $t*m$: F=0.01, p=0.929; $t*l*m$: F=0.26, p=0.6139) indicating that the effects of m, l and t are independent from each other, which means the tests for the individual effects are valid. The effect of m in the Type III sums of squares is significant (F=46.89, p<0.0001). The effects of l and t in the Type III sums of squares are not significant (l: F=1.54, p=0.2172; t: F=0.12, p=0.7322).

In conclusion, the new direct tension test can effectively distinguish between PG 67-22 and PG 76-22 in terms of fracture energy. For these binders, the fracture energy is independent of temperatures and loading rates evaluated.

D.2.2 Two-way Analysis of Variance

D.2.2.1 Modified binders

From our former research project, we knew that current tests do not differentiate between some modified binders. The statistical analyses were performed to test whether the new direct tension test distinguished between them.

Most modified binders were tested at 15°C and multiple loading rates. Therefore, a two-way (materials and loading rates) analysis of variance was performed for all modified binders to test the significance of difference between modified binders' fracture energy density. PG 82-22 was excluded because its very high fracture energy density will obviously make the difference statistically significant.

The statistical regression model used is shown below.

$$e = \mu + \alpha_i + \beta_j + (\alpha\beta)_{ij} + error \qquad\qquad (D\text{-}10)$$

Where:

e – fracture energy density
α_i – i th material
β_j – j th loading rate
$(\alpha\beta)_{ij}$ – interaction between material and loading rate

i=1,…, number of levels of material
j=1,…, number of levels of loading rate

The key statistical analysis results are in Table D-10.

Table D-10 Key statistical analysis results of all modified binders except PG 82-22

Source	DF	F Value	Pr > F
Model	19	3.82	0.0001
R-Square			
0.622610			
Type III sums of squares			
Source	DF	F Value	Pr > F
m	6	4.78	0.0008
l	7	1.01	0.4375
$m*l$	6	0.08	0.9978

From Table D-10, we can see that according to a significance level of 5% (α=0.05), the overall F test is significant (F=3.82, p=0.0001), which means the whole model accounts for a

significant amount of variation in e. With R^2=0.62, the model accounts for 62% of variation in e.

The $m*l$ interaction in the Type III sums of squares is not significant (F=0.08, p=0.9978) indicating that the effects of m and l are independent from each other, which means the tests for the individual effects are valid. The effect of m in the Type III sums of squares is significant (F=4.78, p=0.0008). The effect of l in the Type III sums of squares is not significant (F=1.01, p=0.4375).

In conclusion, the new direct tension test distinguished between modified binders in terms of fracture energy. For these binders, the fracture energy is independent of loading rates evaluated.

D.2.2.2 Hybrid binders and PG 76-22

We have seen a limited difference of fracture energy between hybrid binders and SBS-modified binder PG 76-22. A two-way analysis of variance was further performed for Wright, Hudson, Geotech and SBS-modified binder PG 76-22 to test the significance of difference between their fracture energy density.

The statistical regression model used is shown below.

$$e = \mu + \alpha_i + \beta_j + (\alpha\beta)_{ij} + error \qquad \text{(D-11)}$$

Where:

e – fracture energy density
α_i – i th material
β_j – j th loading rate
$(\alpha\beta)_{ij}$ – interaction between material and loading rate

i=1,…, number of levels of material
j=1,…, number of levels of loading rate

The key statistical analysis results are in Table D-11.

Table D-11 Key statistical analysis results of hybrid binders and PG 76-22

Source	DF	F Value	Pr > F
Model	13	2.87	0.0046

Type III sums of squares

Source	DF	F Value	Pr > F
m	3	4.46	0.0082
l	7	0.96	0.4697
*m*l*	3	0.13	0.9398

From Table D-11, we can see that according to a significance level of 5% (α=0.05), the overall *F* test is significant (*F*=2.87, *p*=0.0046), which means the whole model accounts for a significant amount of variation in *e*. The *m*l* interaction in the Type III sums of squares is not significant (*F*=0.13, *p*=0.9398) indicating that the effects of *m* and *l* are independent from each other, which means the tests for the individual effects are valid. The effect of *m* in the Type III sums of squares is significant (*F*=4.46, *p*=0.0082). The effect of *l* in the Type III sums of squares is not significant (*F*=0.96, *p*=0.4697).

In conclusion, the new direct tension test distinguished between various hybrid binders and SBS-modified binder PG 76-22 in terms of fracture energy. For these binders, the fracture energy is independent of loading rates evaluated.

As for the contrast, due to the limited data of some types of hybrid binder, it is impossible to compare between every two types of modified binders. However, both Hudson and PG 76-22 have adequate data to perform contrast. The statistical model is still two-way, but without the interaction since it is not significant. The key statistical analysis results of the contrast are in Table D-12.

Table D-12 Key statistical analysis results of contrast between Hudson and PG 76-22

Contrast	DF	F Value	Pr > F
Hudson vs. PG 76-22	1	5.17	0.0275

From Table D-12, we can see that according to a significance level of 5% (α=0.05), the F test is significant (F=5.17, p=0.0275), which means the difference of e between Hudson and PG 76-22 is significant.

Furthermore, it is clear that compared to other hybrid binders, Hudson is the closest to PG 76-22. Therefore, the difference between each type of hybrid binder and PG 76-22 is clear.

D.2.2.3 Unmodified binders

All unmodified binders' fracture energy density looks very close. Are they actually different? In other words, did the new direct tension test differentiate between them? For this purpose, a two-way analysis of variance was performed for all unmodified binders.

The statistical regression model used is shown below.

$$e = \mu + \alpha_i + \beta_j + (\alpha\beta)_{ij} + error \qquad (D-12)$$

Where:

e – fracture energy density
α_i – i th material
β_j – j th loading rate
$(\alpha\beta)_{ij}$ – interaction between material and loading rate

i=1,…, number of levels of material
j=1,…, number of levels of loading rate

The key statistical analysis results are in Table D-13.

Table D-13 Key statistical analysis results of unmodified binders

Source	DF	F Value	Pr > F
Model	21	4.09	< 0.0001

Type III sums of squares			
Source		F Value	Pr > F
m	3	9.33	< 0.0001
l	11	0.77	0.6730
$m*l$	7	0.70	0.6684

From Table D-13, we can see that according to a significance level of 5% ($\alpha=0.05$), the overall F test is significant ($F=4.09$, $p<0.0001$), which means the whole model accounts for a significant amount of variation in e. The $m*l$ interaction in the Type III sums of squares is not significant ($F=0.7$, $p=0.6684$) indicating that the effects of m and l are independent from each other, which means the tests for the individual effects are valid. The effect of m in the Type III sums of squares is significant ($F=9.33$, $p<0.0001$). The effect of l in the Type III sums of squares is not significant ($F=0.77$, $p=0.673$).

In conclusion, the new direct tension test differentiated between unmodified binders in terms of fracture energy. For these binders, the fracture energy is independent of loading rates evaluated.

As for the contrast, the statistical model is still two-way, but without the interaction since it is not significant. The key statistical analysis results of the contrast are in Table D-14.

From Table D-14, we can see that according to a significance level of 5% ($\alpha=0.05$), the F test is significant for AC-20 vs. AC-30 ($F=35.3$, $p<0.0001$), AC-20 vs. PG 67-22 ($F=6.12$, $p=0.0145$), AC-30 vs. PG 64-22 ($F=5.4$, $p=0.0215$), AC-30 vs. PG 67-22 ($F=26.74$, $p<0.0001$), PG 64-22 vs. PG 67-22 ($F=9.94$, $p=0.002$), which means the difference of e between them is significant. The F test is not significant for AC-20 vs. PG 64-22 ($F=0.09$, $p=0.7593$), which means the difference of e between them is not significant.

The statistical analysis clearly exhibits that the new direct tension test identified the tiny difference of fracture energy between unmodified binders.

Table D-14 Key statistical analysis results of contrast between unmodified binders

Contrast	DF	F Value	Pr > F
AC-20 vs. AC-30	1	35.30	<.0001
AC-20 vs. PG 64-22	1	0.09	0.7593
AC-20 vs. PG 67-22	1	6.12	0.0145
AC-30 vs. PG 64-22	1	5.40	0.0215
AC-30 vs. PG 67-22	1	26.74	<.0001
PG 64-22 vs. PG 67-22	1	9.94	0.0020

D.3 Summary

All the statistical analyses showed that the new direct tension test significantly differentiated between binders in terms of fracture energy.

Most statistical analyses showed that for the same binder, the fracture energy is independent of loading rates and temperature evaluated.

This is an important finding. It indicates that fracture energy is a fundamental property of binder, which does not depend on test condition, and can be determined by tests performed at a single temperature and loading rate.